MASTER THESIS

IMPROVING POST-TREATMENT DOSIMETRY FOR SELECTIVE INTRA-ARTERIAL RADIATION THERAPY IN LIVER METASTASES

Alienke Ariëlle Kronenberg

27-09-2018

FACULTY OF SCIENCE AND TECHNOLOGY
TECHNICAL MEDICINE

EXAMINATION COMMITTEE
Prof. Dr. Ir. C.H. Slump
Dr. M.P.M. Stokkel
B.J.C.C. Hessink-Sweep, Msc.
Dr. Linda de Wit – van der Veen
J.K. van Zandwijk, Msc.

DAILY MEDICAL SUPERVISOR
M.L. Donswijk, MD

NETHERLANDS CANCER INSTITUTE
ANTONI VAN LEEUWENHOEK

UNIVERSITY OF TWENTE.

List of abbreviations

^{11}Na	Natrium-11
^{18}F	Fluor-18
^{18}F-FDG	^{18}F- fluorodeoxyglucose
4D PET/CT	Respiratory compensated PET/CT
^{64}Cu	Copper-64
^{68}Ga	Gallium-68
^{68}Ge	Germanium-68
^{90}Y	Yttrium-90
^{99m}Tc-MAA	Technetium-99m Macro Aggregated Albumin
AF	Alkalische Fosfatase
ALAT	Alanineaminotransferase
ASAT	Aspartaat Aminotransferase
b_{cold}	Cold background
BoSA	Bovine Serum Albumin
BSA	Body Surface Area
BV	Background Variability
CPS	Counts Per Second
CRC	Colorectal Cancer
CT	Computed Tomography
D_2	Dose received by 2% of the lesion volume
D_{70}	Dose received by 70% of the lesion volume
D_{95}	Dose received by 95% of the lesion volume
D_{98}	Dose received by 98% of the lesion volume
DICOM	Digital Imaging and Communications in Medicine
D_{max}	Maximal received dose
D_{mean}	Mean received dose
D_{min}	Minimal received dose
e^- / β^-	Electron
e^+	Positron
FDA	Food and Drug Administration
FDG	Fludeoxyglucose

FoV	Field of View
FWHM	Full Width Half Maximum
IEC	International Electrotechnical Commission
LD	Local Energy Deposition
MidP	MidPosition
MIRD	Committee on Medical Internal Radiation Dose
MRI	Magnetic Resonance Imaging
NEMA	National Electricals Manufacturers Association
PSF	Point Spread Function
PVE	Partial Volume Effect
PET	Positron Emission Tomography
PET/CT	Positron Emission Tomography / Computed Tomography
RC	Recovery Coefficient
RCs	Recovery curves
RFA	Radiofrequency Ablation
ROI	Regions of Interest
SIRT	Selective Internal Radiotherapy
SPECT/CT	Single Photon Emission Computed Tomography / Computed Tomography
SUV	Standardized Uptake Value
TF/TOF	Time of Flight
ULN	Upper Limit of Normale range
V_{30}	Lesion volume that received more than 30 Gy
V_{50}	Lesion volume that received more than 50 Gy
VOI	Volume of Interest
WHO	World Health Organization
YCl_3	^{90}Y-chloride
^{89}Zr	Zirconium-89

Content

1. Introduction

In the Netherlands, over 15,000 new cases of colorectal cancer (CRC) were reported in 2016, whereas in 2015 almost 5000 patients died due to CRC [1], [2]. CRC is the third most commonly diagnosed cancer in males and second most in females. About 50% of all CRC patients develop liver metastases. The median survival rate of patients with untreated liver metastases is less than 8 months [3]. Comorbidities or lesion location can cause a liver metastasis to be irresectable, which is the case in two-third of the patients. Other treatment options for these patients are chemotherapy, external beam therapy, chemoembolization, radiofrequency ablation and radioembolisation.

1.1 Radioembolisation

In the Netherlands, Yttrium-90 (^{90}Y) radioembolisation is a palliative treatment which is recently approved by 'Zorg Instituut Nederland'. Radioembolisation, also called selective internal radiotherapy (SIRT), is an internal radiation therapy in which ^{90}Y–loaded microspheres are locally delivered intra-arterial to irresectable hepatic malignancies. The microspheres are injected selectively into the proper hepatic artery and are captured in the microvasculature surrounding the liver tumor, which have diameters comparable to those of the microspheres (30μm) [4]–[8]. Accordingly, high radiation doses are delivered to the tumor, whereas healthy liver parenchyma remains mostly unaffected. The rationale behind the treatment is based on the perfusion mismatch between liver parenchyma, which is perfused by the portal vein, and tumor lesions, which are primarily perfused by the hepatic artery [9]. The main advantage of radioembolisation compared with other treatment options is that it is not limited by the distribution and amount of tumor lesions [5].

The effectiveness and safety of ^{90}Y radioembolisation is evaluated in several studies [6], [10]–[13]. Over the past decades more than 18.000 patients in over 150 centers worldwide have been treated with ^{90}Y radioembolisation, either in palliative setting or in combination with chemotherapy [5]. Radioembolisation is in general well tolerated by patients, even if they already have had several types of treatments. In addition, radioembolisation can be safely combined with systemic treatments. In a comparative study by Bester et al., the median survival after radioembolisation in 339 patients was significantly higher compared to the control group who received standard of care (11.9 vs. 6.3 months, respectively) [12]. Seidensticker et al. also reported significant, though much lower, higher survival rates after radioembolisation for 58 patients (8.3 vs. 3.5 months, respectively) [14]. Nevertheless, actual survival rates heavily depend on tumor type, initial disease burden, other sites of disease in the body, comorbidities and patient condition.

A patient will be selected for treatment by a multidisciplinary team. The most important selection criteria are that liver tumor volume needs to be less than 70% of the whole liver volume, good general condition (WHO 1-2) and an acceptable liver- and kidney function (ALAT, ASAT and AF ≤ 5 × ULN, bilirubin and creatinine ≤ 1.5 × ULN). When a patient is selected for radioembolisation a diagnostic CT scan and in some cases a fluor-18 (^{18}F) FDG positron emission tomography (PET) / computed tomography (CT) scan are made to determine healthy liver and tumor volume, furthermore it is used to assess liver vascularization and the presence of extra hepatic disease.

Two weeks before the actual ^{90}Y radioembolisation patients undergo a pre-treatment angiography in which a test dosage of Technetium-99m Macro Aggregated Albumin (^{99m}Tc-MAA) is administered. Figure 1 shows a schematic timeline of the actions involved in ^{90}Y radioembolisation.

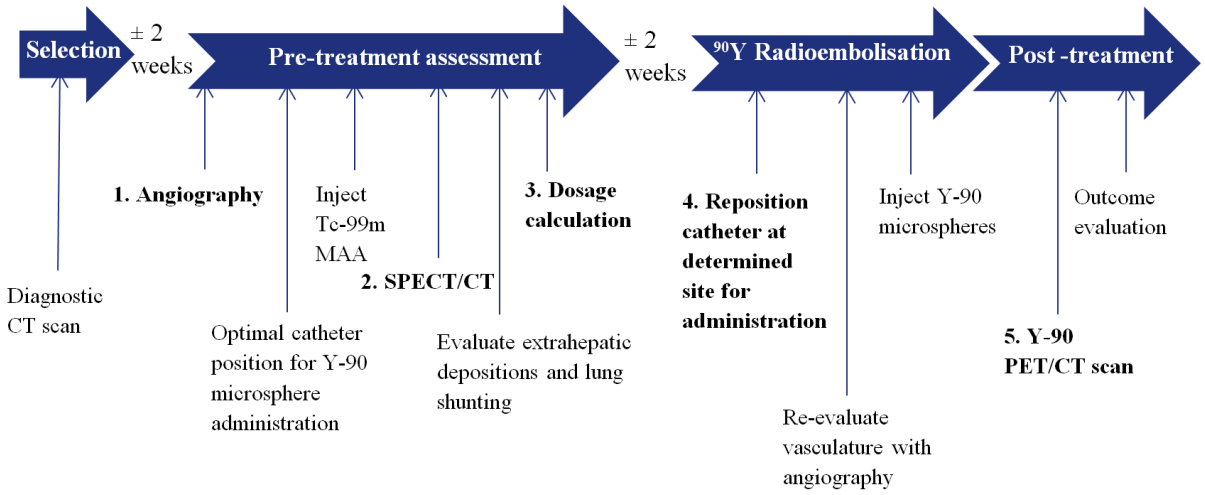

Figure 1. Schematic timeline of ^{90}Y radioembolisation

1.2 Planning angiography and pretreatment nuclear medicine imaging

The planning angiography procedure is the first step after a patient is selected for radioembolisation. During the initial angiography, the abdominal arterial vasculature will be depicted, with specific focus on the vasculature of the liver lesions [15]. In this way, the specific arterial visceral vascularization is visualized and assessed in each patient. The goal is to determine the correct catheter tip position in which the desired liver lesions are reached by the microspheres, while normal tissue is spared. A ‘test dosage’ of ^{99m}Tc-MAA of 75-150 MBq is administered at the optimal catheter position for ^{90}Y microsphere administration. In order to prevent the administered radioactivity to reach other organs like the small intestines or stomach, the right gastric artery or gastroduodenal artery can be coiled [16]. Although ^{90}Y microspheres are permanent once implanted, the ^{99m}Tc-MAA particles are not and therefore do not interfere with ^{90}Y microsphere distribution. The ^{99m}Tc-MAA distribution will never

fully correspond with the ^{90}Y distribution due to differences in injected particle load, particle size (10 – 40 µm), microembolisation, regional blood flow changes and catheter placement [8], [17]. The ^{99m}Tc-MAA particle distribution is analyzed using post-injection SPECT/CT and planar gamma imaging. By means of the planar images, the percentage of administered activity that reaches the lungs (lung shunt) and other extrahepatic organs such as the pancreas and duodenum is assessed. A lung shunt more than 20% is a contraindication for therapy, because it will lead to an unacceptable risk at adverse events like radiation pneumonitis [6], [18].

1.3 Dosage calculation

^{90}Y is a β^--emitting isotope with a half-life of 64 hours. 99.99% of ^{90}Y decays into the ground level ^{90}Zr by β^- emission (2.280 MeV) and 0.0115% is to an excited level of ^{90}Zr by β^- emission (0.519 MeV). The transition from this excited state into the ground state is through internal conversion (0.0083%) or by creation of an e^+/e^- pair (0.0032%). The e^+/e^- pair has a maximum energy of 0.739 MeV. The average range of electrons is 2.5mm, whereas the maximum range is 1.1cm. Therefore, the range of ^{90}Y electrons with the average kinetic energy is approximately 100 cell diameters (25 – 40 µm) [8], [19].

Nowadays, two ^{90}Y microsphere products are FDA-approved for clinical use; TheraSphere (MDS Nordion Inc., Kanata, Ontario, Canada) and SIR-Spheres (SIRTeX Medical Ltd., Sidney, New South Wales, Australia). TheraSphere are glass microspheres, whereas SIR-Spheres are resin-based [4]. In the NKI-AVL (The Netherlands Cancer Institute) resin-based SIR-spheres are used.

Table 1. Characteristics of ^{90}Y microsphere products available for radioembolisation. [6], [8], [20]

	SIR-spheres	**TheraSphere**
Material	Resin	Glass
Particle size (µm) (range)	32.5 (20-60)	25 (20-30)
Activity per sphere (Bq)	40 – 70	1250 - 2700
Number of spheres per 3 GBq vial	$40 – 80 \times 10^6$	1.2×10^6
Activity available (GBq)	3	3 - 20

There are some differences between the two distributors of microspheres (Table 1). For SIR-spheres the calculated dosage is always below 3 GBq, whereas for TheraSpheres up to 20 GBq can be administered. Due to the fact that glass spheres contain a higher activity per sphere, fewer microspheres are needed compared to resin spheres to deliver the same amount of radioactivity. With a lower number of spheres, the glass spheres probably have a less embolic effect in the tumor's microvasculature. On the other hand, the large number of resin spheres may result in a uniform dose distribution and therefore an increased treatment effect [21]. For SIR-spheres the Body Surface Area (BSA) method is used to calculate the desired amount of injected radioactivity (A) with means of a patient's height (h), weight (m) and tumor and liver volume (V), described with equation (1) and (2). It is used to calculate safe treatment activities, but does not incorporate a desired absorbed lesion dose [22], [23].

$$BSA = 0.20247h^{0.725} \times m^{\,0.425} \tag{1}$$

$$A = BSA - 0.2 + \frac{Vtumor}{Vliver} \tag{2}$$

For TheraSpheres non-compartment MIRD (committee on medical internal radiation dose) method is used which incorporates the desired dose (D), described with equation (3). This method assumes the treated area as one 'compartment', no distinction is made between tumor and healthy tissue [8], [22].

$$A = \frac{D \times m}{49.38} \tag{3}$$

1.4 Treatment angiography and post-treatment nuclear imaging

After dosage calculation, the patient is scheduled for the second angiography during which the ^{90}Y microspheres are administered. On average, 2.0 GBq is injected during a whole liver treatment. Within 24 hours after therapy, ^{90}Y-PET is performed to assess whether the ^{90}Y microspheres have reached the tumor and if any extrahepatic accumulations are visible. At present, these images are only visually assessed at the NKI-AVL, and no uptake quantification is performed.

During treatment follow-up with diagnostic CT three aspects are monitored; response of the treated hepatic lesions, the emergence of new lesions and progression of extrahepatic lesions [6]. Rosenbaum et al. reported in a systematic review that only in 18-46% of the patients complete or partial response is observed after radioembolisation [24], [25]. This phenomenon of limited response is not only frequently described in literature, it is also observed in our clinical practice. Figure 2 shows an example of poor local response to radioembolisation whereas Figure 3 shows a good local response to radioembolisation based on post-treatment ^{18}F-FDG PET/CT scans. The origin of heterogeneous responses in metastatic CRC is not yet understood. Differences in therapy response may be explained by under-dosing of specific patients or various phenotypes.

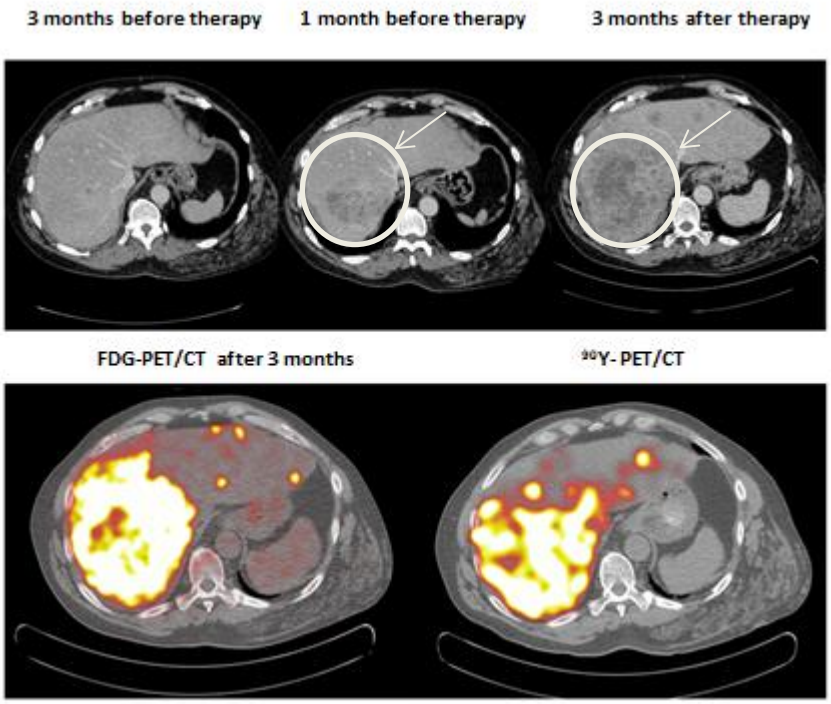

Figure 2. Example of a very poor local response to radioembolisation. This patient has extensive liver metastases, which kept on growing despite chemotherapy. An adequate microsphere accumulation in and around the liver lesions is observed after radioembolisation at the ^{90}Y-PET/CT scan (^{90}Y-dosage 1.7 GBq, total liver volume 3200 ml, estimated tumor volume 980 ml). However, new hepatic lesions are observed at the ^{18}F-FDG PET/CT scan after three months [6].

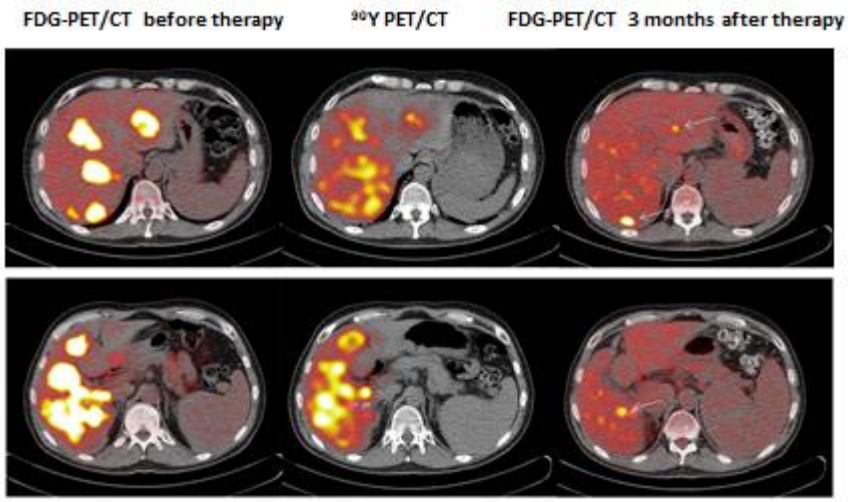

Figure 3. Example of a good local response to radioembolisation. This patient was diagnosed with a metastasized sigmoid carcinoma and was treated with multiple lines of chemotherapy. Sufficient microsphere accumulation in and around the liver lesions is visible after radioembolisation at the ^{90}Y-PET/CT (^{90}Y-dosage 2.0 GBq, total liver volume 1600 ml, estimated tumor volume 620 ml). A very good response is seen at the ^{18}F-FDG PET/CT after three months [6].

1.5 Post-treatment dosimetry

Dosimetry includes either the calculation of the activity that needs to be administered to achieve a desired absorbed dose (pre-treatment) or the calculation of the actual absorbed dose after administration of a radioactive dosage (post-treatment). Absorbed dose is the concentration of energy deposited in tissue by radiation. Post-treatment dosimetry is not routinely performed in radioembolisation, but helps to identify the effective, patient-specific therapeutic dose. Performing dosimetry can reveal that a tumor has not received the calculated amount of radiation and therefore needs additional treatment, thus also directly providing benefit for the individual patient. At this moment, data about the relation between absorbed tumor dose and therapy outcome is limited [26]. Quantification of absorbed doses in radioembolisation has long been assumed to be impossible, due to the inadequate quality of Bremsstrahlung SPECT images [26].

^{90}Y has long been considered to be a pure beta-emitter, although the very low branching ratio (32×10^{-6}) to positron emission was already discovered in 1955 [27]. The first study to the ^{90}Y-PET scan was published in 2009 [6]. Since then, the feasibility of ^{90}Y-PET was established and it was concluded that ^{90}Y PET scan has a superior resolution compared to Bremsstrahlung SPECT, which results in improved quantification possibilities [6], [26]. In 2013 the ^{90}Y-PET/CT has been clinically introduced in the NKI-AVL and is used in the standard work-up of radioembolisation procedure. Even though the introduction of ^{90}Y-PET has led to improved quantification possibilities, PET/CT scanner calibration is eminent for non-pure beta emitting isotopes such as ^{90}Y since the partial volume effect and gamma crosstalk can cause quantification inaccuracies. Additionally, the scanners used in the NKI-AVL do not have a ^{90}Y preset, so acquisition has to be done using the isotope settings of Germanium-68 (^{68}Ge) or Natrium-11 (^{11}Na). This also introduces an offset error for absolute quantification.

Several options to perform post-treatment dosimetry on ^{90}Y-PET scans are available. Dosimetry performed by both dose-point kernel convolution and local energy deposition (LED) method show similar results for ^{90}Y-PET dosimetry, where the LED method has the advantage of easy implementation in the clinical workflow. In LED it is assumed that all emitted β^--particles deposit their energy locally within one voxel. The absorbed dose in each voxel can thus be calculated by multiplying voxel activity concentration with a constant, isotope-dependent scaling factor. The dose-point kernel convolution method is a better representation of reality as it takes interaction between voxels into account [28].

Post-radioembolisation dosimetry provides information about absorbed tumor doses and its relation to therapy outcome. At this moment, data about relation between absorbed tumor dose and therapy

outcome is limited. This is mostly due to a lack of knowledge for PET/CT scan calibration and performing ^{90}Y-PET/CT based dosimetry. The first results of dosimetry performed in radioembolisation based on the LED method show that for similar amounts of absorbed dose, therapy outcome can differ substantially [6]. It is desired to gain more insight into the dose-response relationship of radioembolisation, which may be reached with post-treatment dosimetry. Using post-treatment dosimetry may bring us a step closer in determining the effective, patient-specific therapeutic dose for radioembolisation [20], [26], [29], [30]. Besides that, it will become easier to compare data from multiple clinical centers and to possibly expand this treatment to other types of tumors [6]. Therefore, this research will focus on the best way to perform post-treatment dosimetry in ^{90}Y radioembolisation.

1.6 Research

How can post-treatment dosimetry for selective intra-arterial radiation therapy in liver metastases be improved in the NKI-AVL?

First, the quantification possibilities of the PET/CT scanners in the NKI-AVL for ^{90}Y will be determined in this thesis. These results will be presented in Chapter 2. Second, post-treatment dosimetry will be performed retrospectively on patients treated with ^{90}Y-radioembolisation in the NKI-AVL (Chapter 3). Dosimetry will be performed using PlanetDose (DOSIsoft, Cachan, France), which is dedicated software designed for dosimetry of ^{90}Y microspheres. Finally, future work in post-treatment dosimetry will be discussed in Chapter 4.

2. PET/CT calibration for 90-Yttrium isotope quantification

***Abstract*— ^{90}Y-PET/CT scans are used in ^{90}Y radioembolisation, a targeted radionuclide therapy for irresectable liver metastases. It is desired to quantify ^{90}Y microspheres liver uptake in order to establish a dose-response relationship for radioembolisation. The objective of this study is to assess the quantitative accuracy of two PET/CT scanners (Philips Gemini TF) for the purpose of quantification absorbed doses of ^{90}Y microspheres in radioembolisation. Two experiments were performed with means of the NEMA phantom. In the first experiment the phantom was filled with five different sphere-to-background ratios (1:b_{cold}, 1:15, 1:10, 1:7 and 1:4). In the second experiment the phantom was filled with one ratio (1:9) of ^{90}Y-chloride and imaged on four different timepoints. All results confirm the limited quality of the ^{90}Y-PET scan for quantification purposes. The results indicate that only lesions larger than 11.49 cm^3 and those that receive an activity concentration higher than 70 kBq/ml can be used for quantification. The focus of future research can be the quantification of activity and activity concentrations deposited in liver lesions and healthy liver tissue after radioembolisation, in that way obtaining more insight into the precision of performing post-treatment dosimetry clinically.**

***Index Terms*—Calibration, PET/CT scanner, quantification, Yttrium-90**

2.1 Introduction

In the Netherlands, ^{90}Y radioembolisation is a palliative treatment option that has recently been approved by 'Zorg Instituut Nederland'. Radioembolisation, also called selective internal radiotherapy (SIRT), is an internal radiation therapy in which ^{90}Y–loaded resin (SIR-spheres) or glass (Theraspheres) microspheres are delivered transarterially to hepatic malignancies. The microspheres are injected selectively into the hepatic artery using a catheter and become trapped in the microvasculature surrounding the liver tumor [4], [31], [7], [6]. Accordingly, high radiation doses are delivered to the tumor, whereas the healthy liver parenchyma remains mostly unaffected. The rationale behind the treatment is based on the perfusion mismatch between healthy parenchyma, which is perfused by the portal vein, and tumor lesions, which are primarily perfused by the hepatic artery. The effectiveness and safety have already been demonstrated in several studies [6], [10], [12], [13], [11], [32]–[37]. Over the past decades >18,000 patients in >150 centres worldwide have been treated with ^{90}Y radioembolisation, either in palliative setting or in combination with chemotherapy [31]. Within one day after therapy, ^{90}Y-PET is performed to assess whether the ^{90}Y microspheres have reached the tumor and if any extrahepatic accumulations are visible. No extra injections with ^{90}Y are made before this scan, therefore the microsphere distribution solely caused by the treatment is observed. ^{90}Y has a low branching ratio (32×10^{-6}) to positron emission (b) [17]. With means of equation 4 it is calculated that the amount of counts per second detected per imaged bed position for ^{90} Y is only 0.20% of that of ^{18}F for a similar scanner sensitivity (s), whereas the average activity administered (A) and time per bed position (t) are higher. These calculations demonstrate that ^{90}Y-PET scans are of lesser quality than those of ^{18}F, due to the fact that less counts per second (CPS) are detected [6], [26], [38]. In radioembolisation the quality of ^{90}Y scans is sufficient for visual assessment because the total dose (average 2.0 GBq) is injected locally into the liver and is not distributed over the total body.

$$CPS = b \times s \times t \times A \tag{4}$$

Table 2. The branching ratio (b), scanner sensitivity (s), time per bed position (t) and average activity (A) for ^{90}Y and ^{18}F are given. With these parameters the detected cps per bed position are calculated for both isotopes. [39]

	Yttrium-90	**Fluor-18**
Positron branching ratio (%)	0.0032	96.9
Scanner sensitivity (cps/kBq)	6.6	6.6
Time per bed position (min)	15	2
Average activity (MBq)	1500	190
Cps	0.48×10^6	243×10^6

Ideally, ^{90}Y-PET/CT scans are not only be used for visual assessment after radioembolisation but also for post-treatment dosimetry; quantification of the absorbed liver doses (tumor and healthy tissue) in order to establish a dose-response relationship for radioembolisation [6], [17], [26], [40]. The objective of this study is to assess the quantitative accuracy of the two PET/CT scanners (Philips Gemini TF) in our institute, which is done by performing two experiments with means of the NEMA phantom.

2.2 Methods and materials

2.2.1 PET/CT systems

Data was acquired on two PET/CT scanners; Philips GEMINI TF TOF 16 (2006) and Philips GENIMI TF Big BORE PET/CT (2012) (Philips Medical Systems, Best, The Netherlands), referred to as PETCT06 and PETCT12. The PET component of the Gemini TF is composed of 28 flat modules of a 23×44 array of 4×4×22 mm^3 LYSO crystals. The patient bore has a diameter of 71.7cm (85 Big BORE), with a transverse FOV of 57.6 cm (67.6 Big BORE) and an axial FOV of 18cm. The detection energy window is set to 440-665 keV (default) for a coincidence window of 6 ns [39]. The data were reconstructed with a time of flight (TOF) blob-based OS algorithm (3 iterations, 33 subsets) and TOF correction at 4x4x4mm voxels. Random and scatter corrections are incorporated into the iterative algorithm. The low-dose CT scan was acquired with a slice thickness of 2mm.

2.2.2 Phantom study

In order to simulate different tissue uptake ratios, the International Electrotechnical Commission (IEC) body phantom designed by the National Electricals Manufacturers Association (NEMA) organization was used for the experiments (ECT/IEC-BODY/P, PTW Freiburg GmbH, Freiburg, Germany). The phantom contains a background compartment (9,7 L) and six fillable spheres (internal diameters 10, 13, 17, 22, 28 and 37 mm) and a cold (non-radioactive) insert (diameter 51 mm).

2.2.2.1 Experiment 1

In the first experiment, the phantom was scanned for five different sphere to background ratios; 1:b_{cold} (cold background), 1:15, 1:10, 1:7 and 1:4 created with a total amount of 1.5 GBq ^{90}Y-chloride (YCl_3) (Eckert&Ziegler, Braunschweig, Germany). The ratios measured and used ^{90}Y concentrations are shown in Table 3. In our institute clinical ratios from 1:2 till 1:10 are observed. In literature large differences in tested sphere-to-background ratios are observed, ratios differ from 1:3 till 1:40 [40]. In Table 4, articles are listed that have performed measurements to ^{90}Y calibration with means of a phantom that contained spheres and a background compartment.

2.2.2.2 Experiment 2

In the second experiment, the phantom was filled with an approximate 9:1 sphere-to-background ratio with YCl_3 (Eckert&Ziegler, Braunschweig, Germany). A total amount of 2.4 GBq (5858 GBq/g) YCl_3 was divided into two syringes of approximate 240 MBq and 2160 MBq. The 240 MBq syringe was added to a volume of 100 mL, used to fill the phantom spheres. The 2160 MBq syringe was added to the background compartment together with Bovine Serum Albumin (BoSA, 5000 mg/500 ml), to prevent the YCl_3 from sticking to the phantom walls. Residual in the needles and syringes was considered negligible, as they were thoroughly flushed after usage. The phantom was imaged over the timespan of a week on day 0, 3, 5 and 7.

2.2.3 Scanning protocol

In both experiments the phantom was scanned at both scanners with the clinical scanning protocol for ^{90}Y (68-Germanium (^{68}Ge) isotope preset, 2 bedpositions, 15 minutes per bedposition). ^{68}Ge is a long-lived isotope, which is used to avoid any scanner decay correction during acquisition. In appendix A the decay schemes of both ^{68}Ge and ^{90}Y are shown. The clinical scanning protocol contains ^{68}Ge as isotope instead of ^{90}Y, therefore a rescaling factor was needed to correctly quantify activity in the phantom. The positron fraction of ^{68}Ge is 0.891, whereas that of ^{90}Y is 31.86×10^{-6}. Rescaling in Bq/ml for this difference can be done with means of a correction factor (Equation 5).

$$Theoretical\ correction\ factor = \frac{0.891}{(31.86 \times 10^{-6})} = 27966.1\ Bq/ml \tag{5}$$

Table 3. Measured ratios together with the phantom sphere and background concentrations of ^{90}Y.

Ratio	**1: b_{cold}**	**1:17**	**1:11.7**	**1:6.9**	**1:3.9**
Background concentration (MBq/ml)	0	0.021	0.030	0.051	0.089
Concentration spheres (MBq/ml)	0.35	0.35	0.35	0.35	0.27

Table 4. Articles that performed measurements to ^{90}Y calibration with means of a phantom that contained spheres and a background compartment.

First author	**Concentration spheres**	**Concentration background**	**Ratio (Sphere to background)**	**Scan time (min/bed position)**	**Modality**	**Recovery coefficient**
Maughan [41]	-	-	8:1	30 and 120	PET/MRI	16.6 – 68.7%
Attarwala [42]	2380 kBq/ml	304 kBq/ml	1:8	30 and 120	PET/CT	0.1 – 1.1
Van Elmbt [38]	1.3 MBq/ml	0.44 Mbq/ml	1:3	120, 105, 90, 75, 60, 45, 30 and 15	PET/CT	-
Werner [43]	3.6 MBq.ml	0	1:3.6	40	PET/CT	0.6 – 1.0 for spheres larger than 17 mm
Willowson [40]	2.31 MBq/ml	0.289 MBq/ml	8:1	15 - 20	PET/CT	45 – 100 % for the 37 mm sphere

2.2.4 Dose calibrator accuracy

The accuracy of the dose calibrator used in the NKI-AVL for the ^{90}Y isotope was tested in both experiments, because the dose calibrator is used for activity calibration in every radioembolisation treatment. In both experiments, the activity detected in each syringe by the dose calibrator was compared to the activity calculated from the net weight and the activity concentration determined by the manufacturer (GBq/gram).

2.2.5 Data analysis

In both experiments, the true concentrations in the phantom were determined with the syringe activities and known volumes of the background compartment and spheres. Quantitative accuracy was assessed at each time-point by determining several parameters for both scanners. All parameters were obtained with means of the regular DICOM viewer software in our institute; Osirix and with DOSIsoft (DOSIsoft, Cachan, France), software designed for dosimetry of ^{90}Y microspheres. Concentration in Bq/ml was used in the data analysis instead of standardized uptake value (SUV) values.

The following parameters were determined for every ratio, scanner and data analysis program in the first experiment and for all imaging days in the second experiment.

1. The total activity in the field of view (FoV), which is an indicator for the ability to quantify the total amount of injected activity.
2. Background concentration, determined by following the NEMA NU 2-2007 guidelines [44]. For the first experiment 12 regions of interest (ROI) were drawn for each sphere size (37, 28, 22, 17, 13 and 10mm) in one slice (Figure 4) and then averaged, for the second experiment the 12 ROIs were drawn in 5 separate slices ±1 cm apart (60 in total for each sphere diameter).
3. Mean sphere concentration for all ratios in the first experiment and for the first day of imaging in the second experiment. Assessed with means of Volumes of Interest (VOI) drawn based on the position of the spheres on the CT scan. Results are presented as recovery coefficients (RC), equation 6, in which the measured concentration ($C_{measured}$) is compared to the true concentration (C_{true}).

$$RC(\%) = \frac{C_{measured}}{C_{true}} \times 100 \quad (6)$$

4. Background variability (BV), as an indicator for variation in background concentration measured due to low signal-to-noise ratio. Determined by following the NEMA NU 2-2007 guidelines.

The following parameters were determined only in the second experiment, in addition to the already mentioned parameters

5. Recovery for the largest sphere (37 mm) for all imaging days as an indicator for consistency of recovery with lower activity concentrations.
6. Activity concentration detected in the cold insert of the phantom, assessed as the mean concentration detected across five transversal slices (±1 cm apart) as a percentage of the true background concentration.

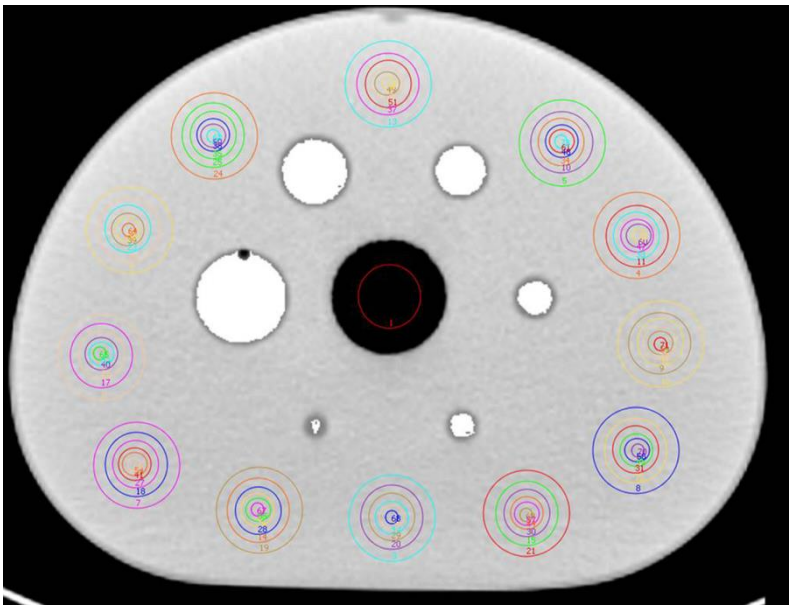

Figure 4. ROI drawn in the background compartment and cold insert, used to determine the background concentration. [45]

2.3 Results

2.3.1 Dose calibrator

Table 5. Dose calibrator accuracy determined for each syringe used in the phantom measurements by comparing the dose calibrator detected activity to the activity determined by the specific activity provided by the manufacturer (GBq/gram).

	Dose calibrator detected activity (Mbq)	**Manufacturer determined activity (Mbq)**	**Accuracy**
Experiment 1			
Spheres	36	31	88%
Ratio 1:15	200	186	93%
Ratio 1:10	93	70	76%
Ratio 1:7	200	187	94%
Ratio 1:4	494	479	97%
Experiment 2			
Spheres	2400	2200	93%
Background	2160	2430	111%

2.3.2 Visual results

a. Ratio 1:b_{cold} experiment 1

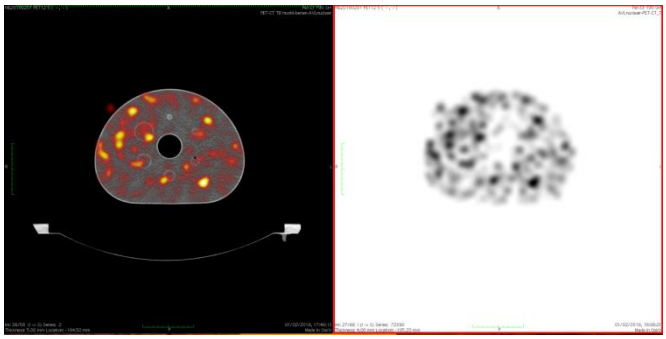

b. Ratio 1:4 experiment 1

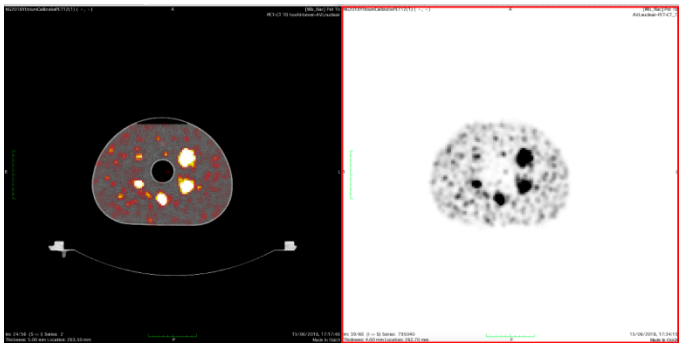

c. Day 1 of imaging experiment 2

Figure 5. PET/CT (left) and PET scan (right) for different ratios. A sample bottle containing the sphere activity concentration was scanned together with the phantom (figure a. and b.).

2.3.3 Total activity in the FoV

In Figure 6 it is observed that the higher the total amount of activity in the phantom, the more is detected by the scanners except for the lowest amount of activity. A maximum of 93% and 87% was quantified for PETCT06 and PETCT12 when 2400 MBq is present in the phantom. Both scanners show similar results for detecting a total amount of activity in the FoV. It is seen that when the total amount of activity becomes less than 700 MBq, quantification accuracy rapidly drops to less than 50%.

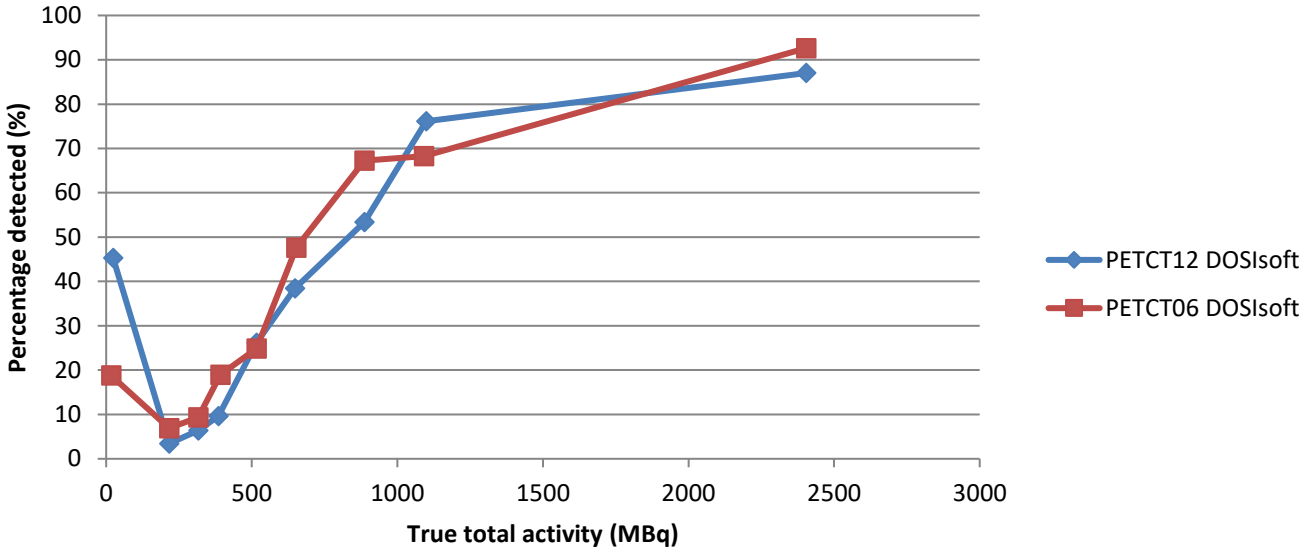

Figure 6. Total amount of activity detected in the FoV for different total activities in both experiments

2.3.4 Background concentration

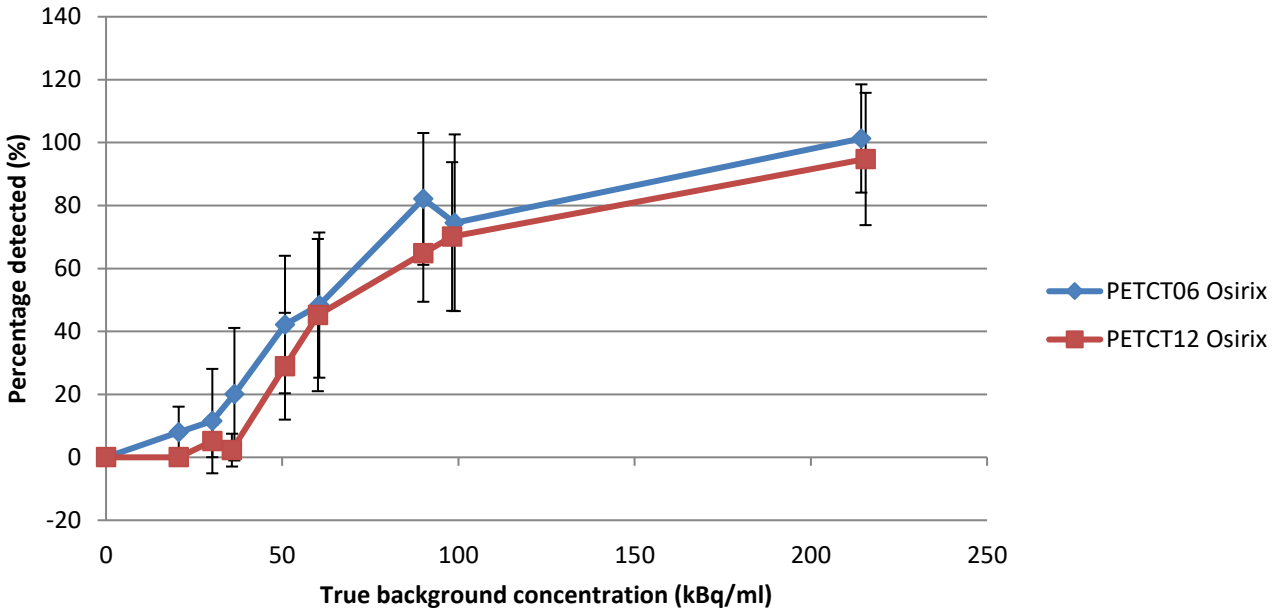

Figure 7. Difference between the true and recovered background concentration (kBq/ml) for different background concentrations for both PET/CT scanners with standard deviation.

In Figure 7, it is observed that higher background concentrations in large VOIs are more accurately quantified than lower background concentrations by both scanners. For the highest background concentration (215 kBq/ml) 100% and 95% is detected for PETCT06 and PETCT12 respectively. When the concentration drops below 70 kBq/ml, quantification accuracy rapidly drops to less than 50%.

2.3.5 Sphere recovery curves

2.3.5.1 Experiment 1

Figure 8 shows the different recovery curves (RCs) for all measured ratios on both PET/CT scanners, measured with both data analysis programs. The smaller spheres of 10, 13 and 17mm could not be accurately segmented in the 1:b_{cold} situation, so in the following ratios only the 22, 28 and 37mm spheres are segmented. Figure 10 and Figure 9 show the differences between sphere to background ratios for both PET/CT scanners. Recovery enhances when sphere diameter becomes larger. It is observed that in general, the recovery curves get better for higher ratios, apart from outliers seen for ratio 1:10 for PETCT06 and for ratio 1:7 and 1:15 for PETCT12.

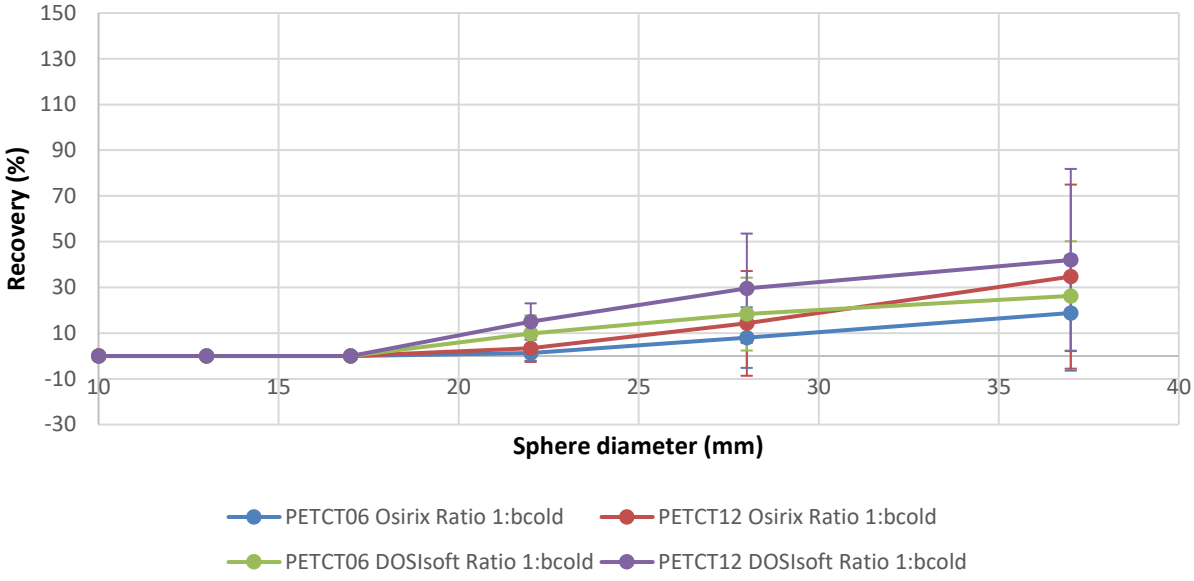

a. Ratio 1: b_{cold}

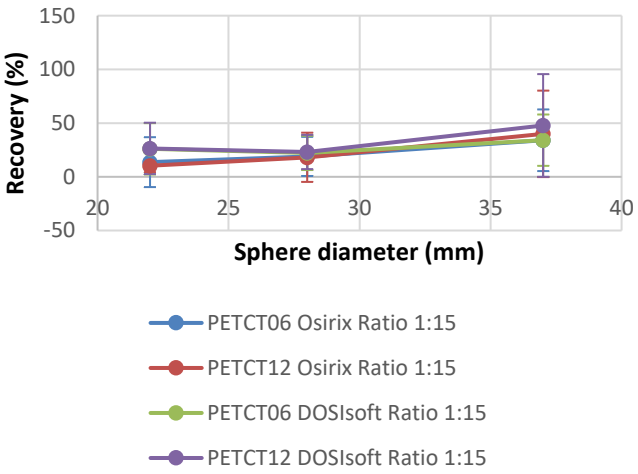

b. Ratio 1:15

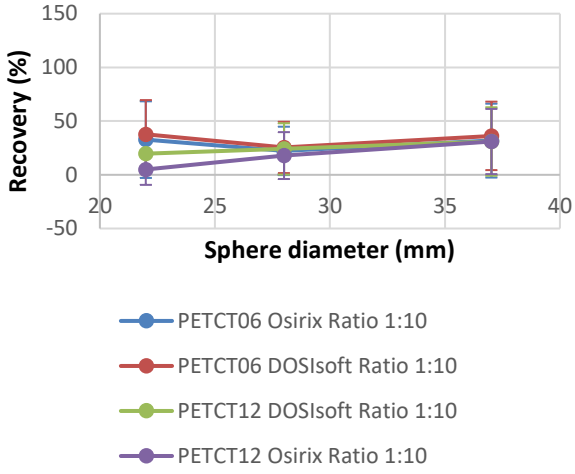

c. Ratio 1:10

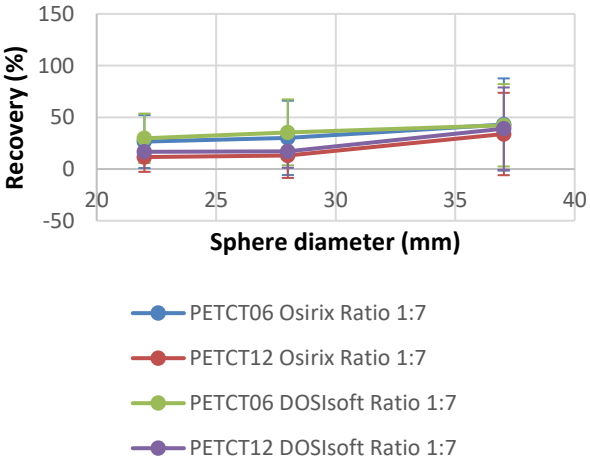

d. Ratio 1:7

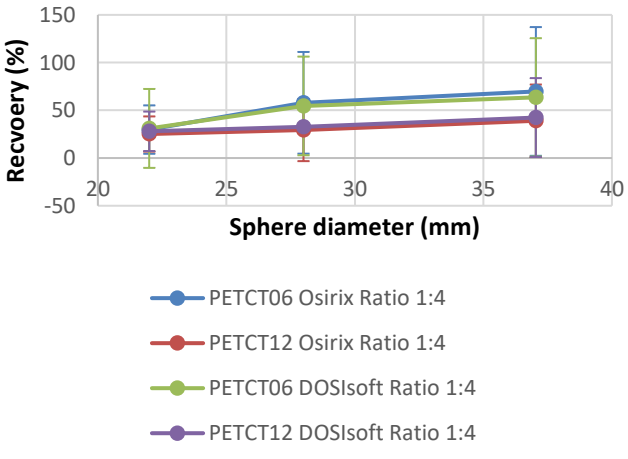

e. Ratio 1:4

Figure 8. Recovery curve for both PETCT scanners and data analysis programs for different ratios.

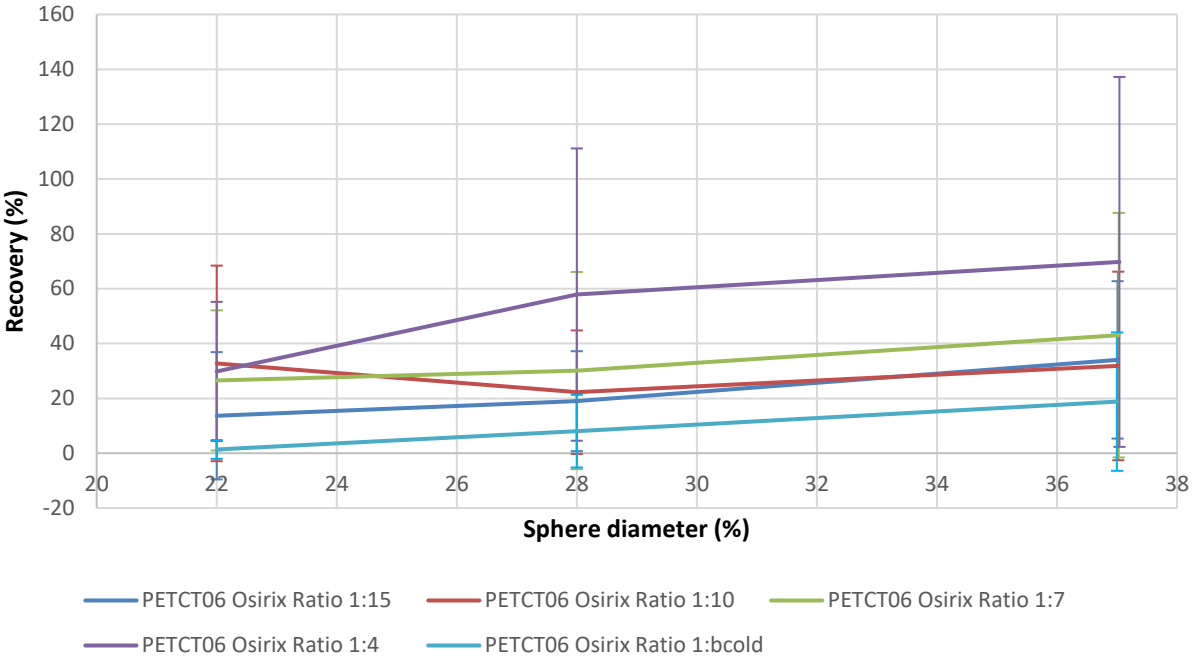

Figure 9. Recovery curves for different ratios and sphere diameters, measured with PETCT06 and Osirix.

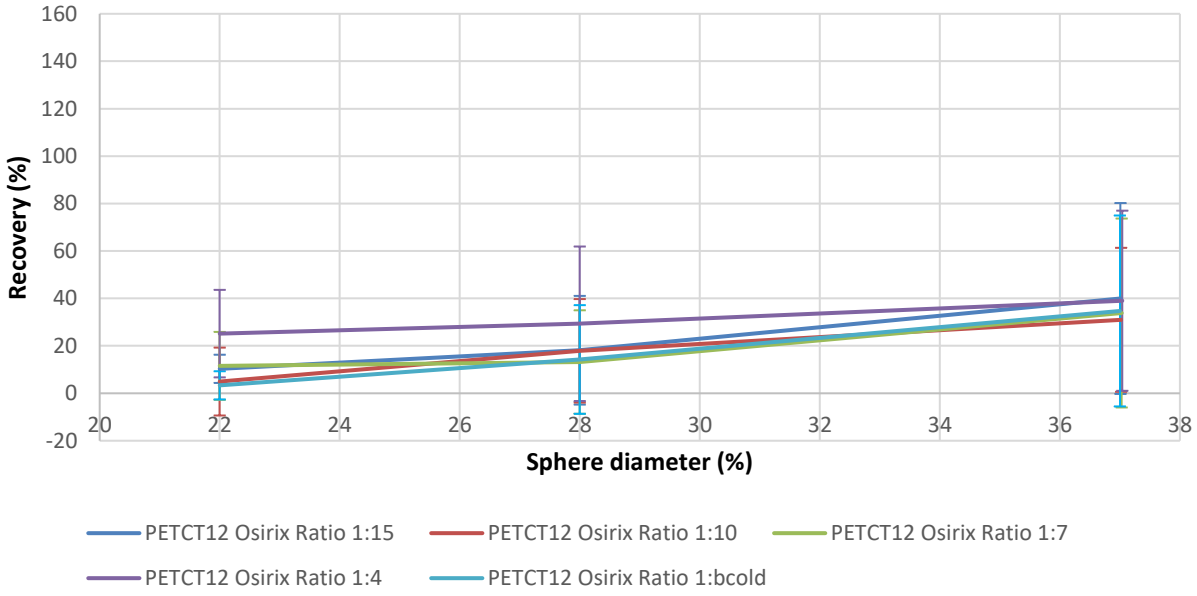

Figure 10. Recovery curves for different ratios and sphere diameters, measured with PETCT12 and Osirix.

2.3.5.2 Experiment 2

The recovery curve for different sphere diameters on day 0 and 3 of imaging are shown in Figure 11 and Figure 12. Due to an artefact discovered in the data of the first day, it was decided to again obtain the recovery curve on the third day of imaging. It is observed that recovery increases with sphere diameter, large standard deviations are seen for every sphere. The largest sphere (37 mm) shows the highest recovery, 68% ± 25% for PETCT06 and 65% ± 35% for PETCT12 (Figure 12).

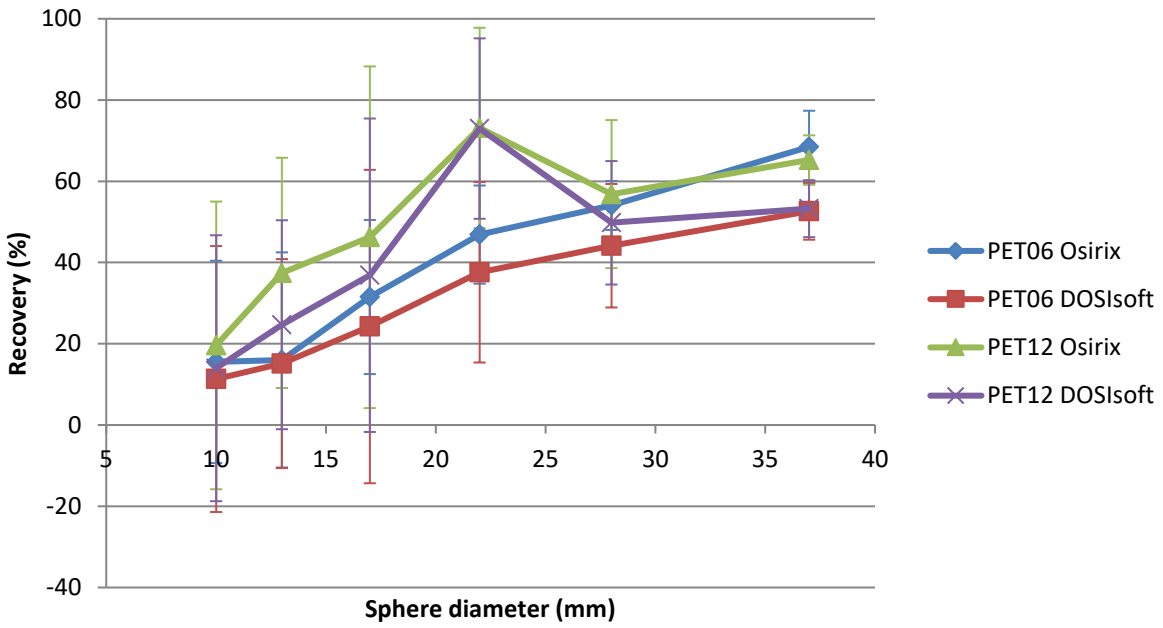

Figure 11. Recovery curve for different sphere diameters (mm) on day 0 of imaging, for both scanners and analysis programs. (spheres: 2404.19 kBq/ml, background: 222.91 kBq/ml)

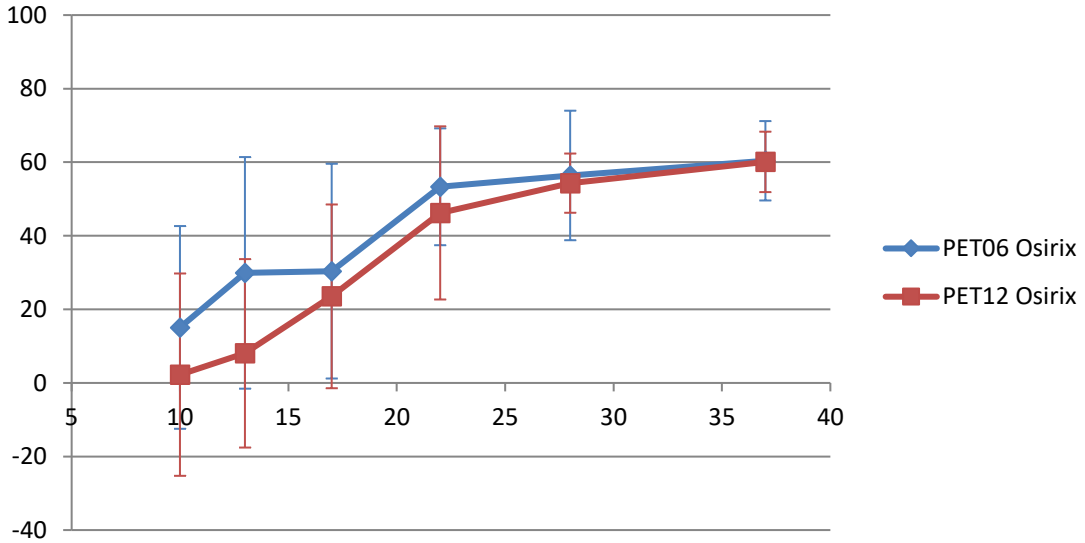

Figure 12. Recovery curve for spheres of different diameters (mm) on day 3 of imaging for both scanners. (spheres: 1100.17 kBq/ml, background: 102.01 kBq/ml)

The recovery for the 37 mm sphere for all days of imaging is shown in Figure 13. It is observed that the recovery of the 37 mm sphere is rather constant at 65% ± 35 % up until the 7th day of imaging (spheres: 387.96 kBq/ml, background: 35.97 kBq/ml), then the recovery drops to around 25% ± 29% for PETCT12.

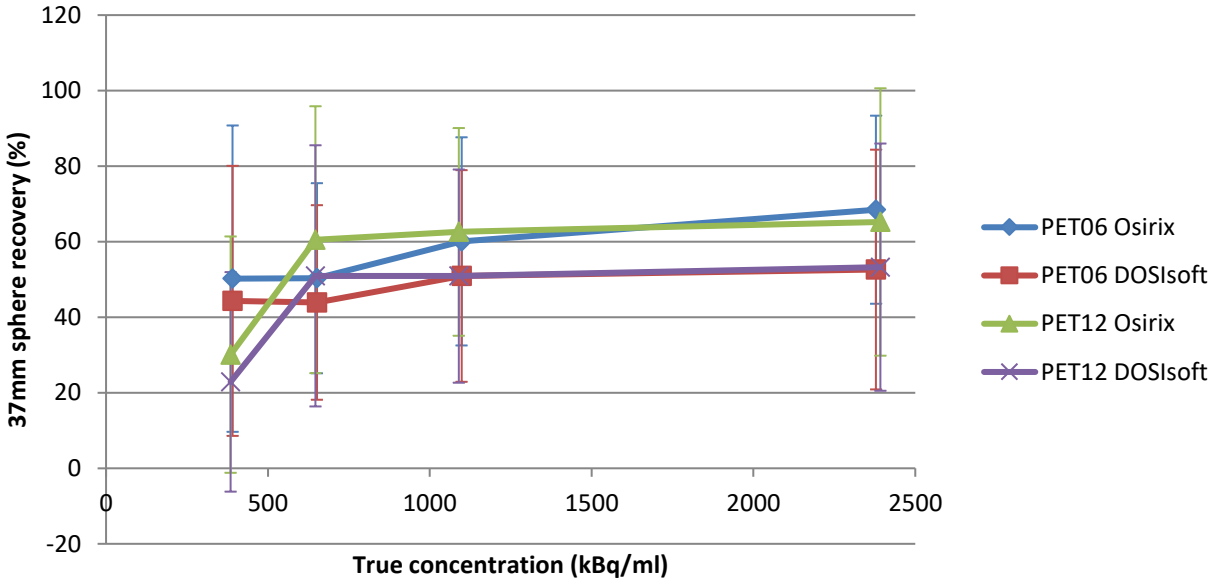

Figure 13. Recovery curve for the largest sphere (37mm) at different concentrations (kBq/ml) for both scanners and analysis programs. (spheres: 2404.19, 1100.17, 653.31 and 387,96 kBq/ml, background: 222.91, 102.01, 60.57, 35.97 kBq/ml)

2.3.6 Cold insert

The activity concentrations detected in the cold insert of the phantom are depicted as a percentage of the true background concentration for different concentrations in Figure 14. Generally, it is observed that the higher the concentration in the background compartment, the higher the concentrations and amount of activity detected in the cold insert (spill-in effect). When a 214 kBq/ml concentration is present in the background compartment an average concentration of 80 kBq/ml is detected in the cold insert, whereas for 60 kBq/ml in the background a concentration of 10 kBq/ml is observed in the cold insert. Again, due to the high noise levels, large variation is seen in the detected counts.

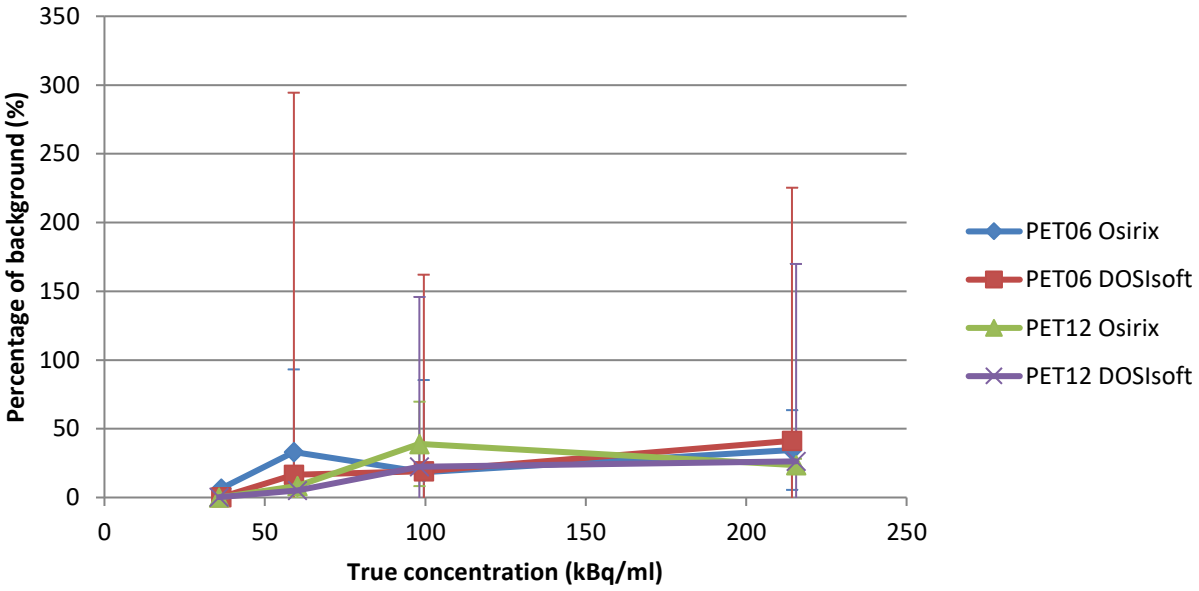

Figure 14. Measured activity concentrations (kBq/ml) in the cold insert as percentage of the true background concentration (kBq/ml) with standard deviation at different concentrations for both scanners and analysis programs.

2.3.7 Background variability

Variability on day 0 of imaging for different diameters, corresponding to the sphere diameters, is shown in Figure 15. The background variability is observed to decrease with increasing region diameter for both scanners. A region diameter of 10mm leads to a BV of 40%, whereas a region diameter of 37 mm leads to a BV of approximately 25% in experiment 2. Higher background variabilities were observed in experiment 1 in which the background was 21×10^{-6} kBq/ml, compared to experiment 2 (background: 222.91 kBq/ml**)**.

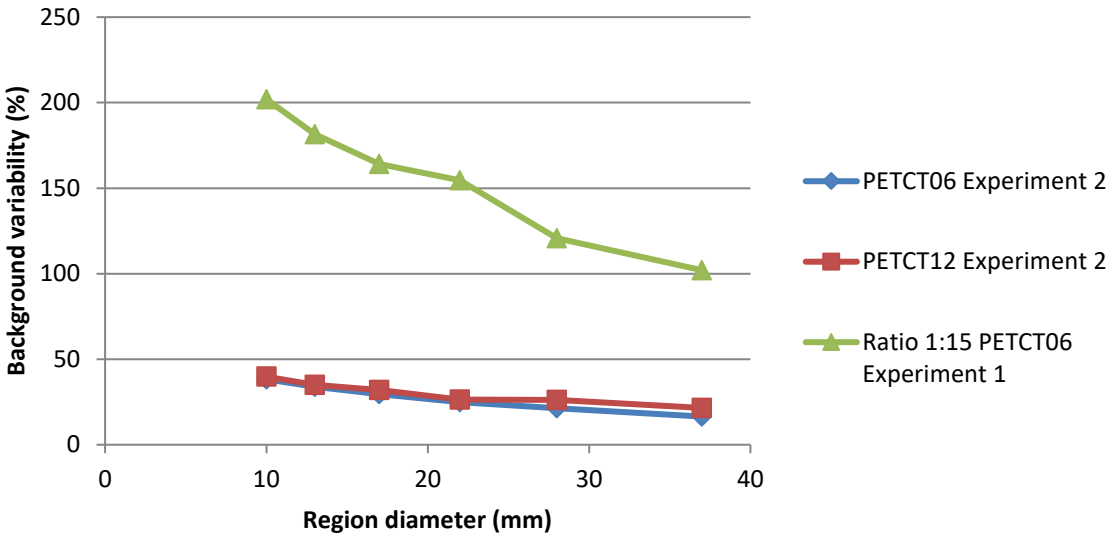

Figure 15. Background variability for different region diameters (mm) for both scanners, measured with means of Osirix on the first day of imaging for experiment 2 together with the results obtained with PETCT06 for ratio 1:15 in experiment 1.

2.4 Discussion

2.4.1 Dose calibrator

It is observed that the dose calibrator shows a higher accuracy for higher activities. The average administered dose for radioembolisation is around 0.5-2.0 GBq, therefore the accuracy of this dose calibrator is sufficient for the clinically used activities of ^{90}Y. Inaccuracies in the measured activities by the dose calibrator could be caused by the fact that the activities were only measured once, measuring all activities multiple times may overcome outliers.

2.4.2 Experiments

It can be concluded that DOSIsoft and Osirix and the two PET/CT scanners show comparable results for ^{90}Y quantification. The large standard deviations found in all experiments are caused by the irregular activity distribution even in a homogenous solution, observed in Figure 5. ^{90}Y-PET scans can contain 'spikes' of activity due to the low positron branching ratio of ^{90}Y. Iterative PET reconstruction protocols are generally optimized for ^{18}F, but the count statistics for ^{90}Y are much lower. In the upper row of Figure 16 it can be seen that at 2-3 iterations the noise levels in the scan are enhanced. Still, the current generation Philips scanners does not allow for any modulation of the standard reconstruction protocol of 3iterations/33subsets. A solution to overcome this problem for clinical visual assessment is the use of Gaussian filtering.

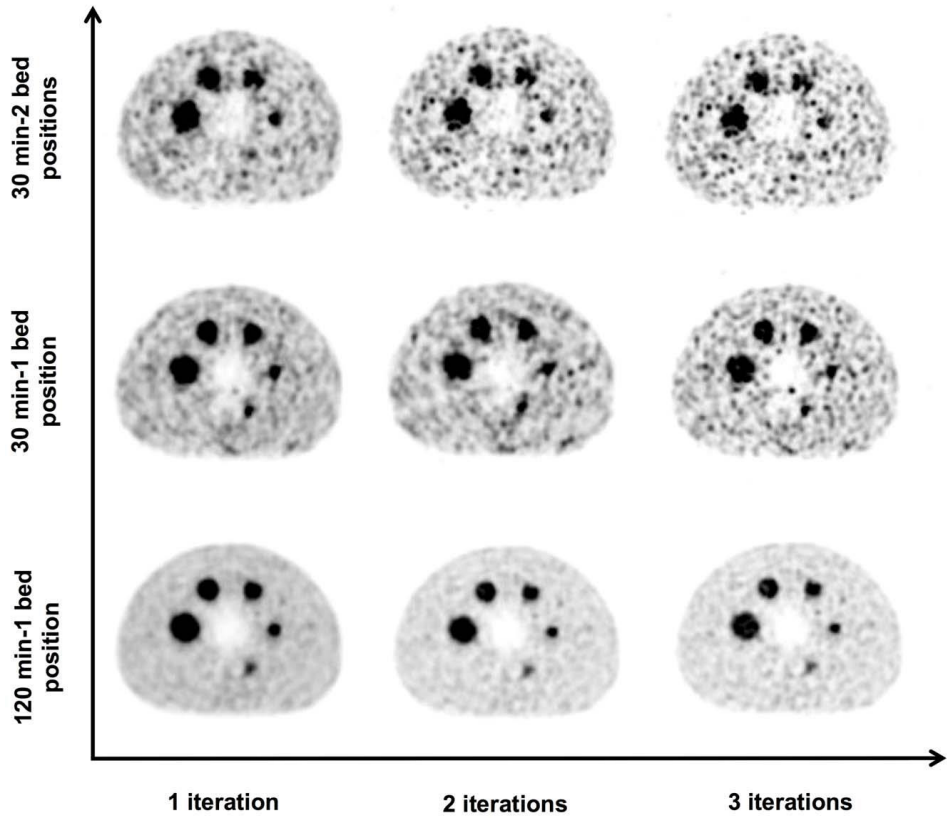

Figure 16. Transverse sections of phantom PET/CT scans reconstructed with 30 min-2 bed positions, 30 and 120 minutes single bed acquisitions and a matrix size of 400 and Gaussian filtering with Full Width Half Maximum (FWHM) of 5mm for 21 subsets and 1-3 iterations of Point Spread Function (PSF) TOF algorithms. [42]

It is seen in Figure 5a that for ratio 1:b_{cold} activity is detected in the three largest spheres by both PET scanners, the activity in the three smaller spheres is thus too low to be detected. Because of this, the recovery curves in Figure 8 are only shown for the three largest spheres. It was observed that even though no activity was detected in the three smallest spheres, activity was detected for the other ratios in these spheres. This indicated the 'spilling in' of activity from the background compartment into the spheres. 'Spilling out' from the background into the cold insert is also observed in Figure 14. It is problematic for the scanners to correctly locate the annihilation events and therefore activity is visualized in wrongful locations, which could lead to wrongful conclusions about delivered lesion dose in the clinical situation.

The recovery curve obtained on the first day of imaging shows an outlier for the 22 mm sphere for PETCT12, which is a known phenomenon for this scanner. For certain activities and concentrations, the scanner erroneously overestimates the activity present in this sphere. It is hypothesized that the BLOB-reconstruction is responsible for this artefact, as BLOB-size is in the order of 2-3 pixels (8-12mm) which corresponds with the dimensions of this sphere. Similar artefacts are also observed for both scanners with ^{18}F, again suggesting that this is not specific to ^{90}Y. Accordingly, the recovery curve on

the third day of imaging shows no erroneous peak for the 22 mm sphere. It is observed in both experiments that the recovery of the 37 mm sphere never exceeds 65% but remains rather constant over multiple days of imaging in the second experiment. Willowson et al. compared the recovery curve of ^{90}Y to the recovery curve of ^{18}F, the differences are shown in Figure 17 [40].

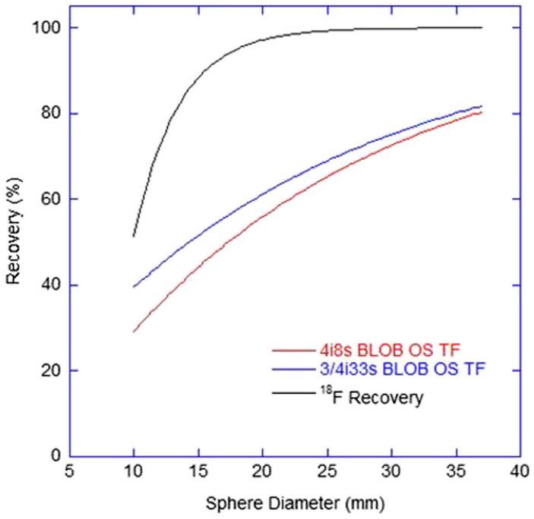

Figure 17. Comparison of ^{18}F (black line) recovery to the recovery of ^{90}Y measured on two types of Philips PET/CT scanners (red and blue line). [40]

The recovery curves of the second experiment indicate that regions up to a diameter of 28 mm (11.49 cm^3) can be used for quantification purposes, for regions with smaller diameters the recovery becomes less than 50% which is unacceptable. Furthermore, it was observed that when more activity was present in the background compartment, higher recovery curves were obtained. Ideally, recovery curves are identical for different ratios, the differences observed may be caused by the 'spilling in' effect explained above. The results of our measurements are comparable to those in the article of Willowson et al. in which measurements were performed with a similar setup and with multiple Philips Gemini TF scanners (BLOB OS TF reconstruction) similar to ours, which ensures that the scanners in our institute are of similar quality as comparable scanners [40].

It is observed that when the background concentration becomes less than 70 kBq/ml, quantification accuracy drops to less than 50%, which is considered unacceptable. Large variabilities are seen in the determined background concentrations. Variability in background concentrations is due to poor signal-to-noise ratio. These results show that the smaller the region to assess, the lower the signal-to-noise ratio will be. Much higher variabilities are observed in the first experiment due to the lower concentrations in which the scanners become less accurate.

Finally, it was observed that when the total amount of activity in the phantom becomes less than 0.7 GBq, quantification accuracy rapidly drops to less than 50%. Activities of 2.0-2.5 GBq are used in whole liver treatment in ^{90}Y radioembolisation, whereas in partial liver treatments activities of 0.6-1.5

GBq are common. The results indicate that accurate quantification of the total injected activity may be problematic in partial liver ^{90}Y radioembolisation. Accurate quantification of specific lesions is nevertheless also dependent on activity concentrations and activity distribution within volumes. An experiment in which the total activity is below 0.7 GBq, whereas lesion activity concentration is over 2000 kBq/ml may better define the scanners capability of quantifying lesions correctly in partial liver treatments.

2.4.3 Future research

^{90}Y-PET quantification is difficult, especially in small lesions (<11.49 cm^3) and for lower concentrations (<70 kBq/ml). The use of higher activities or longer scanning times could improve scan quality. Higher activities will cause more annihilation events and thereby will lead to more signal to be detected, longer scanning times will also lead to more detection of annihilations and thereby a better scan quality. The usage of higher activities is not possible for patient safety reasons. Longer scanning times can be considered but will lengthen the already long ^{90}Y-PET/CT scan (30-45 minutes) for patients. In the near future the department is installing the new digital Vereos PET/CT (Philips), that is roughly twice as sensitive as the Gemini. Therefore, it would be interesting to see how this new scanner handles the low count statistics.
It will be interesting to assess the relationship between the activity concentrations and received dose in treated liver areas. In this research it is intended to provide guidelines about which liver lesions are suitable for quantification and which are not, due to quantification limitations of the PET/CT scanners. Post-treatment dosimetry is becoming more and more popular, but current papers present technical evaluations concerning quantification capabilities of scanners or clinical evaluations examining the dose-response relationship of radioembolisation. It will be interesting to look into the activity and activity concentrations deposited in liver lesions and healthy liver tissue after radioembolisation. Comparing the post-treatment values to the data obtained in these measurements will give more insight into the actual precision of performing post-treatment quantification and the ability to correctly quantify healthy liver activity concentrations and therefore received healthy tissue dose. Lower concentrations are more susceptible to quantification errors and healthy liver is expected to receive lesser amounts of activity than liver lesions.

2.5 Conclusion

^{90}Y-PET quantification is difficult, especially in small lesions and for lower concentrations. The results indicate that only lesions larger than 11.49 cm^3 and receive an activity concentration higher than 70 kBq/ml can be used for quantification. Correct post-treatment dosimetry is dependent on both

activity (concentration) and lesion size. It will be interesting to quantify activity concentrations deposited in liver lesions and healthy liver tissue after radioembolisation to obtain more insight into the precision of performing post-treatment dosimetry clinically.

3. Post-treatment Yttrium-90 PET/CT based dosimetry after radioembolisation with resin microspheres in patients with colorectal liver metastases

Abstract— Radioembolisation is an internal radiation therapy in which ^{90}Y–loaded microspheres are delivered transarterially to hepatic malignancies. Within one day after therapy, ^{90}Y-PET is performed to assess whether the ^{90}Y microspheres have reached the tumor and if any extrahepatic accumulations are visible. In this research, post-treatment dosimetry was performed on ^{90}Y-PET/CT scans in order to determine prognostic factors for treatment response. 13 treatments and 33 lesions were included, patients and individual target lesions were categorized as either having progression or no-progression. Target lesions received an average dose of 61 Gy, 70% of target lesion volume received 47 Gy and the mean whole liver dose was found to be 41 Gy. Progression was observed in 17 of the 33 target lesions and 10 of the 13 patients, indicating underdosing. Only target lesion volume was found to be significantly associated with response to treatment, lesions that showed progression were significantly larger than lesions that did not show progression. Furthermore, it was concluded that time between diagnostic CT and treatment should not be over 30 days to prevent underdosing due to tumor growth and that patients with advanced liver disease do not benefit from ^{90}Y radioembolisation anymore. Post-treatment dosimetry can be improved in the future by developing better segmentation options for target lesions.

***Index Terms*—Colorectal liver metastases, Dosimetry, Radioembolisation, Yttrium-90**

3.1 Introduction

Radioembolisation, also called selective internal radiotherapy (SIRT), is an internal radiation therapy in which ^{90}Y–loaded resin (SIR-spheres) or glass (Theraspheres) microspheres are delivered transarterially to hepatic malignancies. The microspheres are injected selectively into the hepatic artery using a catheter and become trapped in the microvasculature surrounding the liver tumor [4], [6], [7], [31]. Accordingly, high radiation doses are delivered to the tumor, whereas the healthy liver parenchyma remains mostly unaffected. The effectiveness and safety have already been demonstrated in several studies [6], [10]–[13], [32]–[37]. Over the past decades >18.000 patients in >150 centres worldwide have been treated with ^{90}Y radioembolisation, either in palliative setting or in combination with chemotherapy [31]. Within one day after therapy, ^{90}Y-PET is performed to assess whether the ^{90}Y microspheres have reached the tumor and if any extrahepatic accumulations are visible. Ideally, ^{90}Y-PET/CT scans are not only used for visual assessment after radioembolisation but also for post-treatment dosimetry; quantification of the absorbed liver doses (tumor and healthy tissue) [6], [17], [26], [40].

Pre- or post-treatment dosimetry is not routinely performed in radioembolisation but could bring us a step closer in determining the optimal, patient specific therapeutic dose for radioembolisation as it specifies the dose-response relationship in radioembolisation. At this moment, data about the relation between absorbed tumor dose and therapy outcome is very limited for patients with colorectal liver metastases treated with resin microspheres [26]. Van der Hoven et al. concluded that a minimum mean tumor dose of 40-60 Gy is needed for effective treatment, whereas mean absorbed tumor doses between 7 Gy and 174 Gy were observed [24]. Lhommel et al. performed dosimetry on one patient with CRC metastases and found that a tumor with good response received an average dose of 104 Gy, whereas tumors with a poor response received an average dose of 29 Gy [46]. D'Arienzo et al. also performed dosimetry on one patient with CRC metastases and concluded that possibly doses higher than 100 Gy are required to effectively treat liver metastases [47]. It can be concluded that effective tumor doses are uncertain at this moment. This report quantifies the absorbed tumor dose for patients treated with radioembolisation in the NKI-AVL since 2013, using FDA-approved software designed for ^{90}Y dosimetry.

3.2 Methods and materials

Since 2013, 22 patients with CRC liver metastases have been treated with means of radioembolisation with ^{90}Y resin microspheres in the NKI-AVL and have had a ^{90}Y-PET/CT scan afterwards. All patients first underwent a ^{99m}Tc-MAA angiography procedure before ^{90}Y radioembolisation based on which the to be administered activity was determined. Whole liver treatment (n = 10) and partial liver treatment (n = 3) were both applied. Patients were excluded when no follow-up information was present (n = 2). Furthermore, patients were excluded when their lesions showed no pathological FDG uptake at the last follow-up before treatment (n=7). This was chosen because some patients had a recent liver ablation before treatment with ^{90}Y radioembolisation as part of a clinical study, in these patients it cannot be determined if treatment effect is due to the recent ablation or ^{90}Y radioembolisation. ^{90}Y radioembolisation treatments performed after more than a year in one patient were considered to be two separate treatments. Eventually, 13 treatments (12 patients) were included that met all inclusion criteria. Baseline patient characteristics are shown in Table 6.

3.2.1 ^{90}Y-PET/CT imaging

All PET/CT scans were acquired within one day after treatment on one of the two PET/CT scanners at our institute; Philips GEMINI TF TOF 16 (2006) and Philips GENIMI TF Big BORE PET/CT (2012) (Philips Medical Systems, Best, The Netherlands). The data were reconstructed with a time of flight (TOF) blob-based OS algorithm (3 iterations, 33 subsets) and TOF correction at 4x4x4mm voxels. Random and scatter corrections are incorporated into the iterative algorithm. The low-dose CT scan was acquired with a slice thickness of 2mm. All patients were scanned with the clinical protocol for ^{90}Y at our institute; 68-Germanium (^{68}Ge) isotope preset, 2-3 bedpositions, 15 minutes per bedposition. A rescaling factor was needed to correctly quantify absorbed doses in patients, due to the isotope preset difference. The positron fraction of ^{68}Ge is 0.891, whereas that of ^{90}Y is 31.86×10^{-6}. Rescaling in Bq/ml for this difference can be done with means of a correction factor (Equation 5, Chapter 2).

Table 6. Baseline patient characteristics of the 13 included patients.

Clinical variable	**n (%)**
Age, mean (range)	63 (± 8) years
Gender	
Male	11 (84.6%)
Female	2 (15.4%)
Prior local therapies	
Resection	3 (23.1%)
Multiple resections	2 (15.4%)
Ablation	3 (23.1%)
Multiple ablations	3 (23.1%)
Chemotherapy	12 (92.3%)
Multiple chemotherapies	11 (84.6%)
Immunotherapy	5 (38.5%)
Time between last treatment and radioembolisation	
Resection, mean	37.29 weeks
Ablation, mean (range)	34.93 (33 – 37) weeks
Chemotherapy, mean (range)	41.95 (12 – 132) weeks
Immunotherapy, mean (range)	10.21 (1 – 21) weeks
Metastases outside the liver	4 (30.8%)
Tumor burden, mean (range)	22% (3- 90%)

3.2.2 Retrospective post-treatment dosimetry

Post-treatment dosimetry was performed using FDA-approved software designed for ^{90}Y dosimetry by DOSIsoft (DOSIsoft, Cachan, France). The process of performing retrospective post-treatment dosimetry generally consists of three steps; registration, segmentation and dose calculation (Figure 18). First, the diagnostic CT scan made before treatment was registered to the low-dose CT scan made in combination with the ^{90}Y-PET by semi-automatic rigid and elastic registration in DOSIsoft. The whole liver and target lesions were initially segmented based on the diagnostic CT. Unfortunately, the registration of the diagnostic CT to the low-dose CT was less accurate than expected. In only one patient an accurate visual match between the two CT scans was achieved. So, lesion segmentation had to be performed on the low-dose CT alone to avoid the obvious and significant registration inaccuracies (Figure 25 and Figure 26). For each treatment, it was evaluated whether the target lesions showed

progression in the time between the two CT scans. Dosimetry was performed accordingly at voxel level using a kernel convolution algorithm [25], [48]. Several commonly used dosimetry parameters were used to describe the delivered dose to the liver and target lesions; minimal received dose (D_{min}), maximal received dose (D_{max}), mean received dose (D_{mean}), dose received by 98% of the lesion volume (D_{98}), dose received by 95% of the lesion volume (D_{95}), dose received by 70% of the lesion volume (D_{70}), dose received by 2% of the lesion volume (D_2), lesion volume that received more than 50 Gy (V_{50}) and lesion volume that received more than 30 Gy (V_{30}). All before mentioned parameters were determined for a maximum of three target lesions in each patient. Lesions were selected based on their size, from former research it is known that dosimetry is only reliable when performed in lesions larger than 11.49cm^3.

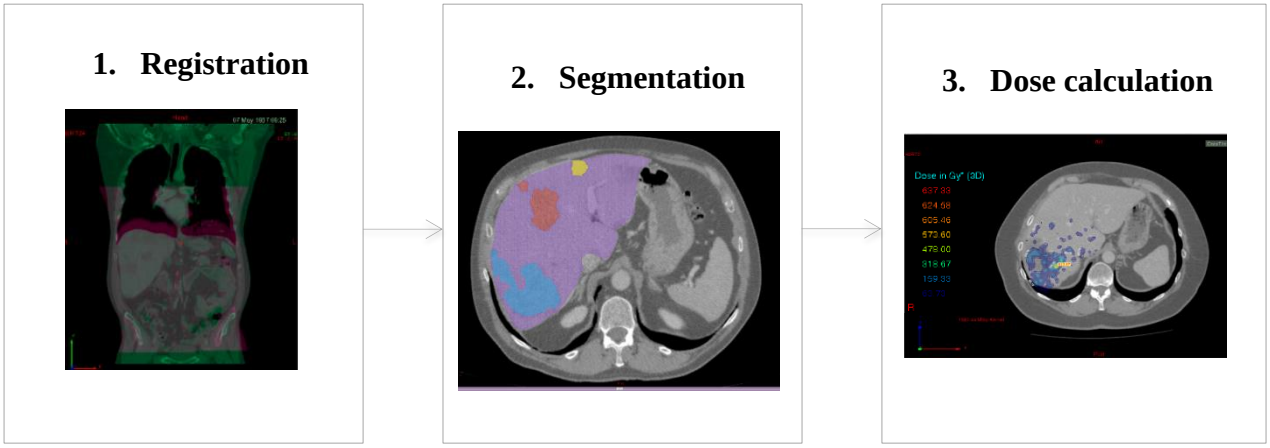

Figure 18. Process of performing retrospective post-treatment dosimetry with means of DOSIsoft.

3.2.3 Therapy response

Treatment response was determined for all treatments and target lesions separately. Not all liver lesions in one liver could be included, therefore lesion response would not always represent whole liver treatment response. Lesion progression was defined as lesion growth determined on CT or the presence pathological FDG-uptake on PET/CT scan, determined by a nuclear physician or radiologist. The development of new liver lesions was considered as progression in evaluating whole liver response. Patients were considered to have no progression when they received other systemic treatment (n=2) or were lost during follow-up before lesion progression was observed (n=1). The date of the start of the new treatment was considered the last day of follow-up for these patients, because it cannot be stated whether progression-free survival is caused by the new treatment or radioembolisation. Furthermore, it

was monitored if patients developed new liver lesions, showed disease progression elsewhere in the body or received any additional liver treatments after radioembolisation. Lesion progression was related to average lesion dose, average liver dose, visual accumulation of microspheres on the post-treatment ^{90}Y-PET/CT and lesion volume.

3.2.4 Statistical evaluation

The evaluations were mainly based on descriptive statistics given the small sample sizes in this study. Continues parameters are presented by mean, standard deviation and ranges; categorical data is presented as a percentage of the total population. Patients and individual target lesions were categorized as either having progression or no-progression (e.g., response and stable disease). Significance of dosimetry outcome parameters and lesion volume for lesion progression was tested with means of independent T-tests when the data was normally distributed and with means of the Mann-Whitney U test otherwise. According to Shapiro-Wilk normality test, $V_{50\text{ and }}D_2$ were normally distributed for both categories. Statistically significant difference was defined as $P < 0.05$.

3.3 Results

The average time between initial diagnosis of liver metastases and radioembolisation was 135 (33 – 451) weeks for the 13 treatments; the time between diagnostic CT and treatment was 57 (21-145) days. Tumor growth was already observed between diagnostic and low-dose CT for one or more lesions in 9 patients. The average administered activity in whole liver treatments (n = 10) was 1.9 GBq, whereas it was 1.3 GBq in partial liver treatments (n = 3). Good visual accumulation was observed in the tumor areas on the post-treatment ^{90}Y-PET/CT in 6 of the 13 treatments, whereas in 7 treatments only partial accumulation was observed. Small extrahepatic depositions in the arteria gastroduodenalis were reported in 2 patients. The time between treatment and follow-up was 5.5 and 13.6 weeks respectively for the first and second follow-up after treatment. Table 7shows the different parameters evaluated regarding therapy outcome. Lesion progression was observed in 10 of the 13 treatments and 17 of the 33 target lesions, 4 patients showed progression at the first follow-up after treatment. 5 patients developed new liver lesions and 9 patients developed lesions elsewhere in the body (lung and lymph tract). 5 patients eventually received other liver therapies (immunotherapy, chemotherapy or radiofrequency ablation (RFA)). Table 8 shows the results of performing post-treatment dosimetry on the 33 target lesions. The different dosimetry parameters calculated separately for the livers and target lesions with and without progression are shown in Table 9, only lesion volume was found to be a significant predictor for lesion response. Figure 21 shows the average liver volume for lesions that did and did not show progression during follow-up. The mean dose received by lesions with a volume over

50cm^3 was 55 ± 18 Gy (13 – 73), whereas lesions smaller than 50 cm^3 received a mean dose of 69 ± 35 Gy (3 – 149). Furthermore, it is seen in Figure 22 that 44% of the lesions that were reported to have good accumulation on the ^{90}Y-PET/CT scan showed progression (Dmean = 70 ± 27 Gy (33 – 149)). Whereas 83% of the lesions that did not have good visual accumulation showed progression (Dmean = 29 ±18 Gy (3 – 51)).

Table 7. Therapy outcome parameters for the 13 treatments (12 patients)

Treatment variable	**n (%)**
General liver progression	10 (76.9%)
Time to liver progression, mean (weeks)	13 (3 – 28)
Target lesion progression	17 (52%)
Time to target lesion progression, mean (weeks)	12.81 (5 – 27)
Development of new liver lesions	5 (38.5%)
Time to new liver lesions, mean (weeks)	28 (3 – 87)
Progression at other sites in the body	9 (69.2%)
Time to progression elsewhere in the body, mean (weeks)	11 (4 – 24)
Have received liver treatment after radioembolisation	5 (38.5%)
Percentage of patients that have died	9 (69.2%)
Time alive after radioembolisation, mean (weeks)	46 (12 – 184)

Table 8. Average dosimetry parameters obtained for 33 target lesions (13 treatments), average whole liver volume and mean whole liver dose.

Parameter	Value ± std. (range)
Lesion volume (cm^3)	108.04 ± 164 (2–742)
Min. dose (Gy)	11.08 ± 13 (0–50)
Max. dose (Gy)	198.30 ± 95 (33-410)
Mean dose (Gy)	62.34 ± 30 (3–149)
D_{98} (Gy)	16.59 ± 16 (0–77)
D_{95} (Gy)	20.90 ± 18 (0–88)
D_{70} (Gy)	43.25 ± 26 (0–120)
D_{2} (Gy)	137.57 ± 56 (16–296)
V_{50} (%)	55.24 ± 26 (0–100)
V_{30} (%)	76.08 ± 25 (0–100)
Whole liver volume (cm^3)	1957.01 ± 675 (1212– 3037)
Mean whole liver dose (Gy)	41.28 ± 10 (23 – 57)

Table 9. Dosimetry parameters and average lesion volume obtained for target lesions with and without progression together with the mean whole liver dose for the livers that did and did not show progression. Average value ± standard deviation (range). The *p* value determined with the Mann-Whitney U test of significance when not normally distributed and with independent T-test of significance (*) when not. Significance is determined as $p < 0.05$.

	Target lesion progression (n = 17)	**No target lesion progression (n = 16)**	**p-value**
Geometric lesion volume (cm^3)	173 ± 201 (2 – 742)	39 ± 65 (4 – 272)	0.005
D_{min} (Gy)	10 ± 15 (0 – 50)	12 ± 11 (0 – 40)	0.146
D_{max} (Gy)	206 ± 87 (33 – 374)	190 ± 105 (74 – 410)	0.09
D_{mean} (Gy)	59 ± 34 (3 – 149)	66 ± 25 (33 – 141)	0.260
D_{98} (Gy)	16 ± 20 (0 – 77)	17 ± 10 (1 – 43)	0.191
D_{95}(Gy)	21 ± 23 (0 – 88)	21 ± 11 (1 – 51)	0.345
D_{70} (Gy)	41 ± 31 (0 – 120)	46 ± 21 (7 – 98)	0.292
D_2 (Gy)	132 ± 54 (16 -248)	143 ± 59 (65 – 296)	0.763*
V_{50} (%)	50 ± 30 (0 – 100)	60 ± 22 (15 – 97)	0.292*
V_{30} (%)	70 ± 30 (0 – 100)	82 ± 15 (42 – 100)	0.402
	Liver progression (n = 10)	**No liver progression (n=3)**	
Mean liver dose (Gy)	40 ± 10 (23 – 51)	47.23 ± 9 (39 – 57)	0.469

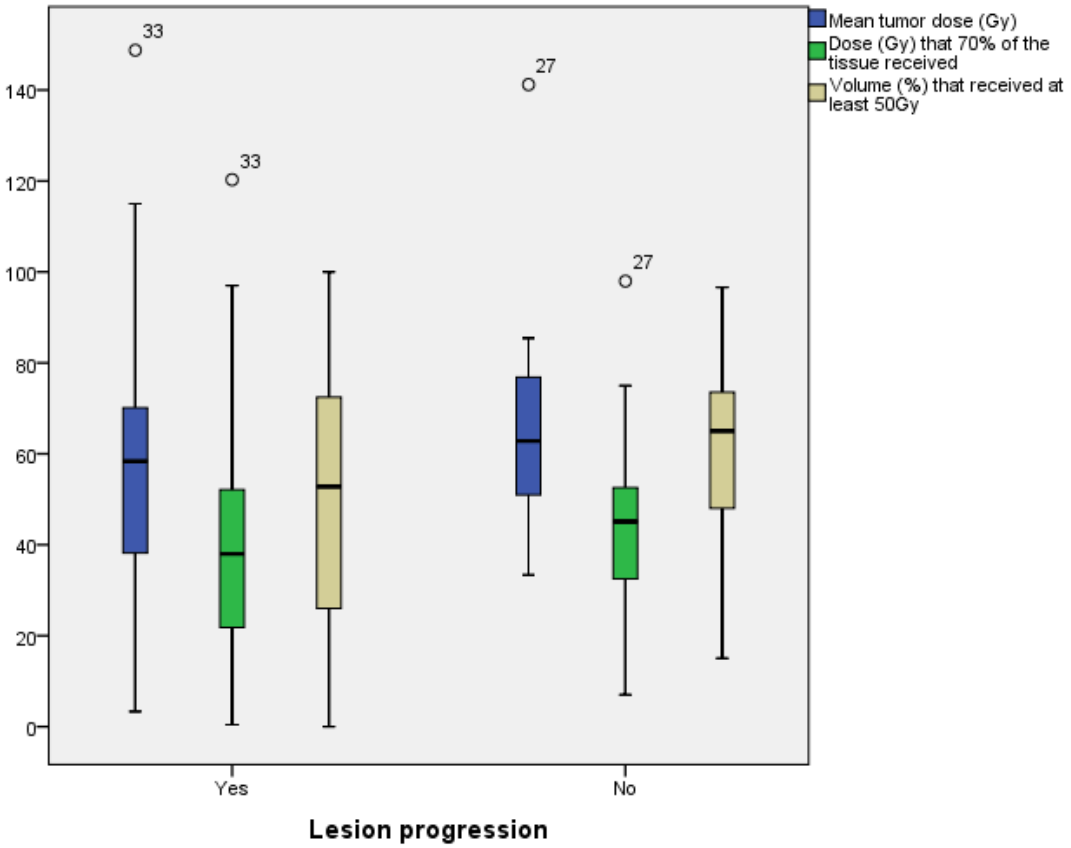

Figure 19. Mean lesion dose (Gy), D_{70} (Gy) and V_{50} (Gy) visualized for target lesions with and without progression. Shaded regions represent the interquartile (IQ) range, the solid line represents the median value. Outliers are visualized by means of circles.

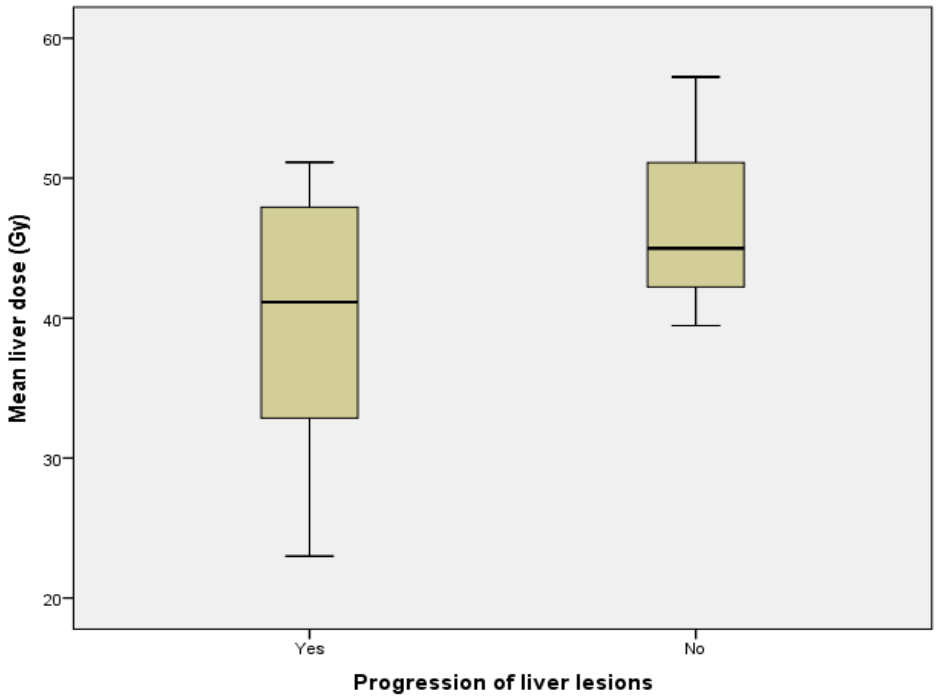

Figure 20. Mean liver dose visualized for the livers that did and did not show progression.

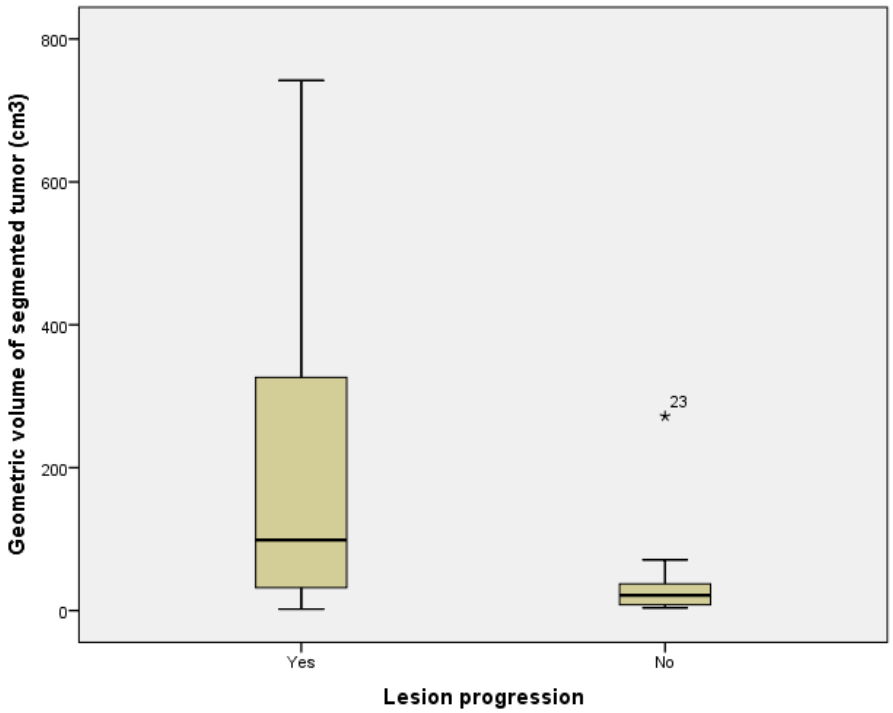

Figure 21. Geometric volume of the liver lesion visualized for the target lesions that did and did not show progression during follow-up. Outliers are visualized by means of asterisks.

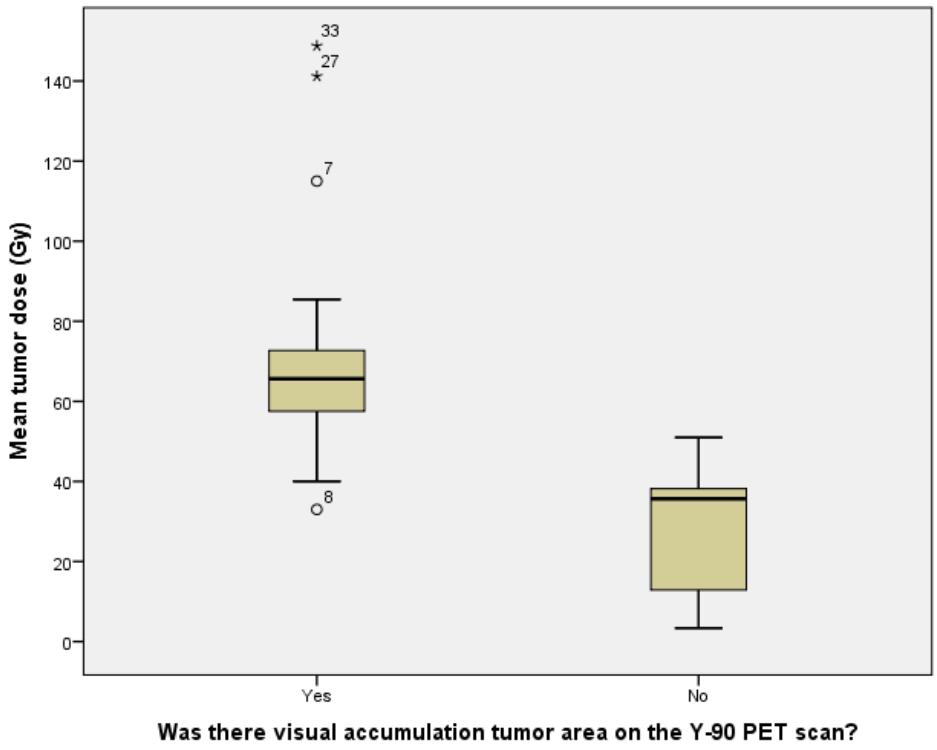

Figure 22. Mean lesion dose visualized for the target lesions that did and did not show visual accumulation in the lesion area on the ^{90}Y-PET scan. Outliers are visualized by means of circles and asterisks.

Figure 23 shows the mean activity injected during radioembolisation compared to the mean activity in the total FoV detected by DOSIsoft. DOSIsoft detected on average 7% (75.18% - 168.15%) higher activities than that were injected during the treatment. Furthermore, it was found that the liver volume segmented based on the low-dose CT was on average 14% higher than the liver volume segmented on the diagnostic CT scan.

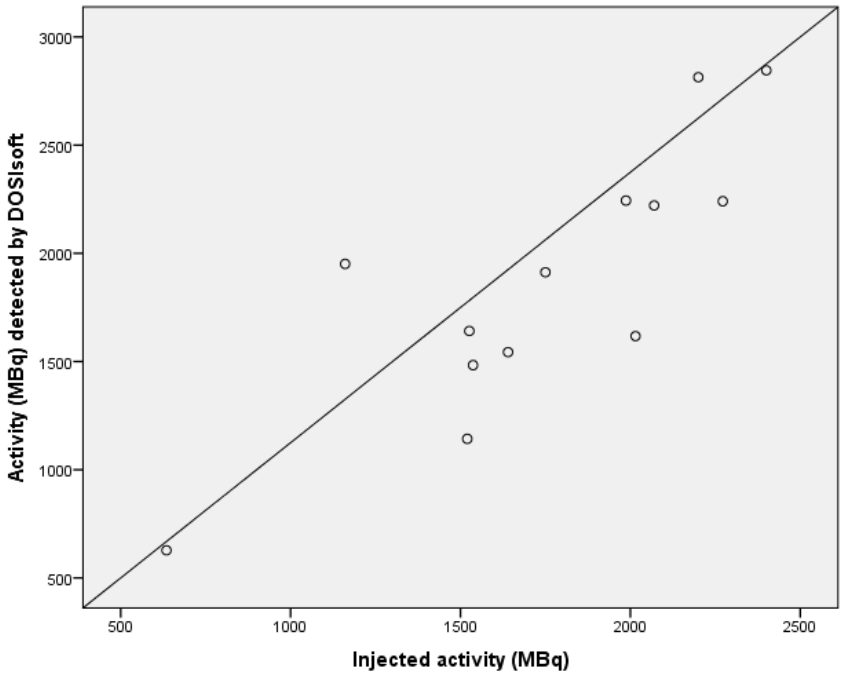

Figure 23. The injected activity of ^{90}Y (MBq) compared to the detected amount of activity in the total FoV by DOSIsoft. The straight line represents the ideal situation that both amount of activities are identical.

In Figure 24, differences in lesion size between the diagnostic CT made before treatment, low-dose CT (^{90}Y-PET/CT) and diagnostic CT at the first follow-up are shown for three liver lesions. All three lesions have grown between the diagnostic CT and treatment of radioembolisation. In 9 of 13 treatments tumor growth was observed between the two timepoints, in one treatment the low-dose CT scan was of too less quality to determine if the tumors had grown. Figure 25 and Figure 26 show the registration difficulties encountered during the segmentation process. A mismatch is observed between the segmented liver on the diagnostic CT when projected onto the registered low-dose CT scan. A larger mismatch between the two CT scans was observed in transversal slices closer to the diaphragm. In Figure 26 it is seen that even though general liver contours match between the two scans, the location of a liver cyst inside the liver differed between the two scans.

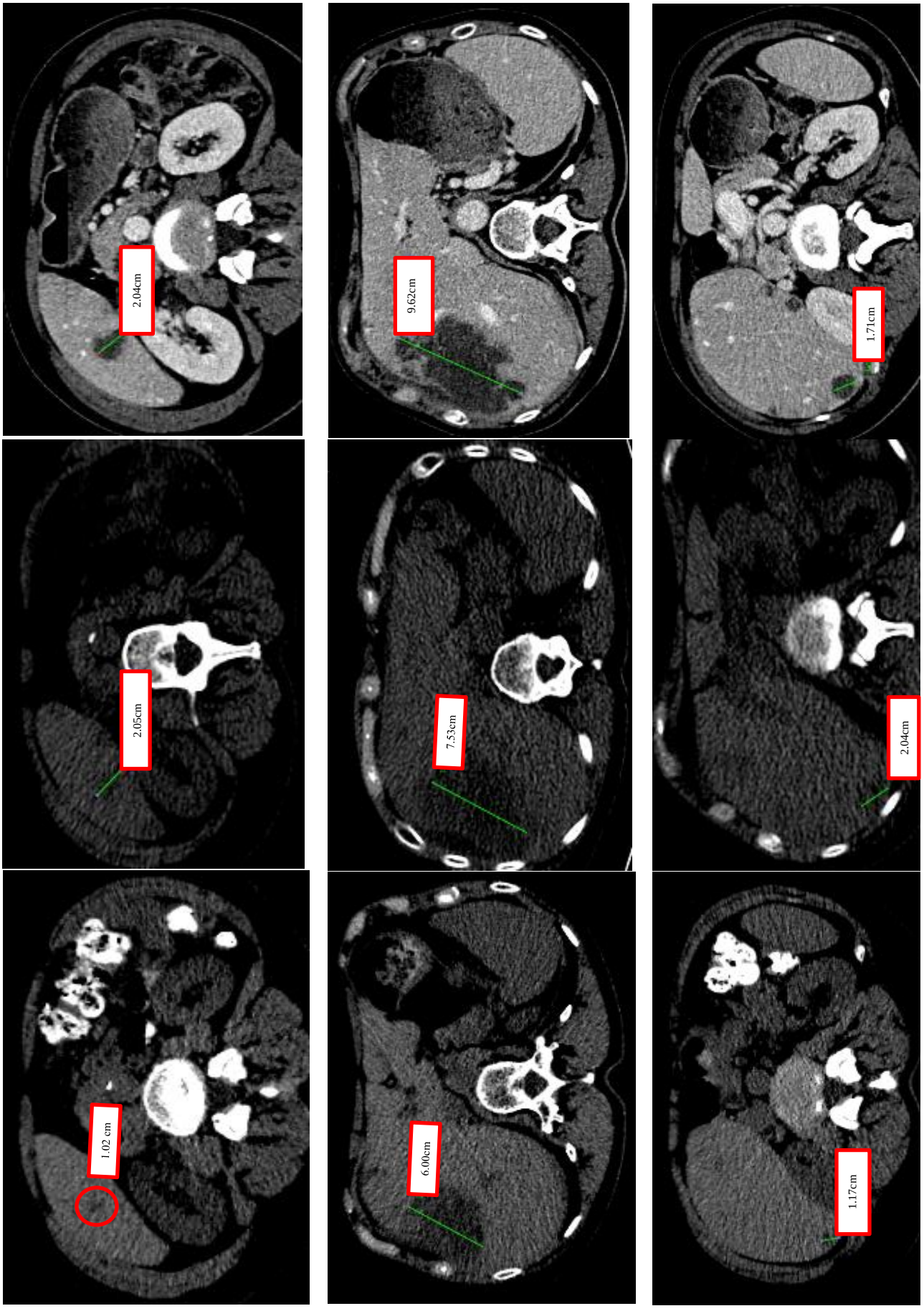

Figure 24. Difference in lesion size for three lesions between the diagnostic CT made before treatment (left), low-dose CT (^{90}Y-PET/CT) (middle)and diagnostic CT at the first follow-up (right)/

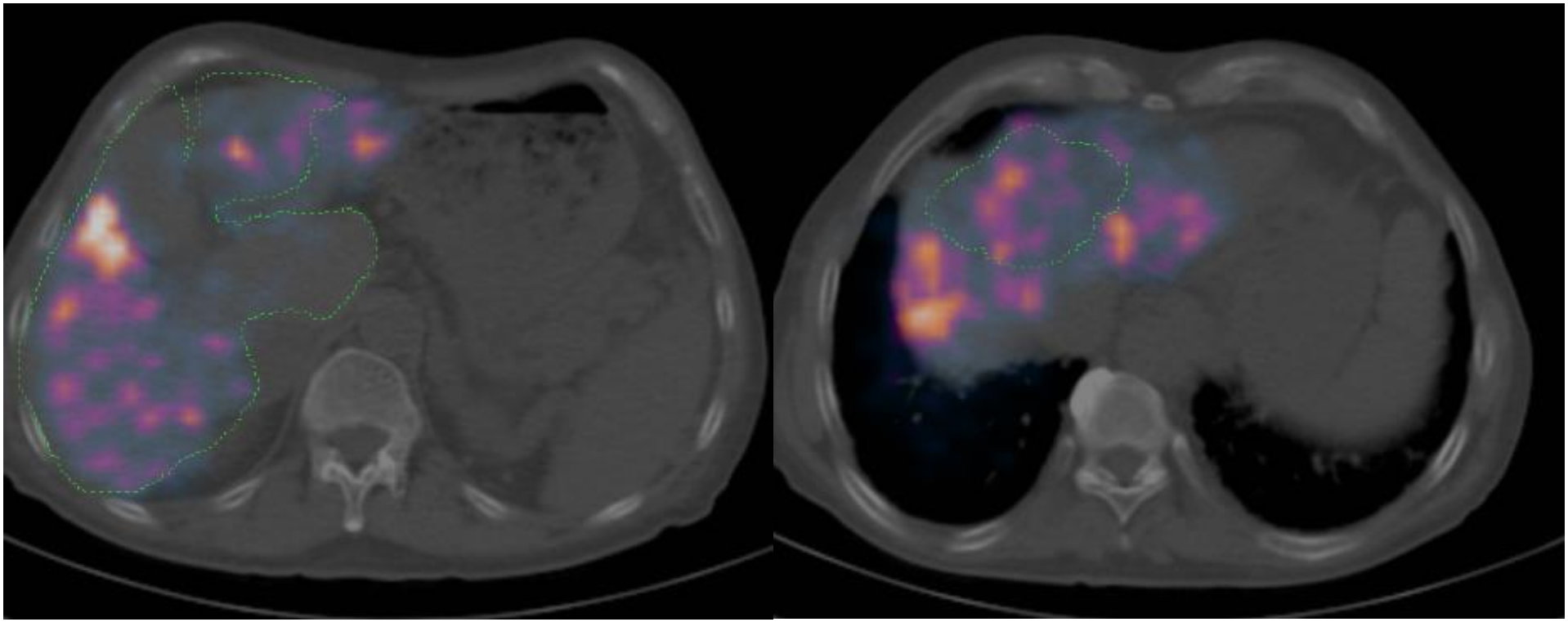

Figure 25. The liver segmented on the diagnostic CT (green lines) projected over the low-dose CT after registration of the two scans for two transversal slices (left and right). Larger differences between the two livers are observed closer to the diaphragm.

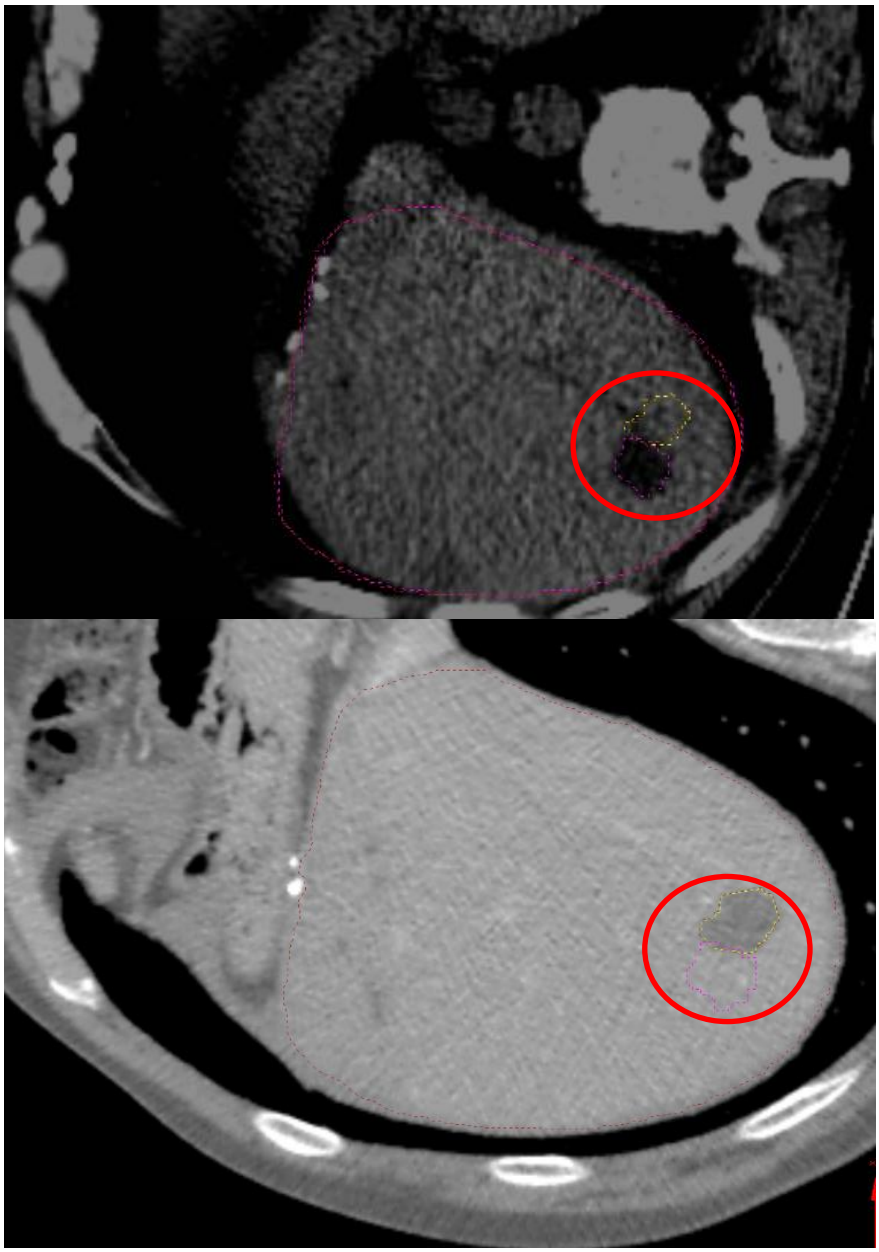

Figure 26. The liver and a cyst segmented on the diagnostic CT (pink and yellow lines) projected over the low-dose CT after registration of the two scans (left), the cyst segmented on the low-dose CT projected over the diagnostic CT is seen on the right side. Even though the liver contours are quite similar after registration, it is observed that the segmented cyst contours do not overlap between the two scans.

3.4 Discussion

3.4.1 Registration and segmentation process

As described in the method section, great difficulties were experienced during the process of registration and segmentation in DOSIsoft which led to the decision to segment the liver and liver lesions based on the low-dose CT instead of the diagnostic CT before performing dosimetry. The use of lower image quality scans has led to several dosimetry inaccuracies. Lesion contours were blurry and therefore harder to segment properly and smaller lesions were not visible at all on the low-dose CT scans. Besides that, it was not possible to exclude necrotic parts of large lesions in the segmentation which is desired in evaluating mean target lesion dose. Dosimetry performed on the whole liver is less influenced by these segmentation inaccuracies, because the liver is better delineated on low-dose CT scans than liver lesions. Though it should be taken into account that a 14% difference was observed between liver volume segmented on the diagnostic CT and the low-dose CT.

Registration of the liver between multiple CT scans is difficult due to its location near the diaphragm and therefore susceptibility for breathing motions. It was also found that for one patient the outer liver structures were matching between the two scans, whereas the location of the cyst within the liver did not match (Figure 26). This phenomenon indicates that also the location of liver tumors can differ while the outer liver structure appears to match between the two scans. Furthermore, registration was troubled due to lesion growth between the two time points. The problems encountered during the registration can be discussed with other institutes also performing ^{90}Y radioembolisation with means of DOSIsoft, also other registration possibilities can be discussed with the manufacturer. Registration is now based on CT scan grayscale values, whereas possibly functional information (lesion location) can be taken into account during the registration process. Making a diagnostic CT in combination with the ^{90}Y-PET scan after radioembolisation would overcome all registration difficulties. Furthermore, it can be concluded that the average time of 57 days between diagnostic CT and treatment is too long because it has led to visible lesion growth in 9 of the 13 patients. The mentioned lesion growth between the two CT scans induces more obstacles than only registration inaccuracies. Lesion size at follow up is compared to lesion size on the diagnostic CT, leading to possible false conclusions about treatment response . Lesion growth could also induce underdosing in radioembolisation because dose calculation is based on lesion size on the diagnostic CT scan. At this moment, a maximum of 30 days between diagnostic CT and

^{99m}Tc-MAA procedure is allowed, which should be changed to a maximum of 30 days between diagnostic CT and radioembolisation procedure.

3.4.2 Retrospective dosimetry

The dosimetry results indicate that although quantification is suboptimal, certain lesions are underdosed during ^{90}Y radioembolisation. The mean lesion dose was found to be 62 Gy (3-149), whereas it is expected that effective lesion doses range from 60 – 100 Gy [24], [46], [47]. Differences in received lesion dose could be caused for example by suboptimal catheter position, central lesion necrosis or tumor heterogeneity. Furthermore, the D_{70} was found to be 43 Gy, implicating that small parts of a lesion receive high doses whereas the majority of a lesion does not receive the assumed minimum required 60-100 Gy. Only lesion volume was found to be significantly predicting for lesion response, proving that especially large lesions are underdosed. Larger lesions could be more difficult to treat effectively because of central necrosis. It should also be taken into account that the patient data dosimetry results are influenced by the scanners capability of quantifying ^{90}Y microspheres. Small lesions are more susceptible to quantification errors due to the partial volume effect; therefore, it is expected that smaller lesions received probably more activity then is shown in the results now. Other articles did find significant relations between dosimetry parameters and therapy outcome [24], [25], which could be caused by larger cohorts or better segmentations procedures.

Progression was observed in 10 of the 13 treatments and 17 of the 33 lesions. It should be taken into account that in some patients without progression, follow-up was no longer than 3-5 months due to death or loss of follow-up. Furthermore, it was observed that 4 of the 13 patients already showed progression at the first follow-up after treatment and died on average within 17 weeks after treatment, indicating that their disease was too extensive for an effective treatment. It is expected that the effects of radioembolisation can be observed in one to two months after treatment, therefore patients should have a life expectation of more than 2 months for a possible effective treatment. Furthermore, it was not possible to obtain a survival analysis from the mortality rate after radioembolisation due to the fact that patients often have had multiple types of previous treatments before radioembolisation, have metastases at other sites in the body or develop metastases elsewhere in the body after radioembolisation (n = 9). It will be interesting to quantify healthy liver tissue dose in the future. It was not possible to

determine healthy liver tissue dose due to the fact that not all lesions could be segmented on the low-dose CT scan. Healthy liver tissue dose will provide knowledge about the damage induced to healthy liver tissue and therefore the capability of healthy liver tissue to receive a possible second treatment of ^{90}Y radioembolisation. Multiple treatments of radioembolisation could be beneficial for larger tumors as most of the ^{90}Y microspheres deposit in the outer layer of tumors [19].

3.5 Conclusion

It can be concluded that post-treatment dosimetry is difficult because of the challenging registration process, caused by breathing motions and tumor growth, between the diagnostic CT made beforehand and the low-dose CT made together with the ^{90}Y-PET after treatment. Making a diagnostic CT together with the ^{90}Y-PET scan after treatment will overcome these registration problems. Furthermore, time between diagnostic CT and the treatment of radioembolisation should be at most 30 days to prevent underdosing caused by tumor growth and to ensure correct assessment of treatment effectiveness. These first results of post-treatment dosimetry indicate that liver lesions are underdosed during treatment, especially larger lesions. Furthermore, it can be concluded that patients with extensive disease do not benefit from ^{90}Y radioembolisation anymore. Post-treatment dosimetry can be improved in the future by developing better segmentation options for target lesions.

4. Future work

4.1 Respiratory gated ^{90}Y-PET/CT scans

Respiratory motions diminish the image quality of ^{90}Y-PET/CT scans. As a result of respiratory motion of the diaphragm, the liver may displace 15 mm on average (maximum of 50mm) during a breathing cycle [49]. Signals that originate from target lesions will therefore be diluted over the trajectory of the liver displacement, leading to loss of contrast, underestimation of tracer uptake and an overestimation of lesion volume [50]. It has already been proven that respiratory motions lead to underestimation of tumor dose and overestimation of normal liver tissue dose in ^{90}Y-PET/CT scans [51]. Respiratory compensated (4D) PET/CT scans, in which PET/CT scans are synchronized with the respiratory cycle of the patient, could be of value to overcome these breathing artefacts.
A data analysis method is already developed at the NKI-AVL to combine scans from different breathing phases to one time-averaged, motion-compensated scan without signal loss. With means of a strain-gauge belt the respiratory cycle of a patient is registered and divided into 10 phases. For each of these 10 breathing phases a PET and low-dose CT reconstruction is made, these 10 different CT and PET reconstructions are deformed to the time-averaged position and combined to one reconstruction, the MidPosition (MidP) scan. The MidP CT and PET scan can then be viewed and used as regular reconstructions (Figure 27). The diagnostic benefit of 4D PET/CT scans has been assessed for lung cancer [52]–[57] and liver lesions [52], [58]–[62]. An example of motion compensated PET/CT scans is given in Figure 28.
Respiratory compensated PET/CT algorithms have not yet been used in ^{90}Y-PET/CT scans, but will likely also lead to the desired higher contrast images and better quantification possibilities especially when lesions are located in close proximity to the diaphragm. Possible drawbacks or risks for patients from this respiratory compensated scan are the longer scanning time (10 minutes) and extra radiation exposure. The respiratory gated ^{90}Y-PET/CT scan will result in an extra 50 mSv radiation exposure for patients. The extra radiation exposure of 50mSv caused by the 4D CT scan does not lead to significant risks in this population with cancer which are already received 2 GBq ^{90}Y (>60 Gy). Appendix F and G contain a report of a brief phantom experiment with a 4D ^{90}Y-PET/CT scan and a METC approval for

performing a feasibility study to assess the clinical value of using 4D ^{90}Y-PET/CT scan in radioembolisation.

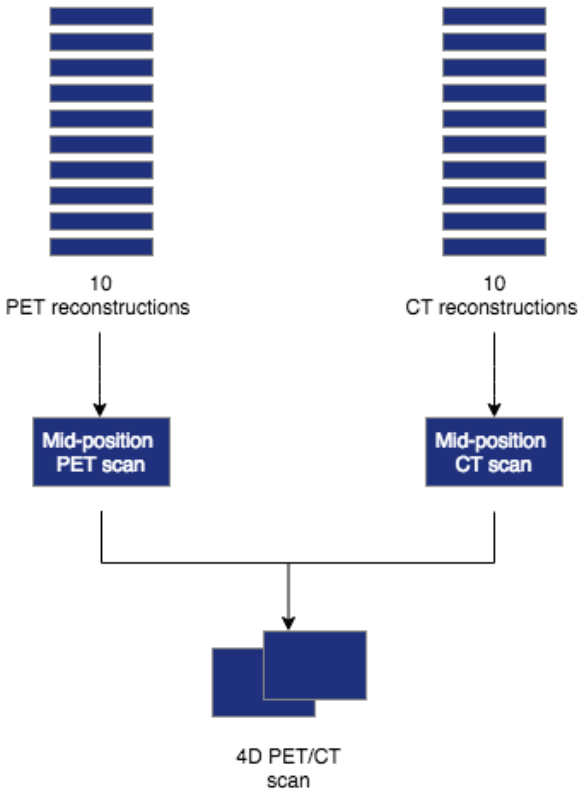

Figure 27. Schematic illustration of the construction of a 4D PET/CT scan.

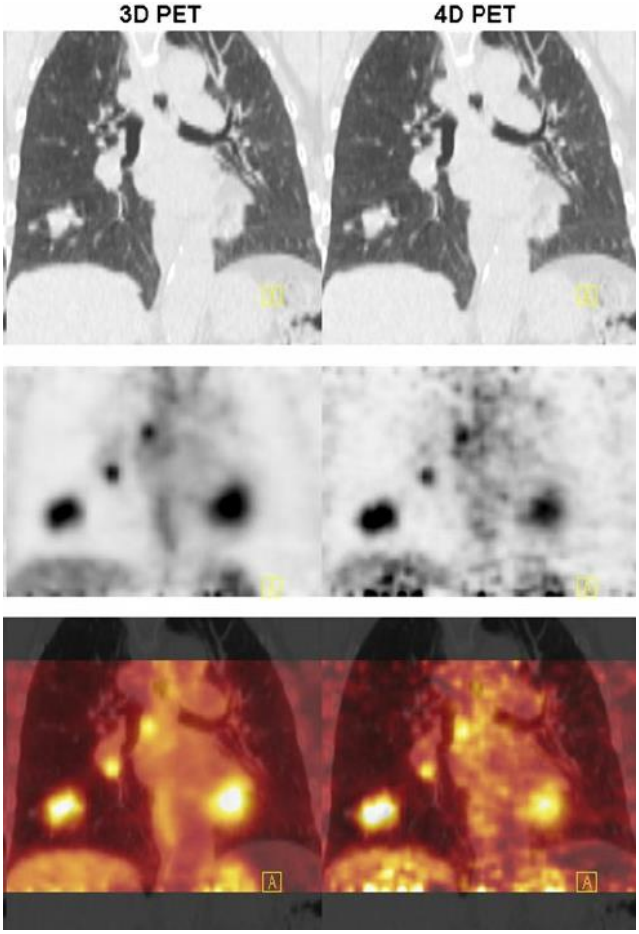

Figure 28. A respiratory compensated (4D) PET/CT acquisition (right) and a regular 3D PET/CT acquisition (left). CT images (top), PET images (middle) and coregistered PET/CT images (bottom), demonstrating the effect of breathing motion on tumor delineation. On the motion-compensated PET/CT it is observed that lesions are easier to identify, mostly due to the higher image contrast [76].

4.2 Labelled ^{90}Y microspheres

The results from the phantom measurements illustrate that the quality of ^{90}Y-PET/CT scans is not optimal for dosimetry purposes. A method to possibly improve post-treatment dosimetry in the future is labelling ^{90}Y microspheres to an isotope that emits large amount of positrons (^{18}F, Gallium-68 (^{68}Ga), Copper-64 (^{64}Cu), Zirconium-89 (^{89}Zr)), because these will 'boost' the positron signal for PET imaging. A microsphere labelled with a positron emitter could produce up to 10^4 more positrons. [19] Detecting and quantifying these surrogate positron emitters is expected to improve the possibility of performing high-quality post-radioembolisation dosimetry. This concept is still far from patient testing, because a safe and stable binding of ^{90}Y microspheres to a high-yield positron emitter needs to be created [19], [63], [64].

4.3 Dosage calculation

The retrospective patient data showed that large lesions are underdosed during radioembolisation, indicating the need for improved dosage calculations or even pre-treatment dosimetry. This thesis has focused on performing post-treatment dosimetry, but in the future thought can also be given to the possibility of performing pre-treatment dosimetry. The results of these first post-treatment dosimetry results may be useful in the first steps towards pre-treatment dosimetry. In the introduction of this thesis it was briefly explained that dosage calculation is performed with means of the BSA-method in our institute. The BSA method can be quantitatively evaluated by calculating the dosage that should have been used in treatment based on post-treatment dosimetry results. Furthermore, retrospective pre-treatment dosimetry performed on 99mTc-MAA scans of these patients will give insight into the possibilities of using 99mTc-MAA scans for pre-treatment dosimetry, by comparing those calculations to the post-treatment dosimetry results already obtained.

5. General discussion

This study is about improving post-treatment dosimetry for ^{90}Y radioembolisation in liver metastases. The calibration experiments from chapter 2 showed that only lesions larger than 11.49 cm^3 and receive an activity concentration higher than 70 kBq/ml can be used for quantification. The target lesions analyzed in the retrospective patient data analysis showed that the 33 included lesions received an average activity concentration of 1166 kBq/ml, indicating that the activity concentrations in liver lesions can therefore be quantified in future post-treatment dosimetry. One lesion received less than 70 kBq/ml and should therefore be excluded in further research.

Furthermore, the total activity recovered in the FoV by DOSIsoft was compared to the injected activity during treatment in the retrospective patient data analysis. An average overestimation of 7% (75.18% - 168.15%) was observed between the activity administered during radioembolisation and the activity detected by DOSIsoft, large variations were seen in these results. Overestimation was even seen in partial liver treatments (<1 GBq), this overestimation by DOSIsoft is striking because of two reasons. Firstly, the administered activity during treatment does not reach the liver completely, it is expected that the activity partly remains in the needles and catheters used. Secondly, the results from the phantom measurements indicate that in high activities (>1.5 GBq) no more than 80%-90% of the total activity in the phantom could be recovered whereas in low activities (<0.7 GBq) no more than 50% could be quantified. These results indicate that DOSIsoft uses a correction for patient data which leads to higher values in patient data than in phantom data. The influence of this overestimation on dosimetry outcome parameters in patient data can be topic of future research. These outcomes have been briefly discussed with the manufacturer, but no explanation has been found yet.

5.1 Summary of recommendations

- Lesions smaller than 11.49 cm^3 and/or lesions that receive less than 70 kBq/ml cannot be quantified correctly and therefore cannot be used for dosimetric purposes.
- There should be a maximum of 30 days between diagnostic CT scan and radioembolisation treatment.

- Performing a diagnostic CT together with the post-treatment ^{90}Y PET scan will overcome registration inaccuracies and thereby improve dosimetry accuracy.
- A stricter patient selection is recommended as results showed that patients with extensive liver disease do not benefit from treatment anymore.

References

[1] A. M. D. Wolf *et al.*, “Colorectal cancer screening for average-risk adults: 2018 guideline update from the American Cancer Society,” *CA. Cancer J. Clin.*, vol. 68, no. 4, pp. 250–281, Jul. 2018.

[2] KNL, “Cancer numbers.” [Online]. Available: http://www.cijfersoverkanker.nl/. [Accessed: 26-Oct-2017].

[3] M. Peeters, “CRC Liver Metastases,” in *Locoregional Tumor Therapy*, Berlin, Heidelberg: Springer Berlin Heidelberg, 2015, pp. 55–72.

[4] M. A. D. Vente *et al.*, “Yttrium-90 microsphere radioembolization for the treatment of liver malignancies: a structured meta-analysis,” *Eur. Radiol.*, vol. 19, no. 4, pp. 951–959, Apr. 2009.

[5] N. H. Nicolay, D. P. Berry, and R. A. Sharma, “Liver metastases from colorectal cancer: radioembolization with systemic therapy,” *Nat. Rev. Clin. Oncol.*, vol. 6, no. 12, pp. 687–697, Dec. 2009.

[6] B. J. de Wit-van der Veen, D. M. V. Huizing, M. L. Donswijk, MD, M. Meier, MD, and M. P. M. Stokkel, MD, “Radioembolisation with yttrium-90 in colorectal liver metastases: current status in the Netherlands,” *J. Nucl. Med.*, vol. 38, no. 4, pp. 1613–1621, 2016.

[7] A. S. Kennedy *et al.*, “Multicenter evaluation of the safety and efficacy of radioembolization in patients with unresectable colorectal liver metastases selected as candidates for ^{90}Y resin microspheres.,” *J. Gastrointest. Oncol.*, vol. 6, no. 2, pp. 134–42, Apr. 2015.

[8] M. Cremonesi *et al.*, “Radioembolization of hepatic lesions from a radiobiology and dosimetric perspective.,” *Front. Oncol.*, vol. 4, p. 210, 2014.

[9] H. R. Bierman, R. L. Byron, K. H. Kelley, and A. Grady, “Studies on the Blood Supply of Tumors in Man. III. Vascular Patterns of the Liver by Hepatic Arteriography,” *JNCI J. Natl. Cancer Inst.*, vol. 12, no. 1, pp. 107–131, Aug. 1951.

[10] R. Murthy *et al.*, “Yttrium-90 Microsphere Therapy for Hepatic Malignancy: Devices, Indications, Technical Considerations, and Potential Complications,” *RadioGraphics*, vol. 25, no. suppl_1, pp. S41–S55, Oct. 2005.

[11] M. F. Mulcahy *et al.*, “Radioembolization of colorectal hepatic metastases using yttrium-90 microspheres,” *Cancer*, vol. 115, no. 9, pp. 1849–1858, May 2009.

[12] L. Bester *et al.*, “Radioembolization versus standard care of hepatic metastases: comparative retrospective cohort study of survival outcomes and adverse events in salvage patients.,” *J. Vasc. Interv. Radiol.*, vol. 23, no. 1, pp. 96–105, Jan. 2012.

[13] A. Hendlisz *et al.*, “Phase III trial comparing protracted intravenous fluorouracil infusion alone or with yttrium-90 resin microspheres radioembolization for liver-

limited metastatic colorectal cancer refractory to standard chemotherapy.," *J. Clin. Oncol.*, vol. 28, no. 23, pp. 3687–94, Aug. 2010.

[14] R. Seidensticker *et al.*, "Matched-Pair Comparison of Radioembolization Plus Best Supportive Care Versus Best Supportive Care Alone for Chemotherapy Refractory Liver-Dominant Colorectal Metastases," *Cardiovasc. Intervent. Radiol.*, vol. 35, no. 5, pp. 1066–1073, Oct. 2012.

[15] R. S. Stubbs and S. K. Wickremesekera, "Selective internal radiation therapy (SIRT): a new modality for treating patients with colorectal liver metastases.," *HPB (Oxford).*, vol. 6, no. 3, pp. 133–9, 2004.

[16] B. Sangro *et al.*, "Survival after yttrium-90 resin microsphere radioembolization of hepatocellular carcinoma across Barcelona clinic liver cancer stages: A European evaluation," *Hepatology*, vol. 54, no. 3, pp. 868–878, Sep. 2011.

[17] Y.-H. Kao *et al.*, "Post-radioembolization yttrium-90 PET/CT - part 2: dose-response and tumor predictive dosimetry for resin microspheres.," *EJNMMI Res.*, vol. 3, no. 1, p. 57, Jul. 2013.

[18] A. Dhabuwala, P. Lamerton, and R. S. Stubbs, "Relationship of 99mtechnetium labelled macroaggregated albumin (99mTc-MAA) uptake by colorectal liver metastases to response following Selective Internal Radiation Therapy (SIRT)," *BMC Nucl. Med.*, vol. 5, no. 1, p. 7, Dec. 2005.

[19] G. Chambers, "Development of a Positron-Emitting Surrogate Microsphere for Image-Based Dosimetry in Yttrium-90 Radioembolization Therapy," *Nucl. Eng. ETDs*, Apr. 2018.

[20] A. K. T. Tong, Y. H. Kao, C. W. Too, K. F. W. Chin, D. C. E. Ng, and P. K. H. Chow, "Yttrium-90 hepatic radioembolization: clinical review and current techniques in interventional radiology and personalized dosimetry.," *Br. J. Radiol.*, vol. 89, no. 1062, p. 20150943, Jun. 2016.

[21] F. Giammarile *et al.*, "EANM procedure guideline for the treatment of liver cancer and liver metastases with intra-arterial radioactive compounds," *Eur. J. Nucl. Med. Mol. Imaging*, vol. 38, no. 7, pp. 1393–1406, Jul. 2011.

[22] W. A. Dezarn *et al.*, "Recommendations of the American Association of Physicists in Medicine on dosimetry, imaging, and quality assurance procedures for ^{90}Y microsphere brachytherapy in the treatment of hepatic malignancies," *Med. Phys.*, vol. 38, no. 8, pp. 4824–4845, Aug. 2011.

[23] A. F. van den Hoven *et al.*, "Insights into the Dose-Response Relationship of Radioembolization with Resin 90Y-Microspheres: A Prospective Cohort Study in Patients with Colorectal Cancer Liver Metastases.," *J. Nucl. Med.*, vol. 57, no. 7, pp. 1014–9, Jul. 2016.

[24] A. F. van den Hoven *et al.*, "Insights into the Dose-Response Relationship of Radioembolization with Resin 90Y-Microspheres: A Prospective Cohort Study in Patients with Colorectal Cancer Liver Metastases.," *J. Nucl. Med.*, vol. 57, no. 7, pp. 1014–9, Jul. 2016.

[25] K. P. Willowson *et al.*, “Clinical and imaging-based prognostic factors in radioembolisation of liver metastases from colorectal cancer: a retrospective exploratory analysis,” *EJNMMI Res.*, vol. 7, no. 1, p. 46, Dec. 2017.

[26] M. L. J. Smits *et al.*, “Radioembolization Dosimetry: The Road Ahead,” *Cardiovasc. Intervent. Radiol.*, vol. 38, no. 2, pp. 261–269, Apr. 2015.

[27] K. W. Ford, “Predicted 0+ Level in (90)Zr 40,” *Phys. Rev.*, vol. 98, no. 5, pp. 1516–1517, Jun. 1955.

[28] A. S. Pasciak, A. C. Bourgeois, and Y. C. Bradley, “A Comparison of Techniques for 90Y PET/CT Image-Based Dosimetry Following Radioembolization with Resin Microspheres,” *Front. Oncol.*, vol. 4, p. 121, May 2014.

[29] Y.-H. Kao *et al.*, “Post-radioembolization yttrium-90 PET/CT - part 1: diagnostic reporting.,” *EJNMMI Res.*, vol. 3, no. 1, p. 56, Jul. 2013.

[30] M. D’Arienzo *et al.*, “Phantom validation of quantitative Y-90 PET/CT-based dosimetry in liver radioembolization,” *EJNMMI Res.*, vol. 7, no. 1, p. 94, Dec. 2017.

[31] N. H. Nicolay, D. P. Berry, and R. A. Sharma, “Liver metastases from colorectal cancer: radioembolization with systemic therapy,” *Nat. Rev. Clin. Oncol.*, vol. 6, no. 12, pp. 687–697, Dec. 2009.

[32] A. S. Kennedy *et al.*, “Resin 90Y-microsphere brachytherapy for unresectable colorectal liver metastases: Modern USA experience,” *Int. J. Radiat. Oncol. Biol. Phys.*, vol. 65, no. 2, pp. 412–425, Jun. 2006.

[33] L. Lim *et al.*, “Prospective study of treatment with selective internal radiation therapy spheres in patients with unresectable primary or secondary hepatic malignancies,” *Intern. Med. J.*, vol. 35, no. 4, pp. 222–227, Apr. 2005.

[34] S. A. Gulec, G. Mesoloras, W. A. Dezarn, P. McNeillie, and A. S. Kennedy, “Safety and efficacy of Y-90 microsphere treatment in patients with primary and metastatic liver cancer: the tumor selectivity of the treatment as a function of tumor to liver flow ratio.,” *J. Transl. Med.*, vol. 5, p. 15, Mar. 2007.

[35] M. Cosimelli *et al.*, “Multi-centre phase II clinical trial of yttrium-90 resin microspheres alone in unresectable, chemotherapy refractory colorectal liver metastases.,” *Br. J. Cancer*, vol. 103, no. 3, pp. 324–31, Jul. 2010.

[36] K. A. Evans, M. G. Richardson, N. Pavlakis, D. L. Morris, W. Liauw, and L. Bester, “Survival Outcomes of a Salvage Patient Population after Radioembolization of Hepatic Metastases with Yttrium-90 Microspheres,” *J. Vasc. Interv. Radiol.*, vol. 21, no. 10, pp. 1521–1526, Oct. 2010.

[37] T. F. Jakobs *et al.*, “Hepatic Yttrium-90 Radioembolization of Chemotherapy-refractory Colorectal Cancer Liver Metastases,” *J. Vasc. Interv. Radiol.*, vol. 19, no. 8, pp. 1187–1195, Aug. 2008.

[38] L. van Elmbt, S. Vandenberghe, S. Walrand, S. Pauwels, and F. Jamar, “Comparison of yttrium-90 quantitative imaging by TOF and non-TOF PET in a phantom of liver selective internal radiotherapy,” *Phys. Med. Biol.*, vol. 56, no. 21, pp. 6759–6777, Nov.

2011.

[39] S. Surti, A. Kuhn, M. E. Werner, A. E. Perkins, J. Kolthammer, and J. S. Karp, "Performance of Philips Gemini TF PET/CT scanner with special consideration for its time-of-flight imaging capabilities.," *J. Nucl. Med.*, vol. 48, no. 3, pp. 471–80, Mar. 2007.

[40] K. P. Willowson, M. Tapner, D. L. Bailey, and D. L. Bailey, "A multicentre comparison of quantitative 90Y PET/CT for dosimetric purposes after radioembolization with resin microspheres," *Eur. J. Nucl. Med. Mol. Imaging*, vol. 42, no. 8, pp. 1202–1222, Jul. 2015.

[41] N. Maughan *et al.*, "Multi-institutional phantom study of yttrium-90 PET-based dosimetry of hepatic radioembolization using PET/MRI: The MR-QUEST Study," *J. Nucl. Med.*, vol. 58, no. supplement 1, pp. 155–155, May 2017.

[42] A. A. Attarwala *et al.*, "Quantitative and Qualitative Assessment of Yttrium-90 PET/CT Imaging," *PLoS One*, vol. 9, no. 11, p. e110401, Nov. 2014.

[43] M. K. Werner, K. Brechtel, T. Beyer, H. Dittmann, C. Pfannenberg, and J. Kupferschläger, "PET/CT for the assessment and quantification of 90Y biodistribution after selective internal radiotherapy (SIRT) of liver metastases," *Eur. J. Nucl. Med. Mol. Imaging*, vol. 37, no. 2, pp. 407–408, Feb. 2010.

[44] National Electrical Manufacturers Association, "NEMA Standards Publication NU 2-2007," Rosslyn, VA.

[45] K. P. Willowson, M. Tapner, D. L. Bailey, and D. L. Bailey, "A multicentre comparison of quantitative ^{90}PET/CT for dosimetric purposes after radioembolization with resin microspheres," *Eur. J. Nucl. Med. Mol. Imaging*, vol. 42, no. 8, pp. 1202–1222, Jul. 2015.

[46] R. Lhommel *et al.*, "Feasibility of 90Y TOF PET-based dosimetry in liver metastasis therapy using SIR-Spheres," *Eur. J. Nucl. Med. Mol. Imaging*, vol. 37, no. 9, pp. 1654–1662, Aug. 2010.

[47] M. D'Arienzo *et al.*, "Absorbed dose to lesion and clinical outcome after liver radioembolization with 90Y microspheres: a case report of PET-based dosimetry," *Ann. Nucl. Med.*, vol. 27, no. 7, pp. 676–680, Aug. 2013.

[48] M. Kafrouni *et al.*, "Retrospective voxel-based dosimetry for assessing the body surface area model ability to predict delivered dose and radioembolization outcome," *J. Nucl. Med.*, p. jnumed.117.202937, Mar. 2018.

[49] M. F. Kruis and Ipskamp), *Motion compensation for 4D PET/CT*. [s.n.], 2014.

[50] V. Bettinardi, M. Picchio, N. Di Muzio, L. Gianolli, M. C. Gilardi, and C. Messa, "Detection and compensation of organ/lesion motion using 4D-PET/CT respiratory gated acquisition techniques," *Radiother. Oncol.*, vol. 96, no. 3, pp. 311–316, Sep. 2010.

[51] L. Ausland, M.-E. Revheim, A. Skretting, and C. Stokke, "Respiratory motion during ^{90} Yttrium PET contributes to underestimation of tumor dose and overestimation of

normal liver tissue dose," *Acta radiol.*, p. 28418511771005, May 2017.

[52] C. Crivellaro *et al.*, "Added diagnostic value of respiratory-gated 4D 18F–FDG PET/CT in the detection of liver lesions: a multicenter study," *Eur. J. Nucl. Med. Mol. Imaging*, pp. 1–8, Aug. 2017.

[53] Y. E. Erdi *et al.*, "The CT motion quantitation of lung lesions and its impact on PET-measured SUVs.," *J. Nucl. Med.*, vol. 45, no. 8, pp. 1287–92, Aug. 2004.

[54] M. K. Werner, J. A. Parker, G. M. Kolodny, J. R. English, and M. R. Palmer, "Respiratory gating enhances imaging of pulmonary nodules and measurement of tracer uptake in FDG PET/CT," *Am. J. Roentgenol.*, vol. 193, no. 6, pp. 1640–1645, Dec. 2009.

[55] L. Guerra *et al.*, "Respiratory gated PET/CT in a European multicentre retrospective study: added diagnostic value in detection and characterization of lung lesions," *Eur. J. Nucl. Med. Mol. Imaging*, vol. 39, no. 9, pp. 1381–1390, Sep. 2012.

[56] A. Lupi, M. Zaroccolo, M. Salgarello, V. Malfatti, and P. Zanco, "The effect of 18F-FDG-PET/CT respiratory gating on detected metabolic activity in lung lesions," *Ann. Nucl. Med.*, vol. 23, no. 2, pp. 191–196, Feb. 2009.

[57] A. M. García Vicente *et al.*, "18F-FDG PET-CT respiratory gating in characterization of pulmonary lesions: Approximation towards clinical indications," *Ann. Nucl. Med.*, vol. 24, no. 3, pp. 207–214, Apr. 2010.

[58] L. Fin *et al.*, "Improved imaging of intrahepatic colorectal metastases with 18 F-fluorodeoxyglucose respiratory-gated positron emission tomography," *Nucl Med Commun Wolters Kluwer Heal. Nucl. Med. Commun.*, vol. 33, no. 33, 2012.

[59] M.-E. Revheim, S.-P. Haugvik, K. Johnsrud, Ø. Mathisen, J. G. Fjeld, and A. Skretting, "Respiratory gated and prolonged acquisition 18F-FDG PET improve preoperative assessment of colorectal liver metastases," *Acta radiol.*, vol. 56, no. 4, pp. 397–403, Apr. 2015.

[60] Y. Suenaga *et al.*, "Respiratory-gated 18F-FDG PET/CT for the diagnosis of liver metastasis," *Eur. J. Radiol.*, vol. 82, no. 10, pp. 1696–1701, Oct. 2013.

[61] A. Schulz *et al.*, "Respiratory gated PET/CT of the liver: A novel method and its impact on the detection of colorectal liver metastases," *Eur. J. Radiol.*, vol. 84, no. 8, pp. 1424–1431, Aug. 2015.

[62] V. Bettinardi, M. Picchio, N. Di Muzio, L. Gianolli, M. C. Gilardi, and C. Messa, "Detection and compensation of organ/lesion motion using 4D-PET/CT respiratory gated acquisition techniques," *Radiother. Oncol.*, vol. 96, no. 3, pp. 311–316, Sep. 2010.

[63] M. A. Avila-Rodriguez *et al.*, "Positron-emitting resin microspheres as surrogates of 90Y SIR-Spheres: a radiolabeling and stability study," *Nucl. Med. Biol.*, vol. 34, no. 5, pp. 585–590, Jul. 2007.

[64] R. G. Selwyn *et al.*, "^{18} F-labeled resin microspheres as surrogates for ^{90} Y resin microspheres used in the treatment of hepatic tumors: a radiolabeling and PET

validation study," *Phys. Med. Biol.*, vol. 52, no. 24, pp. 7397–7408, Dec. 2007.

[65] M. Conti and L. Eriksson, "Physics of pure and non-pure positron emitters for PET: a review and a discussion.," *EJNMMI Phys.*, vol. 3, no. 1, p. 8, Dec. 2016.

[66] K. Tapp, "Evaluation of yttrium-90 positron emission tomography dosimetry," *Open Access Diss.*, Oct. 2014.

[67] B. E. Zimmerman, J. T. Cessna, R. Fritzgerald, B. E. Zimmerman, J. T. Cessna, and R. Fitzgerald, "Standardization of 68 Ge / 68 Ga Using Three Liquid Scintillation Counting based methods," *J. Res. Natl. Inst. Stand. Technol.*, vol. 113, no. 5, pp. 265–280, Sep. 2008.

[68] M. Soret, S. L. Bacharach, and I. Buvat, "Partial-volume effect in PET tumor imaging.," *J. Nucl. Med.*, vol. 48, no. 6, pp. 932–45, Jun. 2007.

[69] S. M. Srinivas, T. Dhurairaj, S. Basu, G. Bural, S. Surti, and A. Alavi, "A recovery coefficient method for partial volume correction of PET images," *Ann. Nucl. Med.*, vol. 23, no. 4, pp. 341–348, Jun. 2009.

[70] CIRS, "CIRS Tissue Simulation and Phantom Technology," *Dynamic thorax phantom; model 008A*, 2018. [Online]. Available: http://www.cirsinc.com/products/all/18/dynamic-thorax-phantom/. [Accessed: 28-Feb-2018].

[71] L. Bester *et al.*, "Radioembolization versus Standard Care of Hepatic Metastases: Comparative Retrospective Cohort Study of Survival Outcomes and Adverse Events in Salvage Patients," *J. Vasc. Interv. Radiol.*, vol. 23, no. 1, pp. 96–105, Jan. 2012.

[72] C. E. N. M. Rosenbaum, M. A. A. J. van den Bosch, W. B. Veldhuis, J. E. Huijbregts, M. Koopman, and M. G. E. H. Lam, "Added value of FDG-PET imaging in the diagnostic workup for yttrium-90 radioembolisation in patients with colorectal cancer liver metastases," *Eur. Radiol.*, vol. 23, no. 4, pp. 931–937, Apr. 2013.

[73] S. A. Nehmeh *et al.*, "Effect of respiratory gating on quantifying PET images of lung cancer.," *J. Nucl. Med.*, vol. 43, no. 7, pp. 876–81, Jul. 2002.

[74] M. K. Werner, J. A. Parker, G. M. Kolodny, J. R. English, and M. R. Palmer, "Respiratory Gating Enhances Imaging of Pulmonary Nodules and Measurement of Tracer Uptake in FDG PET/CT," *Am. J. Roentgenol.*, vol. 193, no. 6, pp. 1640–1645, Dec. 2009.

[75] O. J. O'Connor, S. McDermott, J. Slattery, D. Sahani, and M. A. Blake, "The Use of PET-CT in the Assessment of Patients with Colorectal Carcinoma," *Int. J. Surg. Oncol.*, vol. 2011, pp. 1–14, Jul. 2011.

[76] W. van Elmpt, J. Hamill, J. Jones, D. De Ruysscher, P. Lambin, and M. Öllers, "Optimal gating compared to 3D and 4D PET reconstruction for characterization of lung tumours," *Eur. J. Nucl. Med. Mol. Imaging*, vol. 38, no. 5, pp. 843–855, May 2011.

Appendix A. Decay scheme Yttrium-90 and Germanium-68

99.99% of 90Y decays into the ground level ^{90}Zr by β- (2.280MeV, maximum range 11mm) and 0.0115% into an excited level of ^{90}Zr by β- (0.519MeV). This decays to the ground state through internal conversion (0.0083%) or by creation of an e+/e- pair (0.0032%). The e^+/e^- pair has a maximum energy of 0.739 MeV has a maximum energy of 0.739MeV (short range) [65].

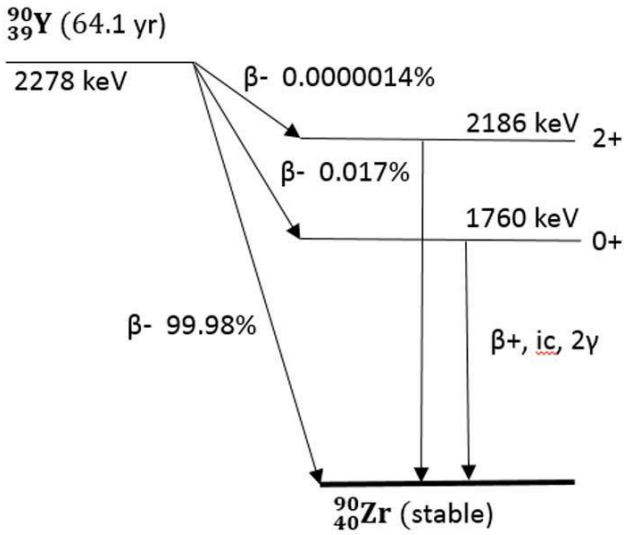

Figure A1. Decay scheme ^{90}Y [66].

^{68}Ge decays by pure electron capture (EC) to the ground state of 68Ga (106.9keV). The half-life of ^{68}Ge is 270.95 days. ^{68}Ga decays with a half-life of 67.71 minutes by a combination of electron capture and positron emission (87.94%, 829.6keV).

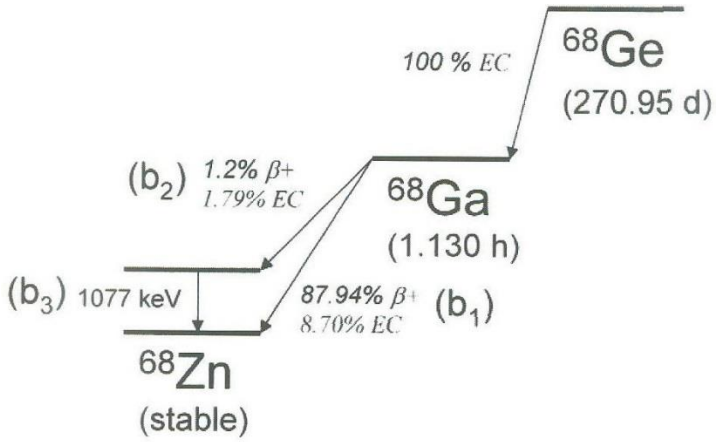

Figure A2. Decay scheme ^{68}Ge. The branching probabilities b_1, b_2, b_3 refer to the two positron emission and gamma emission probabilities [67].

Appendix B. Partial volume effect

PET scans are used to quantify uptake of a radioactive tracer in body tissues. Observed image intensity values can differ from the actual values, which can be caused by the partial volume effect (PVE). The partial volume effect is defined as the loss of image intensity in small regions. PVE can be caused by a limited spatial resolution of the PET scanner, which leads to image blurring. In image blurring part of the observed signal 'spills out' and is seen outside the position of the actual source [68]. As seen in figure B1 (left), the spheres are depicted with blurred delineation to the background. Another phenomenon leading to PVE is image sampling. In PET imaging a voxel grid is used to sample the signal measured. Voxels do generally not match the actual contours of the different tissue types in patient. The intensity measured per voxel is an average of the intensities measured of the underlying tissue types, leading to spilling out or spilling in of the signal (Figure B1) [68]. Spilling in is the phenomenon that signal from outside the Tumor appears to be in the Tumor and therefore leads to an overestimation of activity in the Tumor. Spilling out is the phenomenon that signal from inside the Tumor appears to be outside the Tumor.

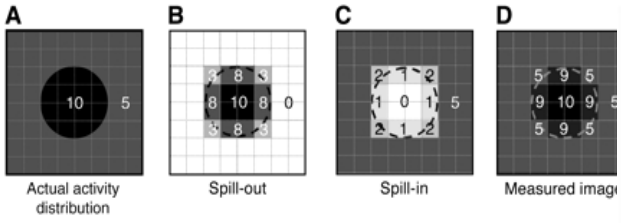

Figure B1. The measured image (D) of the actual activity distribution (A) results from a combination of spilling out (B) and spilling in (C).

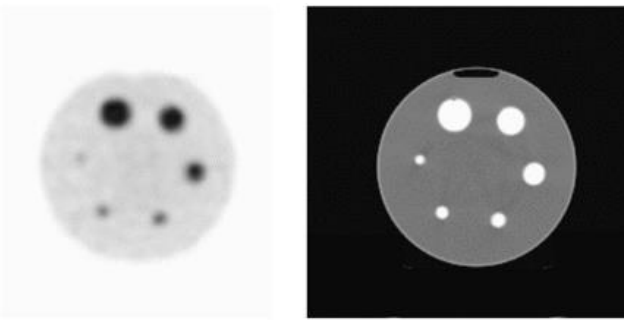

Figure B2. PET slice (left) and corresponding CT slice (right) with six spheres (diameters 10, 12, 16, 22, 28, 34 mm) filled with the same radioactivity concentrations in uniform radioactivity. PVE causes apparent uptake to decrease when sphere size decreases [68].

In summary, PVE will cause that the maximum intensity detected will be lower than the actual intensity value. Besides that, it will also affect the apparent lesion size, lesions can appear to be larger than in reality. PVE does not cause loss of signal, it displaces the signal

and the smaller a lesion, the greater the underestimation of signal intensity as seen in figure B2. One method for PVE correction is the use of the RC. RC's are correction factors precalculated for objects of different sizes, which then can be used for Tumors of similar sizes of that of those precalculated values (Equation B1 and Figure B3).

$$RC = \frac{A_{sphere\_measured} - A_{bck\_measured}}{A_{sphere\_known} - A_{bck\_known}} \quad \text{(B1)}$$

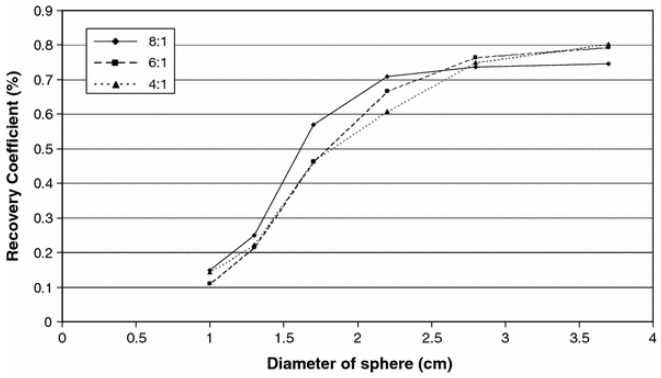

Figure B3. Figure of recovery coefficients for different lesions diameters and different ratios between lesion and background activity [69].

Appendix C. Experiment 1

Table C1. Measurement schedule with scanning start times, file names, scanner number and remarks.

Day 1 (31-01-2018)		**Start time**	**Name**	**Remarks**
Ratio 1:b_{cold}	*PETCT06*	16:37	NG2018130PET06_1	Without sample A
	PETCT12	17:18	NG2018130PET12_1	With sample A
Ratio 1:15	*PETCT12*	18:07	NG2018130PET12_2	With sample A+B
	PETCT06	18:46	NG2018130PET06_2	With sample A+B
Ratio 1:10	*PETCT06*	19:29	NG2018130PET06_3	With sample A+C
	PETCT12	20:06	NG2018130PET12_3	With sample A+C
Ratio 1:7	*PETCT12*	20:49	NG2018130PET12_4	With sample A+D
	PETCT06	21:27	NG2018130PET06_4	With sample A+D
Day 2 (01-02-2018)				
Ratio 1:4	*PETCT06*	16:05	NG20180201PET06_5	With sample A+E
	PETCT12	17:46	NG20180201PET12_5	With sample A+E

Table C2. Syringes with their calibrated activities added to the phantom background compartment to obtain different background to sphere ratios.

	Date	**Calibration time**	**Activity (MBq)**
Syringe 1	31-1-2018	16:00	35.81
Syringe 2	31-1-2018	16:00	199.74
Syringe 3	31-1-2018	16:00	92.53
Syringe 4	31-1-2018	16:00	199.96
Syringe 5	1-2-2018	16:00	493.84

			Spheres			Background				
			Stock (ml)	**Activity (MBq)**	**Concentration (MBq/ml)**	**Background (ml)**	**Concentration (MBq/ml)**	**Total activity (MBq)**	**Activity added (MBq)**	**Actual ratio (sphere to background)**
Day 1 (31-01-2018)		**Ratio 1: b_{cold}**	102	35.81	0.35	9700	0.000	0.00		
		Ratio 1:15	102	35.81	0.35	9700	0.021	199.74	199.74	17.0
		Ratio 1:10	102	35.81	0.35	9700	0.030	292.27	92.53	11.7
		Ratio 1:7	102	35.81	0.35	9700	0.051	492.23	199.96	6.9
	Decay correction			27.08	0.27			372.17		
Day 2 (01-02-2018)		**Ratio 1:4**		27.08	0.27	9700	0.089	866.01	493.84	3.9
								Total	986.07	

Table C3. The concentrations for the spheres and background compartment are given for the two measurement days. For every ratio , the added activity is given and the total activity in the background compartment after adding the new activity. The values of day 2 are corrected for radioactive decay. Finally, the sphere to background ratio is calculated.

Table C4. The net weight of all sphere samples together with the concentration in the bottles.

	Net weight (mg)	Concentration (MBq/ml)
A (spheres)		0.35 (31-01-2018)
	20.33	0.27 (01-02-2018)
B (1:15)	9.27	0.021
C (1:10)	8.85	0.030
D (1:7)	9.47	0.051
E (1:3)	10.23	0.089

Table C5. Results of the gamma counter for the sample bottles.

Bottle	Counts	CPM	Error (%)	Source of sample
A	10616852	16086000	0.03	*Spheres*
B	1694276	936170.9	0.08	*Ratio 1:15*
C	2110925	1199144.8	0.07	*Ratio 1:10*
D	3428933	2146517.5	0.05	*Ratio 1:7*
E	5830405	4573603	0.04	*Ratio 1:4*

Table C6. Weight and activity of the delivered Yttrium-90, corrected for the two measurement days.

	Day of delivery	Day 1	Day 2
Amount (gram)	5.035	5.035	2.96
Total activity (MBq)	1923.37	1214	546.90
MBq/gram	382	241.35	184.76

Table C7. Accuracy of the dose calibrator. The calibrated activity by the dose calibrator, the net weight of the syringes with the activity and the calculated activity based on the net weight of the syringes and the results from table 11.

	Activity calibrated (MBq)	**Net weight (mg)**	**Activity calculated (MBq)**	**Accuracy**
Spheres syringe	35.81	0.13	31.38	88%
1:15 syringe	199.74	0,77	185.84	93%
1:10 syringe	92.53	0,29	69.99	76%
1:7 syringe	199.96	0.775	187.05	94%
1:3 syringe	493.84	2.59	478.53	97%
Average				89%

Table C8. True and recovered background concentrations (kBq/ml) for every ratio measured with PETCT06 with means of Osirx and DOSIsoft.

	Activity in background (MBq)	True concentration (kBq/ml)	Recovered concentration (kBq/ml) Osirix	Percentage detected of true Osirix (%)	Recovered concentration (kBq/ml) DOSIsoft	Percentage detected of true DOSIsoft (%)
Ratio 1: b_{cold}	0	0	0 (± 0)	0	0 (± 0)	0
Ratio 1:15	199.74	20.59	1.64 (± 1.67)	7.97	44.26 (± 10.54)	214.92
Ratio 1:10	292.27	30.13	3.47 (± 5.00)	11.51	31.60 (± 21.49)	104.88
Ratio 1:7	492.23	50.75	21.41 (± 11.09)	42.19	58.24 (± 9.31)	114.77
Ratio 1:5	866.01	90.02	73.91 (± 18.85)	82.11	88.37 (± 14.14)	98.17

Table C9. True and recovered background concentrations (kBq/ml) for every ratio measured with PETCT12 with means of Osirx and DOSIsoft.

	Activity in background (MBq)	True concentration (kBq/ml)	Recovered concentration (kBq/ml) Osirix	Percentage detected of true Osirix (%)	Recovered concentration (kBq/ml) DOSIsoft	Percentage detected of true DOSIsoft (%)
Ratio 1: b_{cold}	0	0	0 (± 0)	0	0 (± 0)	0
Ratio 1:15	199.74	20.59	0 (± 0)	0	0.89 (± 3.07)	4.30
Ratio 1:10	292.27	30.13	1.56 (± 1.55)	5.18	32.81 (± 17.75)	30.13
Ratio 1:7	492.23	50.75	14.69 (± 8.61)	28.95	54.23 (± 12.68)	106.87
Ratio 1:5	866.01	90.02	58.42 (± 13.93)	64.90	81.22 (± 10.46)	90.23

Table C10. True and recovered concentrations (kBq/ml) for every sphere for ratio 1:b_{cold} measured on PETCT06 with means of Osirix and DOSIsoft.

Sphere diameter (mm)	Activity in sphere (MBq)	True concentration (kBq/ml)	Recovered concentration (kBq/ml) Osirix	Percentage detected of true Osirix (%)	Recovered concentration (kBq/ml) DOSIsoft	Percentage detected of true DOSIsoft (%)
10	0.18	351.08	0.00	0.00	0.00	0.00
13	0.40	351.08	0.00	0.00	0.00	0.00
17	0.90	351.08	0.00	0.00	0.00	0.00
22	1.95	351.08	4.81 (±12.08)	1.37	34.40 (±27.97)	9.80
28	4.02	351.08	28.25 (±46.51)	8.05	64.32 (±55.93)	18.32
37	9.28	351.08	66.06 (±88.57)	18.82	92.29 (±83.90)	26.29

Table C11. True and recovered concentrations (kBq/ml) for every sphere for ratio 1:b_{cold} measured on PETCT12 with means of Osirix and DOSIsoft.

Sphere diameter (mm)	Activity in sphere (MBq)	True concentration (kBq/ml)	Recovered concentration (kBq/ml) Osirix	Percentage detected of true Osirix (%)	Recovered concentration (kBq/ml) DOSIsoft	Percentage detected of true DOSIsoft (%)
10	0.18	351.08	0.00	0.00	0.00	0,00
13	0.40	351.08	0.00	0.00	0.00	0,00
17	0.90	351.08	0.00	0.00	0.00	0,00
22	1.95	351.08	11.77 (±20.89)	3.35	52.86 (±27.97)	15.06
28	4.02	351.08	50.06 (±80.43)	14.26	104.03 (±83.90)	29.63
37	9.28	351.08	121.88 (±141.28)	34.71	147.38 (±139.83)	41.98

Table C12. True and recovered concentrations (kBq/ml) for every sphere for ratio 1:15 measured on PETCT06 with means of Osirix and DOSIsoft.

Sphere diameter (mm)	Activity in sphere (MBq)	True concentration (kBq/ml)	Recovered concentration (kBq/ml) Osirix	Percentage detected of true Osirix (%)	Recovered concentration (kBq/ml) DOSIsoft	Percentage detected of true DOSIsoft (%)
10	0.18	351.08	3.36 (±22.82)	0.96	0.00	0.00
13	0.40	351.08	11.75 (±10.10)	3.35	0.00	0.00
17	0.90	351.08	45.70 (±47.18)	13.02	0.00	0.00
22	1.95	351.08	47.93 (±81.49)	13.65	91.45 (±83.90)	34.09
28	4.02	351.08	66.62 (±63.96)	18.97	78,03 (±55.93)	22.22
37	9.28	351.08	119.47 (±100.73)	34.03	119.69 (±83.90)	26.05

Table C13. True and recovered concentrations (kBq/ml) for every sphere for ratio 1:15 measured on PETCT12 with means of Osirix and DOSIsoft.

Sphere diameter (mm)	Activity in sphere (MBq)	True concentration (kBq/ml)	Recovered concentration (kBq/ml) Osirix	Percentage detected of true Osirix (%)	Recovered concentration (kBq/ml) DOSIsoft	Percentage detected of true DOSIsoft (%)
10	0.18	351.08	0.00	0.00	0.00	0.00
13	0.40	351.08	0.00	0.00	0.00	0.00
17	0.90	351.08	0.00	0.00	0.00	0.00
22	1.95	351.08	17.39 (±65.60)	10.32	92.85 (±83.90)	26.45
28	4.02	351.08	62.87 (±62.42)	18.15	81.10 (±55.93)	23.10
37	9.28	351.08	108.76 (±169.64)	39.97	167.80 (±167.80)	47.79

Table C14. True and recovered concentrations (kBq/ml) for every sphere for ratio 1:10 measured on PETCT06 with means of Osirix and DOSIsoft.

Sphere diameter (mm)	Activity in sphere (MBq)	True concentration (kBq/ml)	Recovered concentration (kBq/ml) Osirix	Percentage detected of true Osirix (%)	Recovered concentration (kBq/ml) DOSIsoft	Percentage detected of true DOSIsoft (%)
10	0.18	351.08	0.00	0.00	0.00	0.00
13	0.40	351.08	0.00	0.00	0.00	0.00
17	0.90	351.08	0.00	0.00	38.03 (±27.97)	10.83
22	1.95	351.08	114.94 (±125.20)	32.74	132.28 (±111.86)	36.24
28	4.02	351.08	78.14 (±79.09)	22.26	89.49 (±83.90)	25.49
37	9.28	351.08	111.70 (±120.70)	31.82	127.25 (±111.86)	36.24

Table C15. True and recovered concentrations (kBq/ml) for every sphere for ratio 1:10 measured on PETCT12 with means of Osirix and DOSIsoft.

Sphere diameter (mm)	Activity in sphere (MBq)	True concentration (kBq/ml)	Recovered concentration (kBq/ml) Osirix	Percentage detected of true Osirix (%)	Recovered concentration (kBq/ml) DOSIsoft	Percentage detected of true DOSIsoft (%)
10	0.18	351.08	0.00	0.00	0.00	0.00
13	0.40	351.08	0.00	0.00	0.00	0.00
17	0.90	351.08	51.43 (±62.78)	14.65	79.14 (±55.93)	22.54
22	1.95	351.08	36.22 (±50.26)	4.95	69.08 (±55.93)	19.68
28	4.02	351.08	63.73 (±76.60)	17.91	84.46 (±83.90)	24.06
37	9.28	351.08	140.33 (±106.55)	30.98	108.79 (±111.86)	30.99

Table C16. True and recovered concentrations (kBq/ml) for every sphere for ratio 1:7 measured on PETCT06 with means of Osirix and DOSIsoft.

Sphere diameter (mm)	Activity in sphere (MBq)	True concentration (kBq/ml)	Recovered concentration (kBq/ml) Osirix	Percentage detected of true Osirix (%)	Recovered concentration (kBq/ml) DOSIsoft	Percentage detected of true DOSIsoft (%)
10	0.18	351.08	0.98 (±14.79)	0.28	36.64 (±27.97)	10.44
13	0.40	351.08	15.13 (±31.79)	4.31	50.34 (±27.97)	14.34
17	0.90	351.08	34.96 (±46.59)	9.96	64.60 (±55.93)	18.40
22	1.95	351.08	93.16 (±89.74)	26.53	104.31 (±83.90)	29.71
28	4.02	351.08	105.74 (±126.21)	30.12	124.45 (±111.86)	35.45
37	9.28	351.08	151.10 (±156.50)	43.04	148.50 (±139.83)	42.30

Table C17. True and recovered concentrations (kBq/ml) for every sphere for ratio 1:7 measured on PETCT12 with means of Osirix and DOSIsoft.

Sphere diameter (mm)	Activity in sphere (MBq)	True concentration (kBq/ml)	Recovered concentration (kBq/ml) Osirix	Percentage detected of true Osirix (%)	Recovered concentration (kBq/ml) DOSIsoft	Percentage detected of true DOSIsoft (%)
10	0.18	351.08	0.00	0.00	27.97 (±27.97)	7.97
13	0.40	351.08	71.40 (±107.19)	20.34	118.02 (±55.93)	33.62
17	0.90	351.08	80.32 (±104.03)	22.88	108.79 (±27.97)	30.99
22	1.95	351.08	40.61 (±43.68)	11.57	58.45 (±111.86)	16.65
28	4.02	351.08	46.28 (±47.79)	13.18	60.13 (±83.90)	17.13
37	9.28	351.08	118.86(±152.39)	33.85	137.03 (±27.97)	39.03

Table C18. True and recovered concentrations (kBq/ml) for every sphere for ratio 1:4 measured on PETCT06 with means of Osirix and DOSIsoft.

Sphere diameter (mm)	Activity in sphere (MBq)	True concentration (kBq/ml)	Recovered concentration (kBq/ml) Osirix	Percentage detected of true Osirix (%)	Recovered concentration (kBq/ml) DOSIsoft	Percentage detected of true DOSIsoft (%)
10	0.14	270.45	16.47 (±13.90)	6.09	38.31 (±27.97)	14.16
13	0.31	270.45	30.32 (±25.39)	11.21	44.47 (±27.97)	16.44
17	0.69	270.45	157.78 (±86.92)	58.32	161.08 (±55.93)	59.54
22	1.50	270.45	80.68 (±68.60)	29.82	83.90 (±111.86)	31.01
28	3.10	270.45	156.50 (±144.17)	57.85	147.66 (±139.83)	54.58
37	7.15	270.45	188.72 (±182.48)	69.75	171.99 (±167.80)	63.57

Table C19. True and recovered concentrations (kBq/ml) for every sphere for ratio 1:4 measured on PETCT12 with means of Osirix and DOSIsoft.

Sphere diameter (mm)	Activity in sphere (MBq)	True concentration (kBq/ml)	Recovered concentration (kBq/ml) Osirix	Percentage detected of true Osirix (%)	Recovered concentration (kBq/ml) DOSIsoft	Percentage detected of true DOSIsoft (%)
10	0.14	270.45	0.00	0.00	31.04 (±27.97)	11.47
13	0.31	270.45	58.70 (±45.03)	21.70	79.70 (±55.93)	29.46
17	0.69	270.45	59.60 (±60.88)	22.03	72.71 (±55.93)	26.88
22	1.50	270.45	68.07 (±49.89)	25.16	75.79 (±55.93)	28.01
28	3.10	270.45	79.31 (±88.09)	29.32	88.65 (±83.90)	32.77
37	7.15	270.45	105.57 (±102.75)	39.02	114.66 (±111.86)	42.38

Table C20. Detected total activity present in the phantom by the DOSIsoft software for every ratio measured on scanner 6. These values are rescaled with means of the theoretical rescaling factor. Lastly, the observed activity is presented as a percentage of the actual activity present.

	Activity detected (MBq)	**True activity (Mbq)**	**Percentage detected of true**
Ratio 1: b_{cold}	3.15	16.74	18.82%
Ratio 1:15	14.98	216.67	6.91%
Ratio 1:10	29.47	316.39	9.32%
Ratio 1:7	128.35	516.57	24.85%
Ratio 1:4	596.09	886.77	67.22%

Table C21. BV for each sphere diameter and both PETCT scanners for ratio 1:15 measured with Osirix.

	PETCT06		**PETCT12**	
Region diameter (mm)	*Region concentration (kBq/ml)*	*Background variability (%)*	*Region concentration (kBq/ml)*	*Background variability (%)*
37	1.64 (± 1.67)	102.02	0.00	0.00
28	3.65 (± 4.42)	120.78	0.00	0.00
22	3.36 (± 5.18)	154.50	0.00	0.00
17	3.09 (± 5.07)	164.16	0.00	0.00
13	2.93 (± 5.32)	181.62	0.00	0.00
10	3.33 (± 6.73)	201.98	0.00	0.00

Table C22. BV for each sphere diameter and both PETCT scanners for ratio 1:10 measured with Osirix.

	PETCT06		**PETCT12**	
Region diameter (mm)	*Region concentration (kBq/ml)*	*Background variability (%)*	*Region concentration (kBq/ml)*	*Background variability (%)*
37	3.47 (± 5.00)	144.14	1.56 (± 1.55)	99.24
28	2.24 (± 3.09)	138.11	0.72 (± 1.75)	240.33
22	1.69 (± 2.55)	150.43	0.49 (± 1.46)	295.49
17	1.90 (± 2.88)	151.03	0.72 (± 1.90)	264.13
13	1.82 (± 3.13)	171.95	0.27 (± 0.94)	346.41
10	1.60 (± 2.84)	177.60	0.00	0.00

Table C23. BV for each sphere diameter and both PETCT scanners for ratio 1:7 measured with Osirix.

	PETCT06		**PETCT12**	
Region diameter (mm)	*Region concentration (kBq/ml)*	*Background variability (%)*	*Region concentration (kBq/ml)*	*Background variability (%)*
37	21.41 (± 11.09)	51.78	14.69 (± 8.61)	58.64
28	29.86 (± 17.86)	59.81	12.66 (± 16.68)	131.79
22	26.68 (± 21.13)	79.22	14.91 (± 20.54)	137.79
17	28.42 (± 24.35)	85.70	11.42 (± 13.18)	115.33
13	28.72 (± 31.25)	108.81	8.94 (± 11.67)	130.58
10	27.39 (± 28.43)	103.80	10.41 (± 9.72)	93.38

Table C24. BV for each sphere diameter and both PETCT scanners for ratio 1:4 measured with Osirix.

	PETCT06		**PETCT12**	
Region diameter (mm)	*Region concentration (kBq/ml)*	*Background variability (%)*	*Region concentration (kBq/ml)*	*Background variability (%)*
37	73.91 (± 18.85)	25.50	58.42 (± 13.93)	23.84
28	91.19 (± 43.30)	47.48	59.31 (± 25.54)	43.07
22	93.46 (± 62.12)	66.47	60.56 (± 34.05)	56.22
17	97.41 (± 72.40)	74.32	56.74 (± 30.40)	53.58
13	96.45 (± 103.19)	106.99	62.98 (± 35.63)	56.56
10	103.03 (± 110.84)	107.58	60.12 (± 32.56)	54.17

Experiment 1: Measurement protocol

Volume spheres (alle) = 47.82 ml
Volume achtergrond = 9700 ml

Benodigdheden

- NEMA fantoom
- Weegschaal
- Gamma counter
- BSA
- Activiteit Yttrium-90
    - Spuit voor spheres
    - Spuit voor ratio 1:15
    - Spuit voor ratio 1:10
    - Spuit voor ratio 1:7
    - Spuit voor ratio 1:4
- Karretje om de spuiten en flessen in te vervoeren
- Telflesjes voor gamma counter (totaal = 5)
    - Stock spheres
    - Ratio 1:15
    - Ratio 1:10
    - Ratio 1:7
    - Ratio 1:4
- Fles (100ml) voor de spheres stock, vullen met kraanwater
- Ontluchtingsnaalden (rood, kort)
- 1 afvalfles (500 ml)
- 2 gele afvalzakken (één voor waarschijnlijk niet besmet en één voor waarschijnlijk wel besmet)

Vullen van het fantoom

Achtergrond

Voor de eerste meting de achtergrond vullen met kraanwater. Daarna telkens de correcte spuit toevoegen aan de achtergrond.

- Weeg de spuit.
- Haal 50 ml uit de achtergrond van het fantoom.
- Spuit de activiteit in de achtergrond van het fantoom.
- Weeg de lege spuit.
- Homogeniseer de achtergrond (zwenken)
- Spuit de verwijderde 50 ml weer terug in het fantoom.
- Neem een sample van de achtergrond stock en meet deze met de gamma counter
- Weeg het volle telflesje en plaats deze op het fantoom om meegescand te worden.

Spheres

- Weeg de stock fles
- Vul de fles met 100 ml water
- Weeg de spuit met activiteit
- Leeg de spuit in de fles en flush de spuit
- Weeg opnieuw de fles en de spuit (zonder loodhuls)
- Voeg water toe tot er 100 ml in de fles zit
- Homogeniseer de stock fles (zwenken)
- Vul de spheres met gebruik van de lange naald
- Weeg een leeg telflesje
- Neem een sample van de sphere stock en meet deze met de gamma counter
- Weeg het volle telflesje
- Plaats het telflesje op de zijkant van het fantoom, zodat deze meegescand kan worden

Acquisitieprotocol

Het PET ^{90}Y protocol in het AvL is:
2-3 bedposities (armen omhoog), 15 minuten per bedpositie. Meten voor ^{68}Ge protocol, waarbij de totale dosis gedeeld moet worden door 10.
Er zal gemeten worden op beide PET systemen; de PETCT06 en PETCT12 in 2 bedposities.

- Vul op de scanner de ID, last name, gewicht, lengte in.

ID = NG20180_datum_scanner_meting

Last name = fantoom

Gewicht = 70 kg

Lengte = 170 cm

- Leg het fantoom op de juiste positie en stel de bedhoogte goed in.
- Stel de FOV van de PET en de CT in.

Afronden dag 1

- PET uitzetten
- Weeg alle gevulde telflesjes
- Al het afval weggooien; let op actief afval.

Afronden dag 2

- PET uitzetten
- Weeg alle gevulde telflesjes
- Plaats stock bij Yttrium afval in de kelder
- Al het afval weggooien; let op actief afval.

Appendix D. Experiment 2

Table D1. Sphere diameter (cm) and volume (ml)

Diameter (cm)	3,7	2,8	2,2	1,7	1,3	1.0
Volume (ml)	26,52	11,49	5,58	2,57	1,15	0,52

Table D2. Activities (MBq) added to the spheres and background compartment.

Spheres activity (MBq)	241,14
Background activity (MBq)	2162,27
Total activity in phantom (MBq)	2403,41

Table D3. Concentration (kBq/ml) and activity (kBq) in the background compartment and each sphere at different days of imaging.

	Concentration(kBq/ml)	Activity (kBq)	Day
Background	222,91	2162,27	0
	102,01	989,47	3
	60,57	587,58	5
	35,97	348,92	7
37mm sphere	2404,19	63763,50	0
	1100,17	29178,61	3
	653,31	17327,12	5
	387,96	10289,35	7
28mm sphere	2404,19	27633,83	0
	1100,17	12645,43	3
	653,31	7509,23	5
	387,96	4459,20	7
22mm sphere	2404,19	13404,02	0
	1100,17	6133,77	3
	653,31	3642,41	5
	387,96	2162,97	7
17mm sphere	2404,19	6184,63	0
	1100,17	2830,13	3
	653,31	1680,61	5
	387,96	998,00	7
13mm sphere	2404,19	2765,65	0
	1100,17	1265,58	3
	653,31	751,54	5
	387,96	446,29	7
10mm sphere	2404,19	1258,83	0
	1100,17	576,05	3
	653,31	342,07	5
	387,96	203,13	7

Table D4. True and detected activities (MBq) in the total FoV for both scanners, measured with DOSIsoft software.

	PETCT06			PETCT12		
	True activity (Mbq)	*Detected activity (MBq) DOSIsoft*	*Percentage detected of true (%)*	*True activity (Mbq)*	*Detected activity (MBq) DOSIsoft*	*Percentage detected of true (%)*
Day 0	2403.41	2225.83	92.61	2403.41	2091.25	87.01
Day 3	1091.29	1640.64	68.26	1099.22	1571.06	76.11
Day 5	652.39	1144.66	47.63	647.92	924.54	38.47
Day 7	391.64	454.85	18.93	385.38	231.44	9.63

Table D5. True and detected concentrations (kBq/ml) in the background compartment for PETCT06, measured with Osirix and DOSIsoft

	Activity in background (MBq)	*True concentration (kBq/ml)*	*Recovered concentration (kBq/ml) Osirix*	*Percentage detected of true Osirix (%)*	*Recovered concentration (kBq/ml) DOSIsoft*	*Percentage detected of true DOSIsoft (%)*
Day 0	2162.27	214.32	223.84 (± 36.86)	101.31	221.79 (± 11.60)	100.38
Day 3	989.47	98.95	76.03 (± 27.79)	74.54	72.67 (± 6.93)	71.27
Day 5	587.58	60.51	29.27 (± 13.96)	48.37	30.44 (± 7.50)	50.30
Day 7	348.92	36.39	7.30 (± 7.67)	20.05	6.97 (± 4.24)	6.53

Table D6. True and detected concentrations (kBq/ml) in the background compartment for PETCT12, measured with Osirix and DOSIsoft

	Activity in background (MBq)	*True concentration (kBq/ml)*	*Recovered concentration (kBq/ml) Osirix*	*Percentage detected of true Osirix (%)*	*Recovered concentration (kBq/ml) DOSIsoft*	*Percentage detected of true DOSIsoft (%)*
Day 0	2162.27	215.52	210.64 (± 45.30)	94.80	220.23 (± 21.37)	99.12
Day 3	989.47	98.20	71.04 (± 23.19)	70.17	71.08 (± 12.38)	70.23
Day 5	587.58	60.09	27.16 (± 14.53)	45.20	28.01 (± 11.58)	46.61
Day 7	348.92	35.74	0.81 (± 1.86)	2.28	2.54 (± 2.08)	2.42

Table D7. True and recovered concentrations (kBq/ml) for every sphere diameter on day 0 of imaging for PETCT06, measured with Osirix and DOSIsoft.

Sphere diameter (mm)	*Activity in sphere (MBq)*	*True concentration (kBq/ml)*	*Recovered concentration (kBq/ml) Osirix*	*Percentage detected of true Osirix (%)*	*Recovered concentration (kBq/ml) DOSIsoft*	*Percentage detected of true DOSIsoft (%)*
10	1.26	2378.81	369.54 (± 211.65)	15.53	269.31 (± 83.90)	11.32
13	2.77	2378.81	381.23 (± 143.41)	16.03	359.64 (± 139.83)	15.12
17	6.18	2378.81	749.55 (± 287.41)	31.51	576.66 (± 335.59)	24.24
22	13.40	2378.81	1115.62 (± 451.40)	46.87	894.36 (± 503.39)	37.60
28	27.63	2378.81	1285.35 (± 629.82)	54.03	1049.85 (± 671.18)	44.13
37	63.76	2378.81	1628.75 (± 592.35)	68.47	1252.04 (± 755.08)	52.63

Table D8. Activity (MBq) present and recovered in each of the different spheres on day 0 of imaging for PETCT06

Sphere diameter (mm)	*Activity in sphere (MBq)*	*Recovered activity (MBq) Osirix*	*Percentage detected of true Osirix (%)*	*Recovered activity (MBq) DOSIsoft*	*Percentage detected of true DOSIsoft(%)*
10	1,26	0,19	15,53	0.14	11.32
13	2,77	0,44	16,03	0.41	15.12
17	6,18	1,93	31,51	1.48	24.24
22	13,40	6,22	46,87	4.99	37.60
28	27,63	14,77	54,03	12.07	44.13
37	63,76	43,20	68,47	33.21	52.63

Table D9. True and recovered concentrations (kBq/ml) for every sphere diameter on day 0 of imaging for PETCT12, measured with Osirix and DOSIsoft.

Sphere diameter (mm)	*Activity in sphere (MBq)*	*True concentration (kBq/ml)*	*Recovered concentration (kBq/ml) Osirix*	*Percentage detected of true Osirix (%)*	*Recovered concentration (kBq/ml) DOSIsoft*	*Percentage detected of true DOSIsoft (%)*
10	1.26	2392.20	468.82 (± 145.54)	19.60	334.47 (± 167.80)	13.98
13	2.77	2392.20	895.87 (± 435.85)	37.45	590.64 (± 363.56)	24.69
17	6.18	2392.20	1105.78 (± 590.14)	46.22	882.05 (± 531.36)	36.87
22	13.40	2392.20	1749.14 (± 1006.00)	73.12	1745.64 (± 922.88)	72.97
28	27.63	2392.20	1359.82 (± 677.87)	56.84	1190.80 (± 615.25)	49.78
37	63.76	2392.20	1560.23 (± 847.01)	65.22	1274.14 (± 783.05)	53.26

Table D10. Activity (MBq) present and recovered in each of the different spheres on day 0 of imaging for PETCT12

Sphere diameter (mm)	*Activity in sphere (MBq)*	*Recovered activity (MBq) Osirix*	*Percentage detected of true Osirix (%)*	*Recovered activity (MBq) DOSIsoft*	*Percentage detected of true DOSIsoft(%)*
10	1,26	0,25	19,60	0,18	13,98
13	2,77	1,03	37,45	0,68	24,69
17	6,18	2,84	46,22	2,27	36,87
22	13,40	9,75	73,12	9,73	72,97
28	27,63	15,63	56,84	13,69	49,78
37	63,76	41,38	65,22	33,79	53,26

Table D11. True and recovered concentrations (kBq/ml) on different imaging days for the 37mm sphere for PETCT06, measured with Osirix and DOSIsoft.

	Activity in sphere (MBq)	*True concentration (kBq/ml)*	*Recovered concentration (kBq/ml) Osirix*	*Percentage detected of true Osirix (%)*	*Recovered concentration (kBq/ml) DOSIsoft*	*Percentage detected of true DOSIsoft (%)*
Day 0	63.76	2378.81	1628.75 (± 592.35)	68.47	1252.04 (± 755.08)	52.63
Day 3	29.18	1098.26	663.27 (± 302.68)	60.09	559.04 (± 307.63)	50.93
Day 5	17.33	651.47	334.61 (± 163.97)	50.33	286.09 (± 167.80)	43.92
Day 7	10.29	391.08	196.41(± 158.62)	50.22	391.08(± 139.83)	44.34

Table D12. True and recovered concentrations (kBq/ml) on different imaging days for the 37mm sphere for PETCT12, measured with Osirix and DOSIsoft.

	Activity in sphere (MBq)	*True concentration (kBq/ml)*	*Recovered concentration (kBq/ml) Osirix*	*Percentage detected of true Osirix (%)*	*Recovered concentration (kBq/ml) DOSIsoft*	*Percentage detected of true DOSIsoft (%)*
Day 0	63.76	2392.20	1560.23 (± 847.01)	65.22	1274.14 (± 783.05)	53.26
Day 3	29.18	1089.94	654.94 (± 299.77)	62.60	554.57 (± 307.63)	50.89
Day 5	17.33	647.00	389.29 (± 228.59)	60.54	329.72 (± 223.73)	50.96
Day 7	10.29	384.84	115.84 (± 120.42)	30.10	88.09 (± 111.86)	22.89

Table D13. True and detected concentrations (kBq/ml) in the cold insert for different imaging days for PETCT06, measured with Osirix and DOSIsoft.

	Activity in background (MBq)	*True concentration (kBq/ml)*	*Detected concentration (kBq/ml) Osirix*	*Detected activity (MBq) Osirix*	*Percentage detected of true Osirix (%)*	*Detected concentration (kBq/ml) DOSIsoft*	*Detected activity (MBq) DOSIsoft*	*Percentage detected of true DOSIsoft (%)*
Day 0	2162,27	214.32	76.30 (± 22.13)	2.02 (± 0.59)	34.53	91.17 (± 83.90)	2.42 (± 2.23)	41.26
Day 3	989,47	98.95	18.87 (± 12.63)	0.50 (±0.34)	18.50	19.58 (± 27.97)	0.52 (± 0.74)	19.20
Day 5	587,58	60.51	19.95 (± 12.01)	0.53 (±0.32)	32.96	10.07 (± 27.97)	0.27 (± 0.74)	16.64
Day 7	348,92	36.39	2.38 (± 0.00)	0.06 (±0.00)	6.55	0.28 (± 0.00)	0.01 (± 0.00)	0.26

Table D14. True and detected concentrations (kBq/ml) in the cold insert for different imaging days for PETCT12, measured with Osirix and DOSIsoft.

	Activity in background (MBq)	*True concentration (kBq/ml)*	*Detected concentration (kBq/ml) Osirix*	*Detected activity (MBq) Osirix*	*Percentage detected of true Osirix (%)*	*Detected concentration (kBq/ml) DOSIsoft*	*Detected activity (MBq) DOSIsoft*	*Percentage detected of true DOSIsoft (%)*
Day 0	2162,27	215.52	52.24 (± 10.06)	1.39 (± 0.27)	23.51	58.45 (± 83.90)	1.55 (± 2.23)	26.31
Day 3	989,47	98.20	39.48 (± 30.13)	1.05 (± 0.80)	39.00	22.65 (± 27.97)	0.60 (± 0.74)	22.38
Day 5	587,58	60.09	5.07 (± 5.39)	0.13 (± 0.14)	8.44	3.08 (± 0.00)	0.08 (± 0.00)	5.12
Day 7	348,92	35.74	0.00 (± 0.00)	0.00 (± 0.00)	0	0.28 (± 0.00)	0.01 (± 0.00)	0.27

Table D15. True and recovered concentrations (kBq/ml) for every sphere diameter on day 3 of imaging for PETCT12, measured with Osirix and DOSIsoft.

Sphere diameter (mm)	*True concentration (kBq/ml)*	*Recovered concentration (kBq/ml) PETCT06*	*True concentration (kBq/ml)*	*Percentage detected of true PETCT06(%)*	*Recovered concentration (kBq/ml) PETCT06*	*Percentage detected of true (%)PETCT06*
10	1098.26	165.73 (± 118.52)	1089.94	2.25	24.53 (± 89.46)	2.25
13	1098.26	328.63 (± 193.36)	1089.94	8.05	87.76 (± 87.76)	8.05
17	1098.26	333.80 (± 174.45)	1089.94	23.54	256.53 (± 256.53)	23.54
22	1098.26	585.63 (± 320.60)	1089.94	46.22	503.78 (± 272.22)	46.22
28	1098.26	619.45 (± 345.74)	1089.94	54.31	591.93 (± 279.19)	54.31
37	1098.26	663.27 (± 302.68)	1089.94	60.09	654.94 (± 299.77)	60.09

Table D16. Background variability for each region diameter PETCT06 and PETCT12, measured with Osirix on day 0 of imaging.

	PETCT06		**PETCT12**	
Region diameter (mm)	*Region concentration (kBq/ml)*	*Background variability (%)*	*Region concentration (kBq/ml)*	*Background variability (%)*
10	215.84 (± 82.57)	38.26	210.75 (± 83.86)	39.79
13	223.68 (± 75.90)	33.93	204.48 (± 71.44)	34.93
17	221.78 (± 65.68)	29.61	208.23 (± 66.77)	32.07
22	221.53 (± 55.18)	24.91	207.12 (± 54.79)	26.45
28	221.57 (± 47.43)	21.41	205.03 (± 53.75)	26.21
37	223.85 (± 36.86)	16.47	210.64 (± 45.30)	21.51

Experiment 2: Measurement protocol

Benodigdheden:

- NEMA fantoom; Controleer of het fantoom geleegd is.
- Opgetrokken spuiten: 231 MBq en 2769 MBq
- Spuit en lange naald
- Celstofmatjes
- 500ml BSA oplossing (10mg/ml).
- Weegschaal
- 150 ml glas (voor stock)
- Gele afvalzak
- Lekbak

Procedure

- Achtergrond fantoom vullen met 10L water en BSA. Het fantoom wordt voorgespoeld met een geconcentreerde BSA-oplossing (5000mg/500ml). 30 ml verwijderen met de spuit en de lange naald. Dit gebeurt op 14 juni, zodat het schuim kan wegtrekken (uiteindelijke BSA concentratie ~0,5mg/ml).
- Weeg de volle spuit met activiteit
- Spuit met 2769MBq leegspuiten in het achtergrond compartiment. Daarna het fantoom schudden.
- Weeg de lege spuit van de activiteit, ook nameten als dat mogelijk is.
- 100 ml afwegen in het 150 ml glas
- Weeg de volle spuit
- Spuit met 231MBq toevoegen aan de 100 ml water
- Weeg de lege spuit
- De 6 spheres vullen vanuit deze stock oplossing.
- Radioactief afval weggooien. Overige stockoplossing naar de kelder brengen. Naald en spuit ook laten uitstralen.

Scannen

- Fantoom schudden voor elke keer meten
- Fantoom in lekbak en met matje verplaatsen naar scanner
- Lengte en gewicht instellen; juiste protocol selecteren
  - ID = NG2018_YttriumCalibratie_Scanner(Meting)
  - Last name = NG2018_YttriumCalibratie_Scanner(Meting)
  - Gewicht = 70 kg
  - Lengte = 170 cm
- PET scanner uitzetten

Table D17. For every measurement day and PET scanner the start time and name of the scan are mentioned.

Measurement day	PET/CT scanner	Start time	Name
Day 0	PETCT06	17:59	NG2018YttriumCalibratiePETCT06(1)
Day 0	PETCT12	17:18	NG2018YttriumCalibratiePETCT12(1)
Day 3	PETCT06	17:03	NG2018YttriumCalibratiePETCT06(2)
Day 3	PETCT12	17:43	NG2018YttriumCalibratiePETCT12(2)
Day 5	PETCT06	17:06	NG2018YttriumCalibratiePETCT06(3)
Day 5	PETCT12	17:51	NG2018YttriumCalibratiePETCT12(3)
Day 7	PETCT06	15:51	NG2018YttriumCalibratiePETCT06(4)
Day 7	PETCT12	17:19	NG2018YttriumCalibratiePETCT12(4)

Appendix E. Retrospective dosimetry

Table E1. Injected activities (MBq) during radioembolisation compared to the detected activities by DOSIsoft (MBq).

Injected activity (MBq)	Detected activity detected by DOSIsoft (MBq)	Difference (%)
1520	1142.71	75.18
1537	1483.17	96.50
634.7	627.59	98.88
2070	2221.32	107.31
2015	1617.41	80.27
1750	1912.68	109.30
1525.98	1640.96	107.53
2271.93	2240.6	98.62
1640	1543.5	94.12
1987	2243.93	112.93
1160.38	1951.21	168.15
2400	2845.5	118.56
2200	2813.77	127.90

Table E2. Calculated liver volume before dose calculation compared to the liver volume manually segmented with means of DOSIsoft.

Liver volume dose calculation (cm^3)	Liver volume DOSIsoft (cm^3)	Difference (%)
1790	1960	109.52
1310	1295	98.83
1300	1212	93.27
2200	1995	90.66
3252	3037	93.39
1623	1528	94.12
1460	1543	105.69
1400	1965	140.37
1200	1735	144.57
1650	2328	141.11
1400	1343	95.92
1950	2888	148.12
2500	3017	120.68

Table E3. Average detected activity concentration (kBq/ml) for all 33 lesions segmented and analyzed.

Lesion number	Average kBq/ml	Dmean (Gy)
1	950.85	58
2	1343.21	82
3	1063.83	66
4	1122.28	70
5	600.99	38
6	1153.88	57
7	2382.43	115
8	679.30	33
9	805.50	42
10	808.50	41
11	1091.80	66
12	1462.35	85
13	891.28	51
14	1383.20	71
15	1081.45	51
16	1253.72	60
17	1183.25	51
18	1795.98	72
19	1420.96	59
20	755.36	67
21	1402.22	38
22	1165.07	58
23	1461.23	73
24	791.44	40
25	1550.44	80
26	615.25	33
27	2781.23	141
28	211.42	13
29	1173.46	71
30	982.45	60
31	54.53	3
32	1001.75	61
33	2450.39	149

Table E4. Average concentration (kBq/ml) received by the total liver for each treatment.

Treatment number	Average kBq/ml	Mean liver dose (Gy)
1	377.54	48
2	673.42	33
3	1047.89	51
4	899.39	42
5	461.16	39
6	858.28	22
7	866.67	45
8	937.42	23
9	665.03	51
10	781.09	44
11	1121.44	57
12	650.77	39
13	663.92	40

Table E5. Dosimetry parameters for all 33 analyzed lesions.

Lesion	Volume (cm3)	Min. dose (Gy)	Max. dose (Gy)	Mean dose (Gy)	D98 (Gy)	D95 (Gy)	D70 (Gy)	D2 (Gy)	V50 (%)	V30 (%)	Visual accumulation tumor area	Lesion progression	Time to end of lesion follow-up
1	99	0	374	58	4	7	29	196	46	68	Yes	Yes	25
2	37	1	410	82	6	13	51	213	71	85	Yes	No	25
3	29	3	351	66	13	18	41	174	59	54	Yes	No	25
4	180	7	201	70	20	27	52	137	72	93	Yes	Yes	26
5	74	3	162	38	5	7	22	127	26	52	No	Yes	26
6	45	2	173	57	6	14	38	127	53	80	Yes	Yes	6
7	11	31	211	115	42	55	97	183	97	100	Yes	Yes	6
8	50	0	178	33	0	1	15	112	22	46	Yes	Yes	6
9	26	0	244	42	1	1	7	1932	30	42	Yes	No	184
10	413	3	195	41	8	11	28	97	30	66	Yes	Yes	22
11	12	31	160	66	34	41	53	119	79	100	Yes	Yes	25
12	4	40	120	85	43	54	75	118	97	100	Yes	No	27
13	2	22	78	51	22	26	41	78	50	91	No	Yes	27
14	376	3	217	71	15	21	53	141	73	90	Yes	Yes	7
15	6	17	120	51	18	21	33	102	51	82	Yes	No	28
16	4	19	108	60	21	21	44	106	65	88	Yes	No	28
17	71	3	171	51	8	11	28	139	45	68	Yes	No	40
18	51	14	188	72	25	31	54	139	76	95	Yes	No	40
19	38	10	117	59	17	24	48	103	67	92	Yes	No	40
20	7	2	163	64	7	10	39	150	57	82	Yes	No	13

Lesion	Volume (cm3)	Min. dose (Gy)	Max. dose (Gy)	Mean dose (Gy)	D98 (Gy)	D95 (Gy)	D70 (Gy)	D2 (Gy)	V50 (%)	V30 (%)	Visual accumulation tumor area	Lesion progression	Time to end of lesion follow-up
21	333	0	352	38	1	2	15	139	26	47	Partial	Yes	13
22	5	25	150	67	27	29	49	141	70	93	Yes	No	22
23	272	2	269	73	10	14	44	185	64	83	Yes	No	22
24	10	17	71	40	19	21	32	65	25	73	Yes	No	22
25	15	14	182	80	20	25	62	147	80	93	Yes	No	18
26	18	6	91	33	8	11	24	75	15	53	No	No	18
27	24	8	349	141	16	23	98	296	86	92	Yes	No	18
28	742	0	139	13	0	0	3	63	4	11	No	Yes	5
29	326	0	301	71	2	6	42	184	64	78	Yes	Yes	5
30	120	4	251	60	11	15	37	159	53	78	Yes	Yes	5
31	27	0	33	3	0	0	0	16	0	0	No	Yes	5
32	100	12	199	61	23	28	46	124	63	93	Yes	Yes	5
33	32	50	275	149	77	88	120	248	100	100	Yes	Yes	5

Table E6. Patient and disease characteristics together with treatment, dosimetry and progression information for each included patient.

Treatment	Gender	Age	Tumor burden (%)	Metastases at other sites	Injected activity (MBq)	Accumulation tumor area	Progression	New liver lesions	Progression other than liver	Mean liver dose (Gy)	Death or last FU alive
1	Male	66	22.35	No	1520	Yes	Yes (25 weeks)	No	Yes (16 weeks)	48	99 weeks
2	Male	68	13.74	No	1537	Partial	Yes (26 weeks)	No	Yes (4 weeks)	33	28 weeks
3	Female	64	3.08	Yes	634 (partial)	Yes	Yes (6 weeks)	Yes (6 weeks)	Yes (6 weeks)	51	12 weeks
4	Male	56	2.73	No	2070	Yes	No	Yes (87 weeks)	Yes (24 weeks)	42	184 weeks
5	Male	59	30.14	No	2015	Partial	Yes (13 weeks)	No	No	39	21 weeks
6	Male	61	5.55	Yes	1750 (partial)	Partial	Yes (6 weeks)	Yes (27 weeks)	Yes (14 weeks)	22	59 weeks
7	Female	63	15.75	No	1525 (partial)	Yes	Yes (3 weeks)	Yes (3 weeks)	No	45	28 weeks
8	Male	52	39.24	No	2272	Yes	Yes (28 weeks)	Yes (15 weeks)	Yes (15 weeks)	23	75 weeks
9	Male	80	89.97	Yes	1640	Partial	Yes	No	Yes (13 weeks)	51	13 weeks
10	Male	56	16.48	Yes	1987	Yes	No	No	Yes (4 weeks)	44	22 weeks
11	Male	60	6.29	No	1160	Partial	No	No	No	57	18 weeks
12	Male	74	20.00	No	2400	Partial	Yes (5 weeks)	No	No	39	13 weeks
13	Male	57	22.00	No	2200	Partial	Yes (5 weeks)	No	Yes (5 weeks)	40	24 weeks

Appendix F. Experiment respiratory gated 90Y PET/CT

The scanning protocol for performing respiratory gated ^{90}Y-PET/CT scans was tested with means of the CIRS Dynamic Thorax Phantom, Model 008A (CIRS Inc., Norfolk, VA, USA). The phantom represents an average human thorax in shape, proportion and composition. In the lung region of the phantom a lung tissue-like cylindrical rod can be inserted, which can be moved by a powered actuator thereby simulating thorax movements.

Methods and materials

Phantom

The CIRS Dynamic Phantom simulates respiratory movements. The phantom is used in combination with the corresponding software (Figure F1), in which the parameters for the respiratory motions can be determined. The amplitude and cycle time of the actuator were set to 10 mm and 4 seconds, simulating a regular respiratory movement.

^{90}Y chloride

A bottle filled with 10 ml of YCl_3 (0.089 MBq/ml) was positioned outside of the movable cylindrical rod. Normally, activity is positioned within the rod, but the bottle did not fit and therefore was positioned outside of the rod (Figure F2).

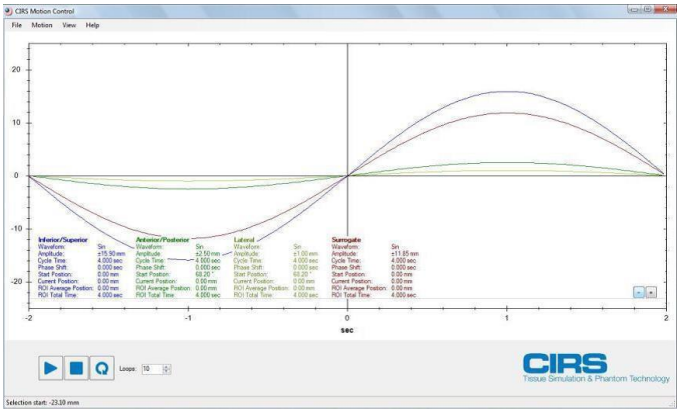

Figure F1. Example of CIRS software settings for amplitude and cycle time [70].

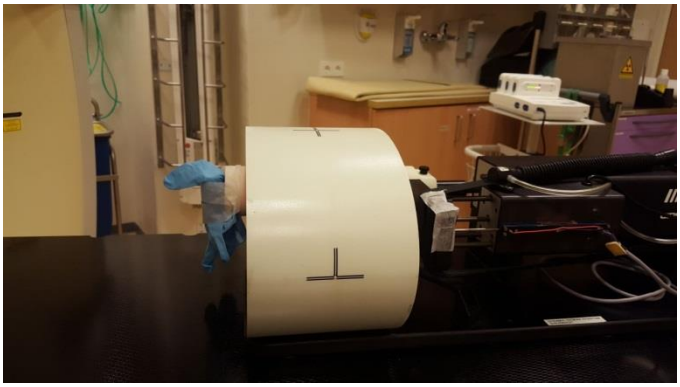

Figure F2. Measurement setup; the activity was positioned outside of the phantom in a blue glove.

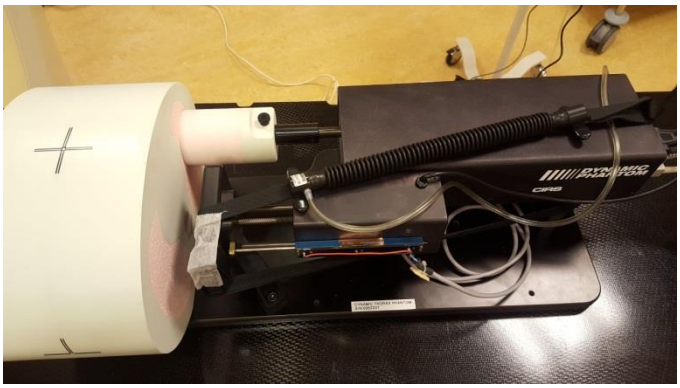

Figure F3. Measurement setup; the strain-gauge belt is placed around the actuator.

Detection of the respiratory movements

Clinically a respiratory monitoring device (Breath Hold ES RMD, Medspira, Minneapolis, USA) is used to detect respiratory movements. It consists of a strain-gauge belt, which is positioned around the waist of patients. The strain-gauge belt was positioned around the actuator (Figure F3), in that way registering the simulated breathing motions.

PET/CT acquisition

The CIRS phantom was scanned with the Philips Gemini TF Big bore PET/CT scanner, originating from 2012 (Philips Medical Systems, Cleveland, OH, USE). Respiratory gated PET/CT is used in the NKI-AVL for research purposes in patients treated with radiotherapy for lung metastasis. The clinical scanning protocol for this was adapted to be applied to the liver area in ^{90}Y-PET/CT scans. The clinical scanning protocol for ^{90}Y-PET scans is 15 minutes per bed position. Therefore, the 4D protocol was set to 3 minutes, which corresponds with 15 minutes per bed position. The PET/CT data was divided into 10 breathing phases, registered by the waist belt. Afterwards, image reconstruction was performed in software

tools developed at our institute.

Results

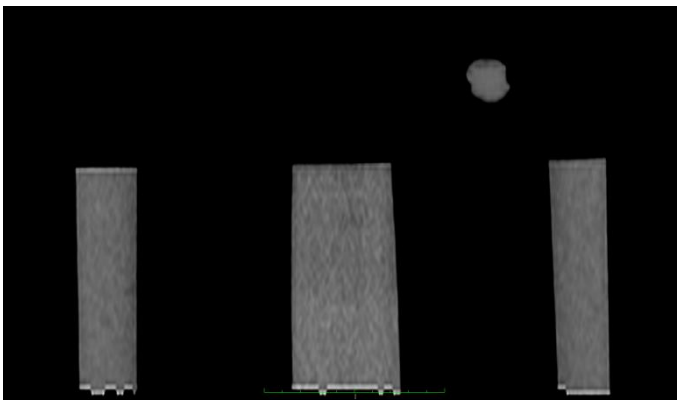

Figure F4. 4D CT image of CIRS phantom and bottle with activity on top. Black compartments in the phantom are the simulated lungs.

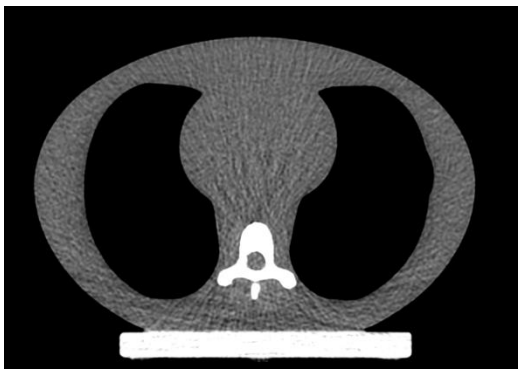

Figure F5. 4D CT image of breathing phantom with backbone and lungs.

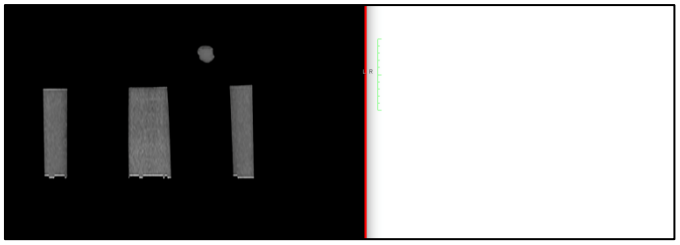

Figure F6. 4D CT (left) and PET (right) reconstruction.

Discussion and conclusion

The measurements were performed without technical failures. It was possible to reconstruct a 4D PET and CT scan (Figure F4-F6). No activity was detected by the PET scanner and therefore no activity was observed in the 4D PET scan. Unfortunately, the activity concentration was too low to be detected by the scanner, because this experiment was

performed at the same moment as the first calibration experiment from chapter one. In which some of the used activity concentrations were too low to be detected by the scanners.

Appendix G. METC approval form

LIST OF ABBREVIATIONS AND RELEVANT DEFINITIONS

AE	**Adverse Event**
AR	**Adverse Reaction**
CA	**Competent Authority**
CRC	**Colorectal cancer**
DSMB	**Data Safety Monitoring Board**
DVF	**4D deformation vector field**
EU	**European Union**
EudraCT	**European drug regulatory affairs Clinical Trials**
FOV	**Field of view**
IC	**Informed Consent**
METC	**Medical research ethics committee (MREC); in Dutch: medisch ethische toetsing commissie (METC)**
MidP	**Mid position scan**
PET	**Positron emission tomography**
(S)AE	**(Serious) Adverse Event**
SIRT	**Selective internal radiotherapy**
Sponsor	**The sponsor is the party that commissions the organisation or performance of the research, for example a pharmaceutical company, academic hospital, scientific organisation or investigator. A party that provides funding for a study but does not commission it is not regarded as the sponsor, but referred to as a subsidising party.**
SUSAR	**Suspected Unexpected Serious Adverse Reaction**
Wbp	**Personal Data Protection Act (in Dutch: Wet Bescherming Persoonsgevens)**
WMO	**Medical Research Involving Human Subjects Act (in Dutch: Wet Medisch-wetenschappelijk Onderzoek met Mensen**

SUMMARY

Rationale: ^{90}Y radioembolisation is an internal radiation therapy of which the effectiveness and safety has been demonstrated extensively, over 18.000 patients in more than 150 centres worldwide have been treated with ^{90}Y radioembolisation. The emergence of post-treatment dosimetry is of importance in future therapy optimization and patient selection. However, respiratory movements can cause severe degradation in PET/CT images that lead to incorrect dose measurements. Respiratory compensated (4D) PET/CT could be of value to overcome these artefacts in post-treatment dosimetry. Through this study we aim to assess the usability and clinical value of respiratory-gated ^{90}Y-PET/CT compared to traditional PET/CT in patients with colorectal liver metastases treated with ^{90}Y radioembolisation.
Objective: The primary objective is to evaluate the technical feasibility and assess the clinical value of using respiratory-gated ^{90}Y-PET/CT for post-treatment dosimetry in patients with colorectal liver metastases treated with ^{90}Y radioembolisation. The secondary objective is to assess scan quality of the respiratory gated ^{90}Y-PET/CT, by letting a nuclear physician assess the two reconstructions made; with and without respiratory compensation. For the following parameters, the physician will state which one of the two reconstructions is better: presence of artefacts, alignment of the liver between the PET and CT scan, visibility of Tumor(s) and delineation of Tumor(s).
Study design: The proposed study is a non-randomized prospective single center feasibility study (Antoni van Leeuwenhoek, Amsterdam), aimed to prove the technical feasibility and clinical value of using respiratory-gated ^{90}Y-PET/CT for post-treatment dosimetry in patients with colorectal liver metastases treated with ^{90}Y radioembolisation.
Study population: All patients who are eligible for radioembolisation can enter the study. Patients must have met all inclusion and exclusion criteria of this study. The NKI-AVL treats ±15 patients a year with means of radioembolisation, therefore the inclusion will be done within 2 years. The study will have no follow up after the treatment.
Main study parameters/endpoints: The main parameters of this study are Tumor volume, maximal tissue dose to healthy and Tumor tissue and absorbed Tumor dose.
Nature and extent of the burden and risks associated with participation, benefit and group relatedness: Participation in this study has no significant risks. Patients will receive a respiratory gated ^{90} Yttrium PET/CT scan, which is about 10 minutes longer than a regular ^{90}Yttrium PET/CT scan. During this respiratory gated scan an additional 4D CT scan is made, which takes 100 seconds. The expected additional radiation exposure caused by this 4D CT scan is 50 mSv . This extra radiation exposure does not induce a significant risk in these patients with liver metastases, treated with the salvage treatment of radioembolisation

INTRODUCTION AND RATIONALE

In 2016 over 15.000 new cases of colorectal cancer (CRC) were reported in the Netherlands and almost 5000 deaths were reported in 2015 due to CRC [2]. About 50% of all CRC patients develop metastases, most of which are located in the liver during the course of their disease. When these metastases are not treated, the median survival rate of these patients is less than 8 months [3]. Roughly 25-50% of the patients with advanced CRC are considered eligible for lesion or partial liver resection, which is aimed to be curative (5-year survival rates of 30-60% have been reported). Comorbidities, extensive disease load or lesion location can cause the metastases to be classified as 'irresectable'. A subgroup of these patients will still be considered for non-surgical local therapies such as radiofrequency ablation or stereotactic radiotherapy. Local therapies are often combined with systemic treatments such as capecitabine, oxaliplatin or irinotecan, or targeted systemic treatments such as cetuximab or bevacicumab. When these first and second line treatment options fail, the next step in treatment is dependent on previous treatment and extensiveness of the disease.

Radioembolisation

In the Netherlands, Yttrium-90 (^{90}Y) radioembolisation is a salvage treatment option that has recently been approved by 'Zorg Instituut Nederland'. Radioembolisation, also called selective internal radiotherapy (SIRT), is an internal radiation therapy in which ^{90}Y–loaded resin (SIR-spheres®) or glass (Theraspheres®) microspheres are delivered transarterially to hepatic malignancies. The microspheres are injected selectively into the hepatic artery using a catheter and become lodged in the microvasculature surrounding the liver Tumor [4]–[7]. Accordingly, high radiation doses are delivered to the Tumor, whereas healthy liver parenchyma remains mostly unaffected. The rationale behind the treatment is based on the perfusion mismatch between parenchyma, which is perfused by the portal vein, and Tumor lesions, which are primarily perfused by the hepatic artery.

The effectiveness and safety has already been demonstrated in several studies [6], [10]–[13], [32]–[37]. Over the past decades more than 18.000 patients in more than 150 centers worldwide have been treated with ^{90}Y radioembolisation, either in salvage setting or in combination with chemotherapy [5]. Radioembolisation is well tolerated by patients, even if they already have had several types of treatments and can be combined safely with additional systemic treatments. In a comparative study by Bester *et al.,* the median survival after radioembolisation was significantly higher compared to the control group who received standard of care (11.9 vs. 6.3 months, respectively) [71]. Seidensticker *et al.* also reported a significant, though much lower, survival rates after radioembolisation (8.3 vs. 3.5 months, respectively) [14]. So in general, 3-7 months is gained on average compared to standard care [6].

The complete radioembolisation procedure consists of 5 steps; the planning angiography, pre-treatment nuclear imaging, dose calculation, treatment angiography and post-treatment nuclear imaging. During the initial angiography, the abdominal arterial vasculature will be

depicted, with specific focus on the vasculature of the liver lesions. A ‘test dosage’ of Technetium-99m (^{99m}Tc) labelled albumins is administered at the proposed arterial injection site of the microspheres. Immediately after angiography, patients are transferred to the nuclear medicine department to visualize the distribution of the ^{99m}Tc-particles. These images are used to exclude the presence of shunting to the lungs or accumulation of radioactivity in the intestinal tract, which are both contraindication for the eventual radioembolisation. Additionally, these images are used to calculate the actual dosage of ^{90}Y, and subsequently, the patient is scheduled for the second angiography during which the ^{90}Y microspheres are administered. Within one day after therapy, ^{90}Y positron emission tomography (PET) is performed to assess whether the ^{90}Y microspheres have reached the tumor and if any extrahepatic accumulations are visible. At present, these images are only visually assessed at the NKI-AVL, and no quantification of uptake is performed.

During treatment follow-up with diagnostic CT three aspects are described: response/ progression of the hepatic lesions, the emergence of new lesions and the presence of (new) extrahepatic lesions [6].Rosenbaum *et al.* reported in a systematic review that in only 18-46% of the patients complete or partial response is observed after radioembolisation [25], [72]. This phenomenon of limited response is not only frequently described in literature, it is also seen in our clinical practice (Figure G1 and G2). Still, the origin of this heterogeneous response in metastatic CRC is not yet understood. It is hypothesized that it can be due to under-dosing of specific patients, differences in phenotype or tumor heterogeneity.

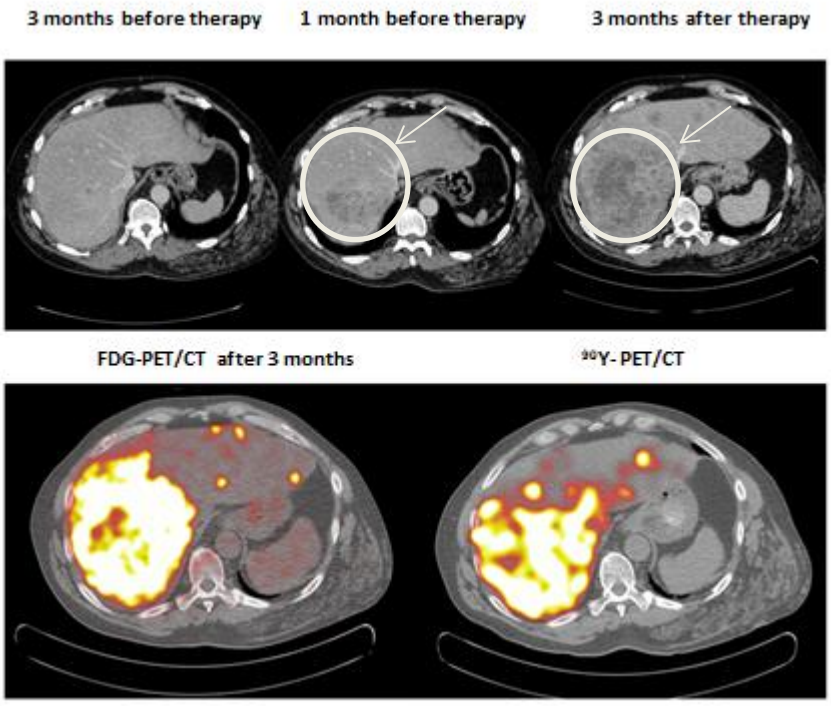

Figure G1. Example of a very poor local response to radioembolisation. This patient has extensive liver metastases, which keep growing despite chemotherapy. An adequate microsphere accumulation in and around the liver lesions is observed after radioembolisation at the ^{90}Y-PET/CT scan (^{90}Y-dose 1.7 GBq, total liver volume 3200ml, estimated tumor volume 980ml). However, new hepatic lesions are observed at the FDG PET/CT scan after three months [6].

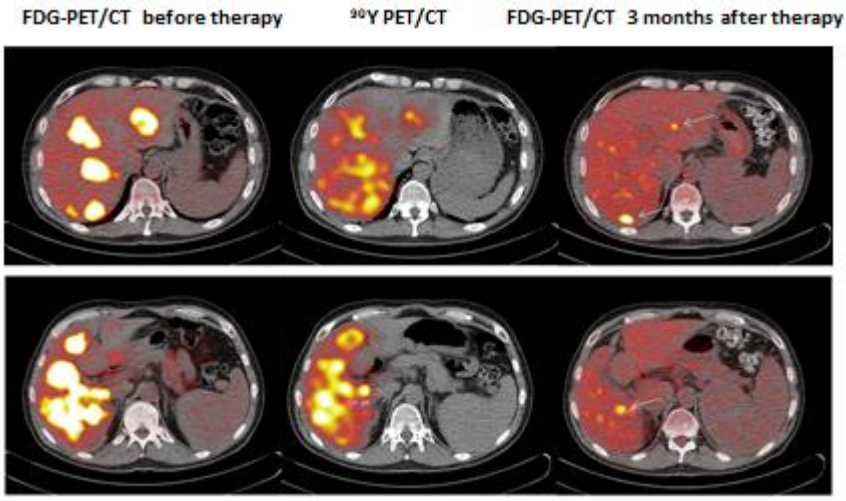

Figure G2. Example of a good local response to radioembolisation. This patient was diagnosed with a metastasized sigmoid carcinoma and has had multiple lines of chemotherapy. An adequate microsphere accumulation in and around the liver lesions is visible after radioembolisation at the ^{90}Y-PET/CT (^{90}Y-dose 2.0 GBq, total liver volume 1600ml, estimated tumor volume 620ml). A very good response is seen at the FDG PET/CT after three months [6].

Post-treatment dosimetry in ^{90}Y radioembolisation

Dosimetry is the calculation of the activity that needs to be administered to achieve a desired absorbed dose or the calculation of the actual absorbed dose after administration of a radioactive dosage. Post-treatment dosimetry is not routinely performed in radioembolisation but could bring us a step closer in determining the optimal, patient specific therapeutic dose for radioembolisation as it specifies the dose-response relationship in radioembolisation. At this moment, data about the relation between absorbed Tumor dose and therapy outcome is very limited [26]. Besides that, post-treatment dosimetry can reveal that a Tumor has not received the calculated amount of radiation and therefore needs additional treatment, thus also directly providing benefit for the individual patient. Quantification of absorbed doses in radioembolisation has long been considered impossible, due to the inadequate quality of ^{90}Y-PET images [26]. Recently, ^{90}Y-PET/CT has been introduced in the clinical practice and has become the standard modality used for post-treatment imaging [27]. The first case study with ^{90}Y-PET was published in 2009 [6]. Since then, the feasibility of ^{90}Y-PET was established and it was concluded that ^{90}Y has a superior resolution compared to Bremsstrahlung SPECT, which results in improved quantification possibilities [6], [26]. In 2013 the ^{90}Y-PET/CT has been clinically introduced in the AVL and is used in the standard work-up of radioembolisation procedure. At this moment, retrospective dose quantification of all patients treated between 2013 and 2017 is already performed in the AVL to relate clinical outcome to absorbed tumor dose. Based on these initial efforts, it can be concluded that the image quality is still not optimal due to the low positron branching ratio of ^{90}Y together with the respiratory movements of the liver. In order to optimize dose quantification and determine the optimal and patient specific therapeutic dose for radioembolisation, a higher image quality is desired.

Respiratory compensated PET/CT

As a result of respiratory motion of the diaphragm, the liver may displace 15 mm on average (maximum of 50mm) [49]. During the lengthy PET-acquisition protocols (10-40 minutes), these respiratory movements cause degradation of the PET-signal. The signal that arises from a lesion will be diluted over the trajectory of the displacement, leading to loss of contrast, underestimation of tracer uptake and an overestimation of the lesion volume [50]. In addition, the customary use of a snap-shot 3D CT for attenuation correction of the PET signal causes inaccuracies. Using 4D CT to attenuate the motion-correlated PET signal, phase-by-phase, provides more accurate, quantitative PET images.

One of the options to incorporate breathing motions is the respiratory-gated PET scan (4D-PET). In this technique the acquisition of the PET/CT scan is synchronized with the patients respiratory cycle [50]. Monitoring the respiratory cycle can be performed in several ways; by means of a pressure sensor, spirometry system, strain-gauge belt, temperature sensor, opto-electronic system [50]. At the AVL we have clinically implemented respiratory compensated 4D-PET/CT using a strain-gauge belt that is positioned around the chest of the patient. The diagnostic benefit of this technique has been assessed in our institution for lung cancer [52],

[53], [55]–[57], [73]–[75] and liver lesions [52], [58]–[62], [75]. In this way, no PET signal is lost to acquisition in contrast to methods that only acquire signal during the exhale phase in which motion is limited. At the AVL we have developed a technique to combine the different PET phases to one time-averaged, motion-compensated 3D PET scan without signal lost. Examples of motion compensated PET/CT scans are given in figure G3 and G4. Respiratory compensated 4D-PET/CT algorithms have not yet been used in ^{90}Yttrium PET/CT scans, but will likely also lead to the desired higher contrast images and better quantification possibilities especially when lesions are located in close proximity to the diaphragm.

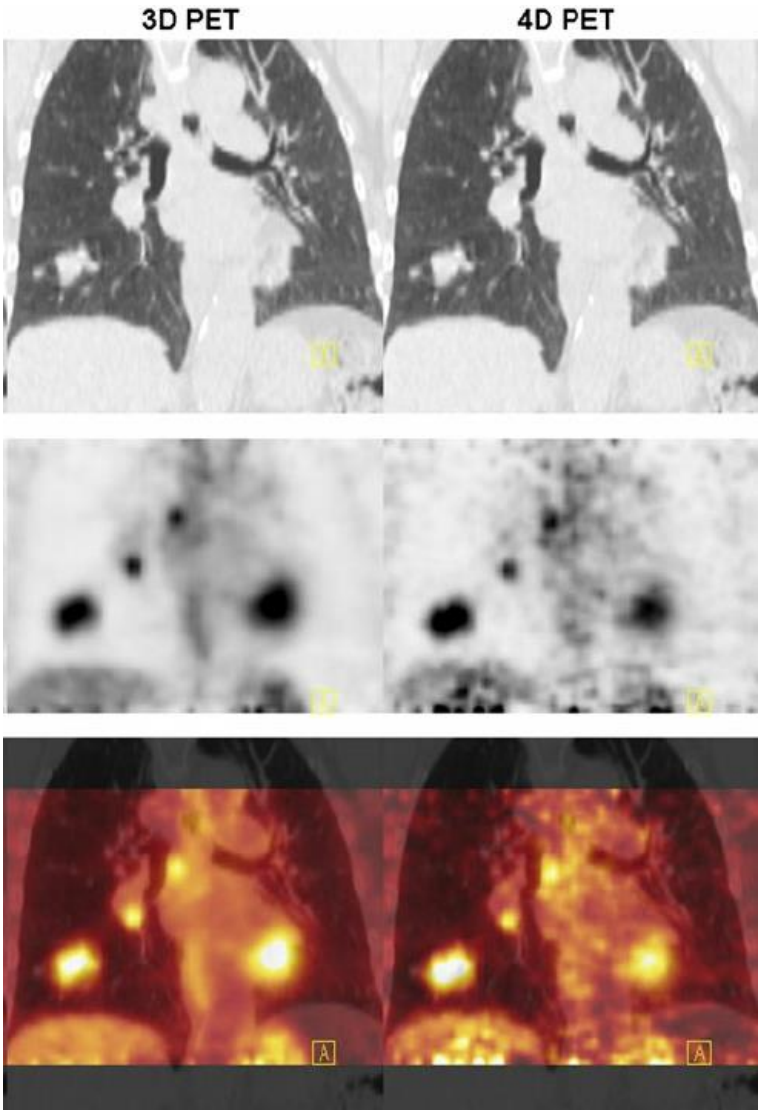

Figure G3. A respiratory compensated (4D) PET/CT acquisition (right) and a regular 3D PET/CT acquisition (left). CT images (top), PET images (middle) and coregistered PET/CT images (bottom), demonstrating the effect of breathing motion on Tumor delineation. On the motion-compensated PET/CT it is observed that lesions are easier to identify, mostly due to the higher contrast in this image [76].

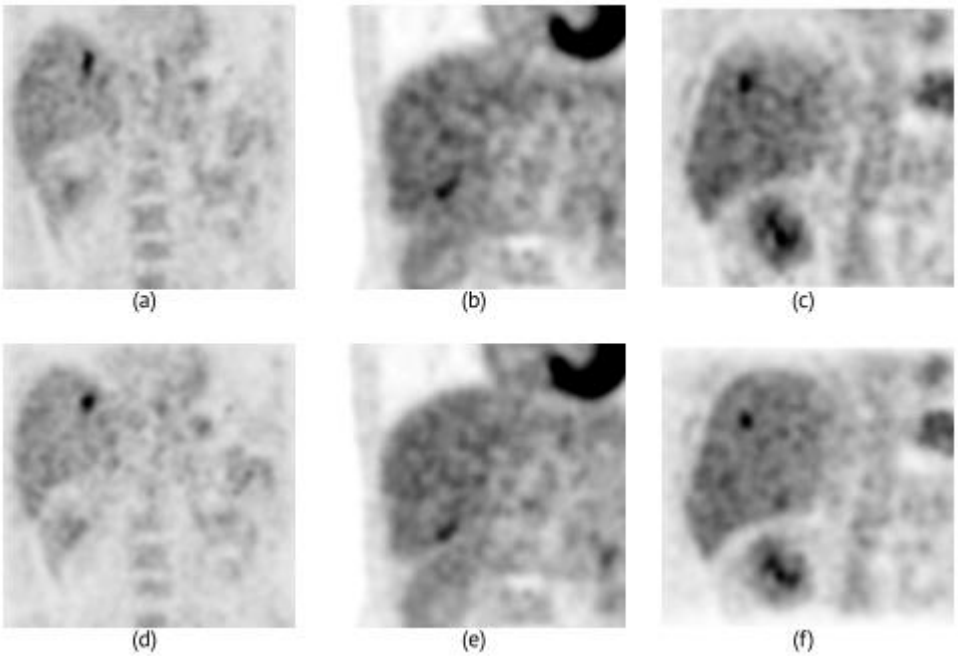

Figure G4. Three patient examples of differences between 3D-PET/CT images (top) and respiratory compensated PET/CT images (bottom). In the first patient (a),(d) it is clearly seen that Tumor activity is more focused after motion compensation. In the second patient, (b),(e) a more clear distinction between the liver and the kidney is seen. In the third patient, (c),(f) the target lesion is more clearly delineated after motion compensation [49].

Study rationale

^{90}Y radioembolisation is an internal radiation therapy of which the effectiveness and safety has been demonstrated extensively, over 18.000 patients in more than 150 centres worldwide have been treated with ^{90}Y radioembolisation. The emergence of post-treatment dosimetry is of importance in future therapy optimization and patient selection. However, respiratory movements can cause severe degradation in PET/CT images that lead to incorrect dose measurements. Respiratory compensated (4D) PET/CT could be of value to overcome these artefacts in post-treatment dosimetry. Through this study we aim to assess the usability and gain insight into the clinical value of respiratory-gated ^{90}Y-PET/CT compared to traditional PET/CT in patients with colorectal liver metastases treated with ^{90}Y radioembolisation.

OBJECTIVES

Primary Objective:

To evaluate the technical feasibility and gain insight into the clinical value of using respiratory-gated ^{90}Y-PET/CT for post-treatment dosimetry in patients with colorectal liver metastases treated with ^{90}Y radioembolisation.

Secondary Objective(s):

To assess scan quality of respiratory-gated ^{90}Y-PET/CT scans.

STUDY DESIGN

The proposed study is a non-randomized prospective single center feasibility study (Antoni van Leeuwenhoek, Amsterdam), aimed to prove the technical feasibility and gain insight into the clinical value of using respiratory-gated ^{90}Y-PET/CT for post-treatment dosimetry in patients with colorectal liver metastases treated with ^{90}Y radioembolisation.

A total of 15 patients already undergoing ^{90}Y radioembolisation are asked to undergo respiratory gating during the standard post-treatment PET/CT. Patients will be asked to participate in this study, receive written patient information and an informed consent form, prior to their treatment of radioembolisation.

4D PET/CT acquisition

As in the standard clinical scanning protocol patients will undergo a ^{90}Y-PET/CT scan within a day after treatment with radioembolisation. In addition to the regular scan, a strain-gauge belt will be positioned around the chest of patients to record their breathing motions. As part of the study an additional 4D-CT (100 mAs, 10 phase) will be made of the liver region. This will take a maximum of 100 seconds, and results in an extra radiation burden of 50 mSv. Different tube currents have been used in the past at our institute for 4D PET/CT of the liver region. A tube current of 30 and 40 mAs (figure G6) led to obvious ring artefacts in the CT images, whereas a tube current of 100 mAs did not cause these artefacts (figure G5).

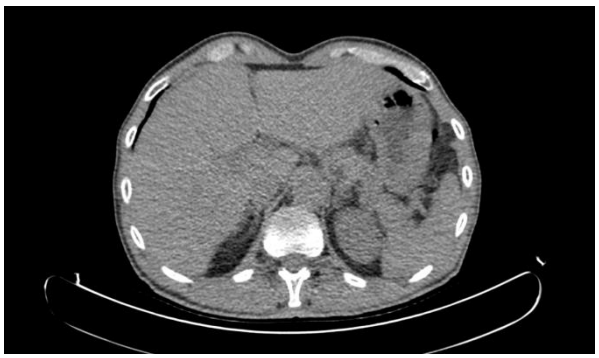

Figure G5. 4D CT of the liver made with 100mAs. No ring artefacts are seen.

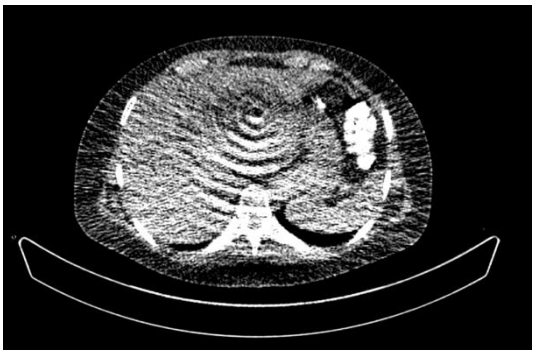

Figure G6. 4D CT of the liver made with 30mAs. Ring artefacts are seen.

For all patients the regular reconstruction algorithm and the respiratory compensated algorithm are applied afterwards (see section 5.3 for more detailed information). The standard reconstruction will be used for clinical evaluation, whereas the respiratory compensated reconstruction will only be used for research purposes. The difference in Tumor volume, maximal tissue dose (D_{max}) for healthy and Tumor tissue and absorbed dose (V_{50} and D_{70}) between the two reconstructed scans will be analysed. Furthermore, a nuclear physician will assess the two reconstructions made; with and without respiratory compensation. The physician will state which one of the two reconstructions shows more artefacts, has a better alignment for the liver between the PET and CT scan, better visibility of Tumor(s) and has a better Tumor(s) delineation.

STUDY POPULATION

Population (base)

All patients who are eligible for radioembolisation can enter the study. Patients must have met all inclusion and exclusion criteria of this study. The NKI-AVL treats ±10 patients a year with means of radioembolisation, therefore the inclusion will be done within 2 years. The study will have no follow up after the treatment.

Inclusion criteria

In order to be eligible to participate in this study, a subject must meet all of the following criteria:

- Patients who have given written informed consent
- Patients have to be clinically suitable for ^{90}Y radioembolisation (work-up conform standard clinical treatment protocol)
- Patients older than 18 years

Exclusion criteria

A potential subject who meets any of the following criteria will be excluded from participation in this study:

- Patients who cannot lie still for 45 minutes (average duration of an ^{90}Y-PET/CT)

Sample size justification

The aim of this study is based on a technical feasibility and initial clinical usability assessment. Although a formal sample size calculation may not be appropriate in this study, a justification of the sample size will be provided.

Given that ^{90}Y-PET is quite different from the standard ^{18}F-PET, from a technical point of view, we first need to optimize the imaging workflow and determine if our proposed protocol is technically feasible. To answer this question, we will perform an interim analysis after the first 5 patients and determine whether or not the tube current should be raised. If the acquisition and reconstruction protocols prove technically feasible, we will include another 10 patients to eventually assess clinical usability based on the 15 patients in total.

METHODS

Study parameters/endpoints

Main study parameter/endpoint

The main objective is to evaluate the technical feasibility and to gain insight into the clinical value of respiratory-gated ^{90}Y-PET/CT for post-treatment dosimetry in patients with colorectal liver metastases treated with ^{90}Y radioembolisation.

> **Outcome measure:** Technical feasibility is defined as the ability to determine the following parameters: Tumor volume, maximal tissue dose (D_{max}) to healthy and Tumor tissue and absorbed Tumor dose (V_{50} and D_{70}). In order to get insight into the clinical value, the mentioned parameters will be compared for the regular and 4D reconstruction of the ^{90}Y-PET/CT scan.

Secondary study parameters/endpoints (if applicable)

The secondary objective is to assess scan quality, a nuclear physician will assess the two reconstructions made; with and without respiratory compensation.

> **Outcome measure:** For the following parameters, the physician will state which one of the two reconstructions is better: presence of artefacts, alignment of the liver between the PET and CT scan, visibility of Tumor(s) and delineation of Tumor(s).

Randomisation, blinding and treatment allocation

> No randomisation or treatment allocation is applied.

Study procedures

Respiratory gated ^{90}Y-PET/CT

Within a day after radioembolisation with ^{90}Yttrium, patients will undergo a respiratory-correlated ^{90}Y-PET/CT scan instead of the regular ^{90}Y-PET/CT scan. The difference for patients will be that they will wear a strain-gauge belt around their waist, just below the ribs, that will register their breathing movements during the acquisition of the scan. Figure G7 shows an example of the registration of a patients breathing motion.

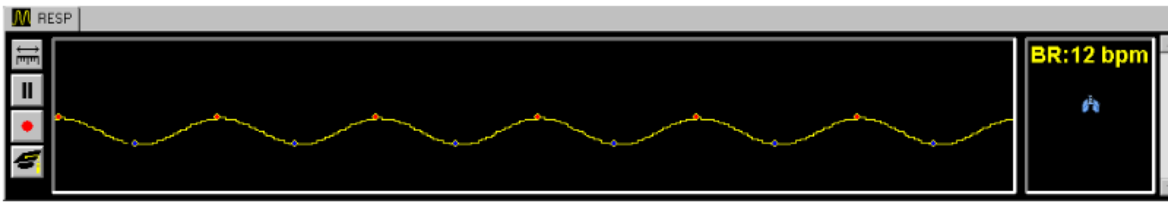

Figure 5. Registration of breathing cycle with means of a belt around the waist.
The acquisition protocol of the ^{90}Y-PET/CT scan consists of 4 different subparts:

1. An expiration-breath-hold surview scan of the liver.
2. Low-dose 3D CT scan
3. 4D-PET scan. Each patient is scanned for 2 bed positions, 15 minutes each. No Yttrium isotope pre-set is present on the PET/CT scanners, therefore the isotope Germanium is used (clinical scanning protocol).
4. 4D CT-scan, duration is one minute, only for the 2 bed positions.

Reconstruction

The 4D PET/CT data will be divided into 10 breathing phases, for which the breathing cycle is registered by the waist belt. This respiratory cycle is checked manually before the following 4 steps are performed.

1. 4D CT reconstruction. For each breathing phase a CT reconstruction is made, this results effectively in 10 different 3D CT reconstructions.
2. 4D PET reconstruction. The PET scan is also reconstructed for each of the 10 breathing phases. The attenuation in each frame of the PET data is corrected with the corresponding 4D CT frame.
3. Creating the MidP CT scan. The 10 different CT reconstructions made in step 1 are deformed to the time-averaged position and combined, resulting in an artificial 3D CT dataset, representing the time-averaged 3D CT dataset. This set is called the mid-position (MidP) CT scan.
4. Creating the MidP PET scan. The 10 different PET reconstructions made in step 2 are deformed using the vector fields calculated in step 3, resulting in an artificial 3D PET dataset, representing the time-averaged 3D PET dataset. This set is called the mid-position (MidP) PET scan [49].

The MidP CT and PET scan can then be viewed and used as regular reconstructions.

Regular reconstruction

Besides the motion-compensated datasets the conventional 3D reconstructions of the ^{90}Y-PET/CT images are made on the 3D low-dose CT scan. The reconstruction voxel size of the PET data is 4x4x4mm, the voxel size for the CT data is 1x3x3 mm. These datasets are used for clinical follow-up.

Determination of Tumor volume

The liver and tumors in the liver will be segmented semi-automatically on the pre-treatment made high-dose CT scan. Segmentation based on the low-dose CT scan made during the ^{90}Y-PET/CT scan is almost impossible, due to the lower quality.

Determination of absorbed and maximal tissue dose

Firstly, the high-dose CT scan will be registered to the low-dose CT scan of the ^{90}Y CT scan. Secondly, the absorbed tissue dose is calculated based on the segmented structures, the D_{max}, V_{50} and D_{70} will be determined for liver lesions and for healthy liver tissue.

D_{max} = maximal received tissue dose.

V_{50} = Percentage of lesion volume receiving at least 50Gy.

D_{70} = Dose to 70% of the lesion volume.

Assessment by nuclear physician

A nuclear physician will assess the two reconstructions made; with and without respiratory compensation. For the following parameters, the physician will state which one of the two reconstructions is better: presence of artefacts, alignment of the liver between the PET and CT scan, visibility of Tumor(s) and delineation of Tumor(s).

Withdrawal of individual subjects

Subjects can leave the study at any time for any reason if they wish to do so without any consequences. The investigator can decide to withdraw a subject from the study for urgent medical reasons.

Replacement of individual subjects after withdrawal

<Not applicable>

Premature termination of the study

The study will be terminated when the investigators become aware of factors that prevent reaching the described aims. In that case, the METC and included patients will be informed according to current guidelines.

SAFETY REPORTING

Temporary halt for reasons of subject safety

In accordance to section 10, subsection 4, of the WMO, the sponsor will suspend the study if there is sufficient ground that continuation of the study will jeopardise subject health or safety. The sponsor will notify the accredited METC without undue delay of a temporary halt including the reason for such an action. The study will be suspended pending a further positive decision by the accredited METC. The investigator will take care that all subjects are kept informed.

AEs, SAEs and SUSARs

Adverse events (AEs)

Adverse events are defined as any undesirable experience occurring to a subject during the study, whether or not considered related to [the investigational product / trial procedure/ the experimental intervention]. All adverse events reported spontaneously by the subject or observed by the investigator or his staff will be recorded.

Serious adverse events (SAEs)

A serious adverse event is any untoward medical occurrence or effect that

- results in death;
- is life threatening (at the time of the event);
- requires hospitalisation or prolongation of existing inpatients' hospitalisation;
- results in persistent or significant disability or incapacity;
- is a congenital anomaly or birth defect; or
- any other important medical event that did not result in any of the outcomes listed above due to medical or surgical intervention but could have been based upon appropriate judgement by the investigator.

An elective hospital admission will not be considered as a serious adverse event.

The sponsor will report the SAEs through the web portal *ToetsingOnline* to the accredited METC that approved the protocol, within 7 days of first knowledge for SAEs that result in death or are life threatening followed by a period of maximum of 8 days to complete the initial preliminary report. All other SAEs will be reported within a period of maximum 15 days after the sponsor has first knowledge of the serious adverse events.

Suspected unexpected serious adverse reactions (SUSARs)

<Not applicable>

Annual safety report

<Not applicable>

Follow-up of adverse events

All AEs will be followed until they have abated, or until a stable situation has been reached. Depending on the event, follow up may require additional tests or medical procedures as indicated, and/or referral to the general physician or a medical specialist. SAEs need to be reported till end of study within the Netherlands, as defined in the protocol

STATISTICAL ANALYSIS

All the data will be collected and analysed within the NKI-AVL. The findings will be in descriptive manner.

Primary study parameter(s)

The main parameters will be determined for each metastasis in the liver; Tumor volume, maximal tissue dose (D_{max}), absorbed Tumor dose (V_{50} and D_{70}). No further statistical analysis is performed in this feasibility stage

Secondary study parameter(s)

Scan quality will be assessed through the following parameters: presence of artefacts, visibility liver, visibility of Tumor(s) and delineation of Tumor(s).

Interim analysis

After 5 subjects an interim analysis is performed to assess the technical feasibility of the acquisition and reconstruction protocol when scanned with 40mAs. When the scans are proven to be of good quality, it will be concluded that the scanning protocol is technical feasible and another 10 patients will be included to assess clinical usability.

ETHICAL CONSIDERATIONS

Regulation statement

The study will be conducted according to the principles of the Declaration of Helsinki and in accordance with the Medical Research Involving Human Subjects Act (WMO) and other guidelines, regulations and Acts.

Recruitment and consent

Patients will be asked by their treating physician. Patients will receive verbal and written information and will be provided with a minimum of 24 hours to consider participation.

Objection by minors or incapacitated subjects (if applicable)

<Not applicable.>

Benefits and risks assessment, group relatedness

Participation in this study has no significant risks. Patients will receive a respiratory gated ^{90} Yttrium PET/CT scan, which is in total 10 minutes longer than a regular ^{90} Yttrium PET/CT scan. The 4D CT scan will be scanned with 100mAs, which will lead to an additional radiation exposure of 50mSv for patients. The average activity administered during radioembolisation is 2GBq, which leads to an estimated dose of 60Gy in patients. The 50mSv is inferior compared to the dose already received during radioembolisation. This extra radiation exposure does not induce a significant risk in these patients with liver metastases treated with the salvage treatment of radioembolisation.

Compensation for injury

The sponsor/investigator has a liability insurance which is in accordance with article 7 of the WMO. The sponsor (also) has an insurance which is in accordance with the legal requirements in the Netherlands (Article 7 WMO). This insurance provides cover for damage to research subjects through injury or death caused by the study. The insurance applies to the damage that becomes apparent during the study or within 4 years after the end of the study.

Incentives (if applicable)

<Not applicable>

ADMINISTRATIVE ASPECTS, MONITORING AND PUBLICATION

Handling and storage of data and documents

Data will be handled confidentially and anonymously. This way of handling of personal data complies with the Dutch Personal Data Protection Act (in Dutch: De Wet Bescherming Persoonsgegevens, Wbp).

Monitoring and Quality Assurance

Not applicable

Amendments

Amendments are changes made to the research after a favourable opinion by the accredited METC has been given. All amendments will be notified to the METC that gave a favourable opinion.

A 'substantial amendment' is defined as an amendment to the terms of the METC application, or to the protocol or any other supporting documentation, that is likely to affect to a significant degree:

- the safety or physical or mental integrity of the subjects of the trial;
- the scientific value of the trial;
- the conduct or management of the trial; or
- the quality or safety of any intervention used in the trial.

All substantial amendments will be notified to the METC and to the competent authority.

Non-substantial amendments will not be notified to the accredited METC and the competent authority but will be recorded and filed by the sponsor.

Annual progress report

The sponsor/investigator will submit a summary of the progress of the trial to the accredited METC once a year. Information will be provided on the date of inclusion of the first subject, numbers of subjects included and numbers of subjects that have completed the trial, serious adverse events/ serious adverse reactions, other problems, and amendments.

Temporary halt and (prematurely) end of study report

The investigator/sponsor will notify the accredited METC of the end of the study within a period of 8 weeks. The end of the study is defined as the last patient's last visit. The sponsor will notify the METC immediately of a temporary halt of the study, including the reason of such an action. In case the study is ended prematurely, the sponsor will notify the accredited METC within 15 days, including the reasons for the premature termination. Within one year after the end of the study, the investigator/sponsor will submit a final study report with the results of the study, including any publications/abstracts of the study, to the accredited METC.

Public disclosure and publication policy

All results derived from this study will be disclosed unreservedly.

STRUCTURED RISK ANALYSIS

Participation in this study has no significant risks. The complaints and survival of patients will be determined entirely by their cancer, and its response to the standard treatment. The respiratory gated ^{90}Y-PET/CT scans acquired in this study have no impact on the diagnosis or treatment of the patients. The respiratory gated ^{90}Y-PET/CT scan will result in an extra 50 mSv for patients, which brings no significant risks in this population with cancer. The average activity administered during radioembolisation is 2GBq, which leads to an estimated dose of 60 Gy in patients. The 50 mSv is inferior compared to the dose already received during radioembolisation. This extra radiation exposure does not induce a significant risk in these patients with liver metastases treated with the salvage treatment of radioembolisation.

The results of this study will contribute to better dosimetry in radioembolisation and therefore to a more optimal determination of therapeutic doses in radioembolisation for future patients. In summary, the disadvantages of participation in the study are outbalanced by the potential benefit for future patients.

Appendix H. DOSIsoft dosimetry manual

Loading scans & generating a study

At this moment the DOSIsoft system is not connected to the internet, due to privacy safety reasons. The scans therefore need to be downloaded from the Osirix server and manually loaded into the DOSIsoft system. A study needs to be created before the tools of the software program can be used. Several 'studies' can be created for one patient.

Scan details

For radioembolisation, the following scans should be downloaded and loaded into the system:

1. Diagnostic CT
   Choose the most recent diagnostic CT scan made on which the target lesions are clearly visible. Choose the reconstruction with the most slices, for precision reasons. Furthermore, look on which reconstruction the lesions are best delineated. That is of importance for the segmentation later on.

2. Technetium MAA procedure
   a. SPECT AC without scatter correct
   b. Low dose CT (B30)

3. ^{90}Y-PET/CT
   a. Low-dose CT
   b. CTACT ^{90}Y-PET

Loading scans on the workstation

1. Select the 'Dicom list' icon on the desktop.

Figure H1. 'Dicom list' desktop pictogram

2. Select ‘ file’; ‘open folder’ and choose the right folder to select your data (Run/media/planet for USB ports) *or* drag your files from another folder to the ‘DICOM list’ screen. The system will now load your files, you can see the progression of that at the bottom of your screen. Multiple patients can be loaded into the system at once.

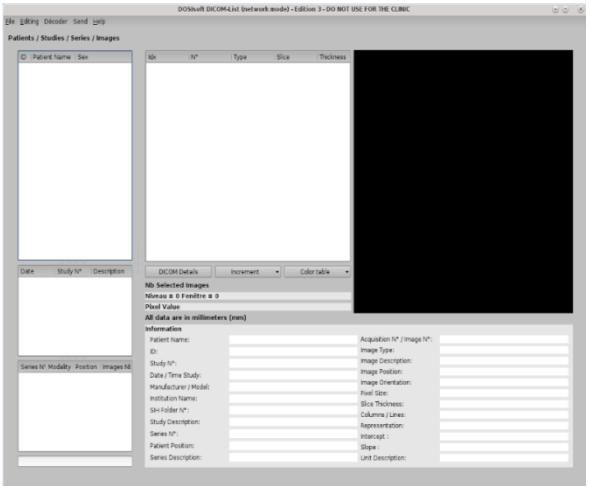

Figure H2. ‘Dicom list’ start screen. The ‘file’ button is seen in the upper left corner.

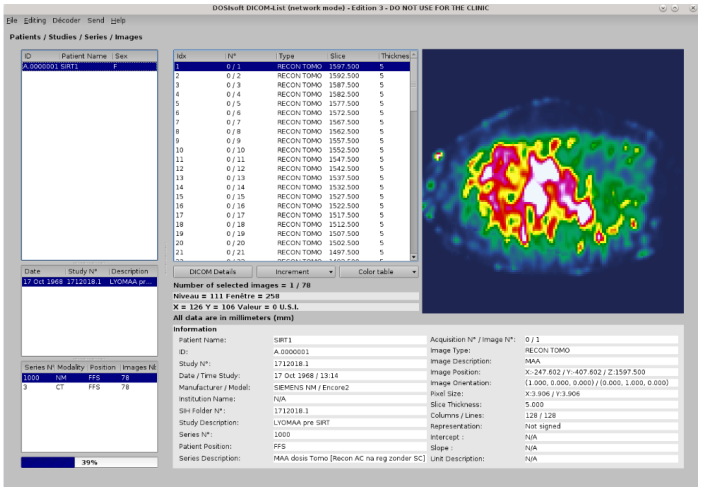

Figure H3. ‘Dicom list’ screen when loading the selected files. Patient and scan information is shown in the box in the right lower part of the screen. The three boxes on the left part of the screen show consecutively: patient, exam, scans in the exam.

3. Select ‘decoder selected *[patient/studies/serie/images]*’. It is the most convenient to decoder the selected patient at once, then all three scan types will be decoded. After decoding your files, they will be ready for use in the main working screen of DOSIsoft; ‘Planet DB Front’.

> **Warning:** brackets [ ] are not allowed in file names. They need to be removed from file names before the decoding process, otherwise they will generate an error.

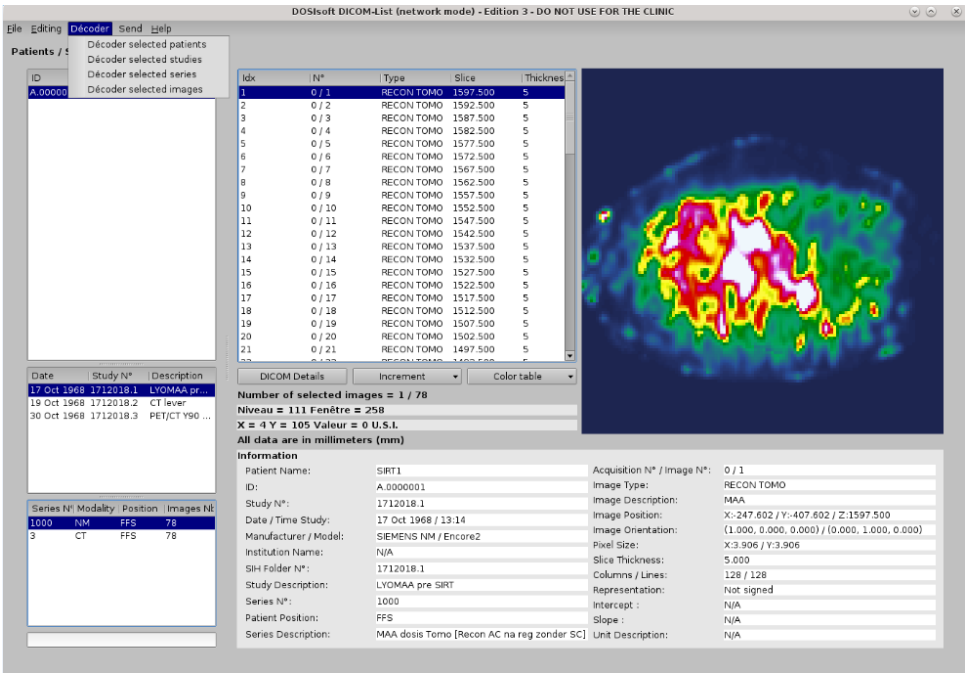

Figure H4. Screen shot of selecting the ‘decoder’ button.

Generate a study

1. Open ‘Planet DB front’ from the desktop and select your patient.

Figure H5. ‘Planet DB Front’ desktop pictogram

2. Select one of the scans available for this patient and press the right mouse button for selecting ‘create start PLANET onco’, this will open a new screen in which a study can be created.

3. Add all the needed scans to your patient study. For radioembolisation, the three mentioned type of scans need to be added to a study. When all studies are added to ‘longitudinal studies in progress’, you can finish creating the study by clicking ‘ok’. After creating a study, it will be present in the ‘studies’ box of your patient and can be used for data analysis.

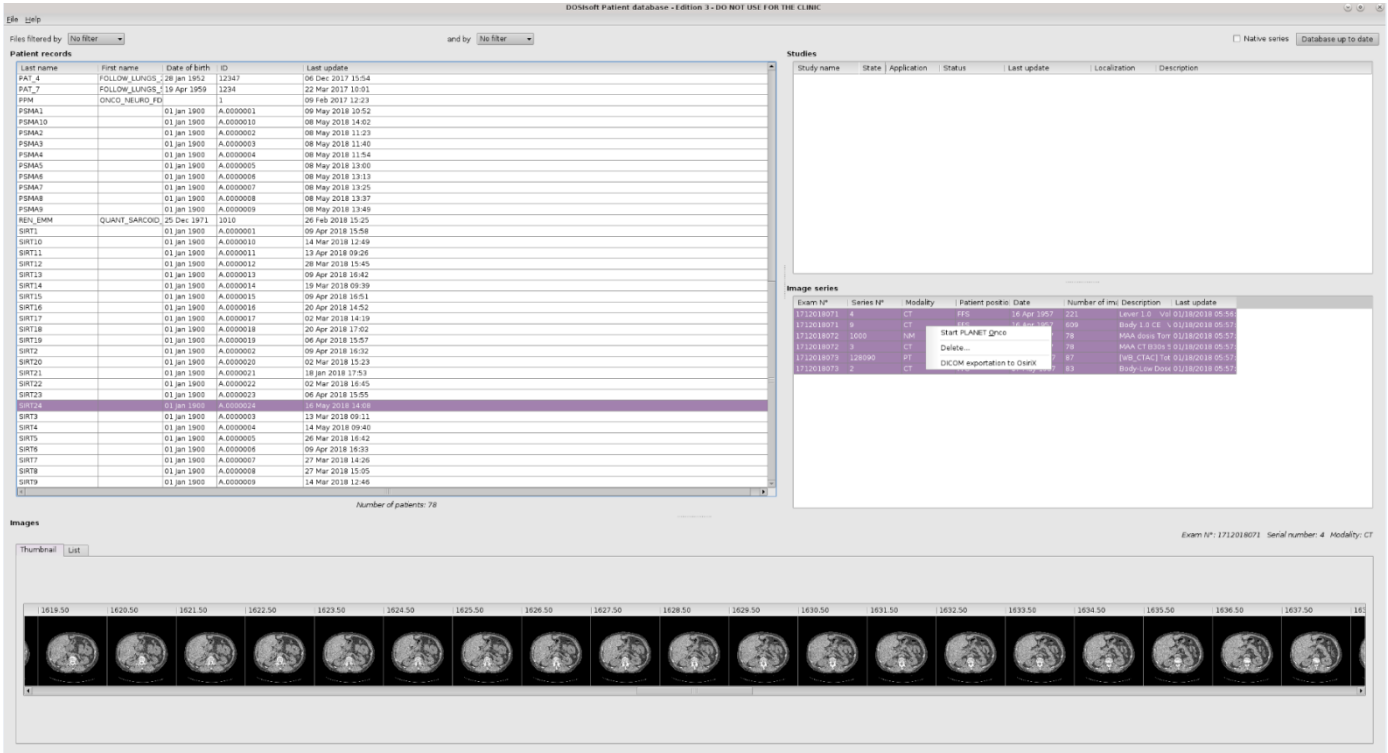

Figure H6. Planet Front starting screen. On the left a list of all patients in the database is seen. When a patient is selected, the scans available for this patient are shown in the right lower box. Studies created for a patient are shown in the upper right box.

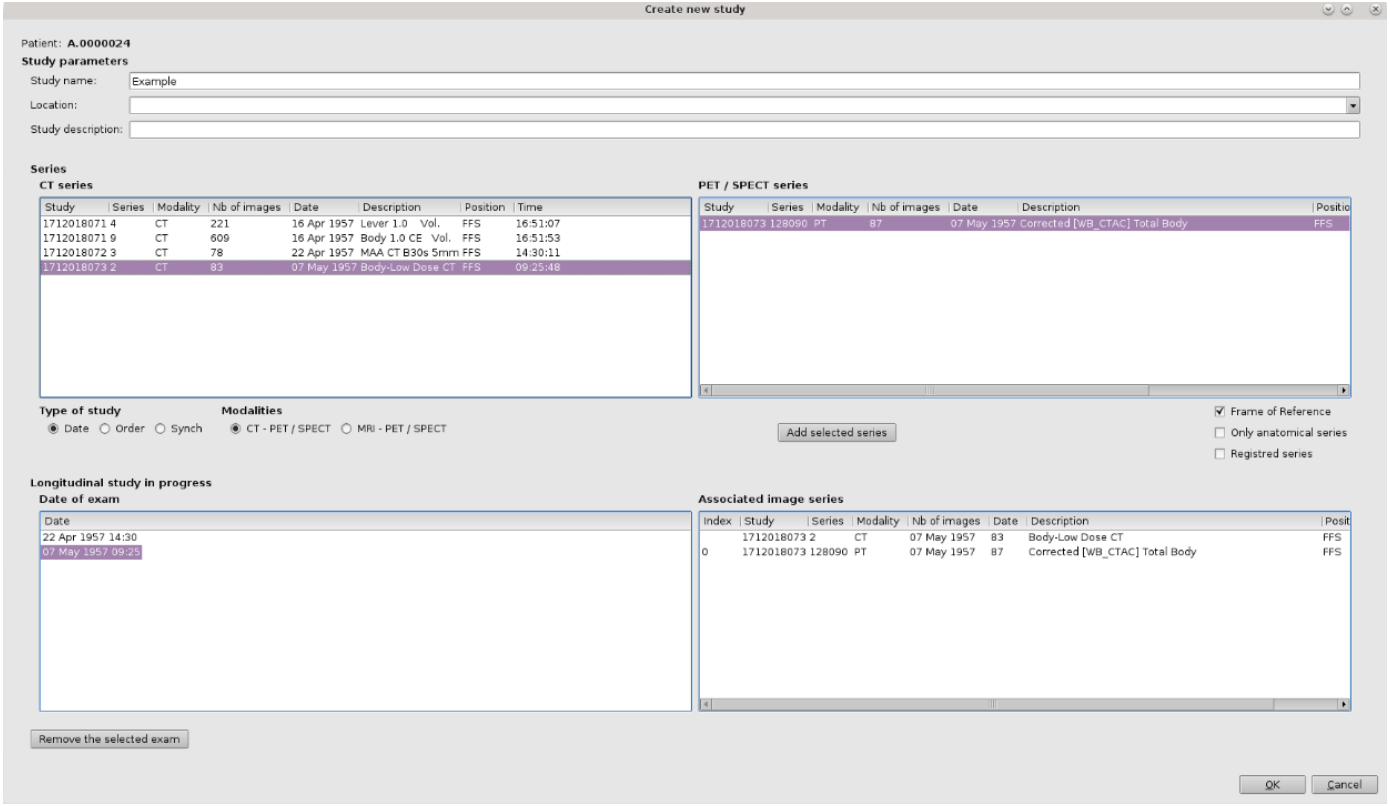

Figure H7. Adding the scans to a ‘study’.

Registration and segmentation

After creating a patient study, the study can be used for data analysis. Double click on the study to open the DOSIsoft Onco tool. In figure H8, an overview of the start screen is shown. The start screen consists of 4 views; transverse (upper left), frontal (lower left), sagittal (lower right) and 3D views (upper right) of scans are shown.

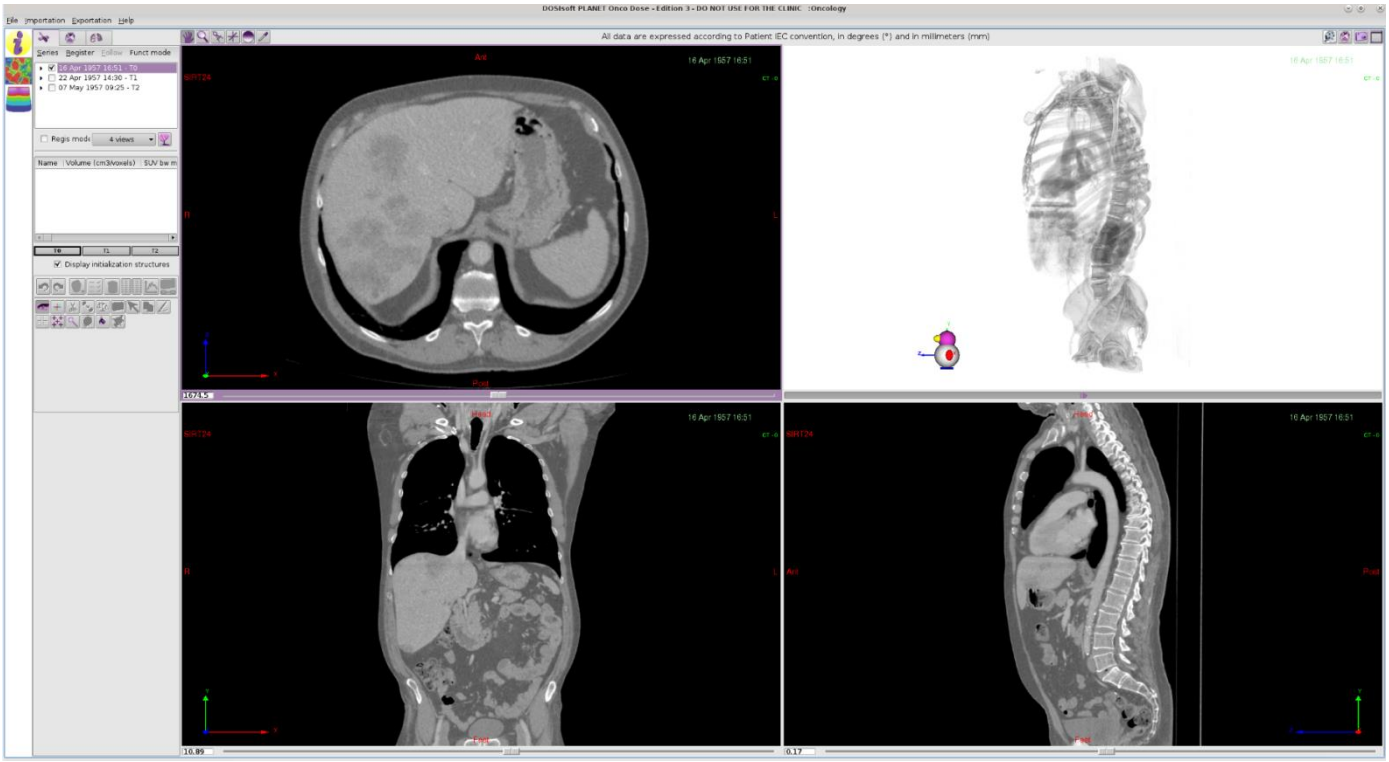

Figure H8. Overview of the DOSIsoft onco screen.

The main toolbox is located on the left side of the screen. In the red box (figure 9), it can be chosen to show the available scans in functional or anatomical mode. Functional mode is needed to view and work with functional scans, like PET scans. Anatomical mode is needed when working with anatomical views of the scans, for example when segmenting structures on CT. In the blue box, the available scans are shown, defined by T0, T1 and T2. Representing their chronological order; diagnostic CT, MAA scan, Yttrium PET scan. It is important that the diagnostic CT scan is the first scan in the system (T0), because the rest of the scans will be registered onto the first scan. Each of the scans can be viewed by selecting one of the scans.

Registration

1. The first step for the radioembolisation procedure is to register the three scans to each other. This is needed because the liver and Tumor(s) will be segmented based on the diagnostic CT scan, because of the better quality of this scan. The registration procedure starts by clicking on ‘Register’ as seen in the green box (figure H9).

2. Several options for the registration process are available, select ‘Rigid’ registration. This is done based on manually delineating the liver in the three views of the CT scans. After this semi-automatic rigid registration, the software automatically performs an elastic registration. Each of the two low-dose CT scans needs to be registered separately, so the procedure of registration has to be performed twice.

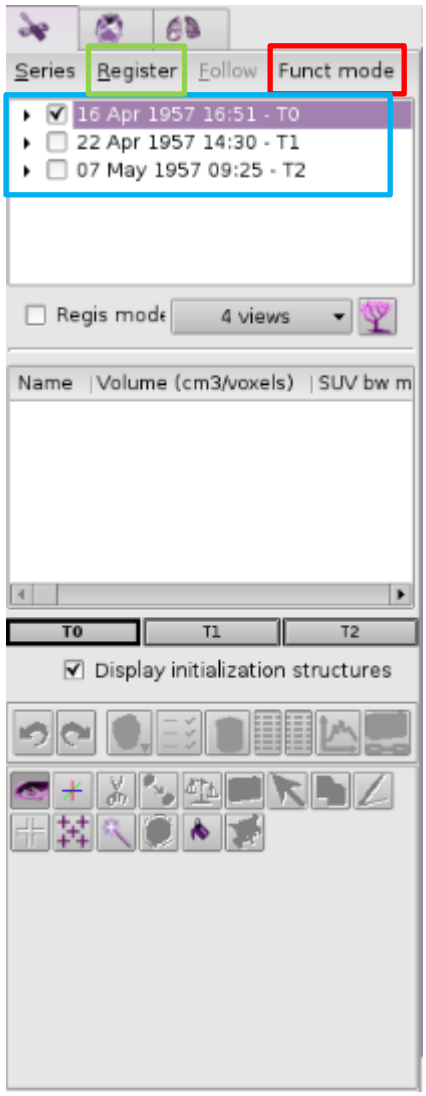

Figure H9. Overview left toolbox of DOSIsoft Onco.

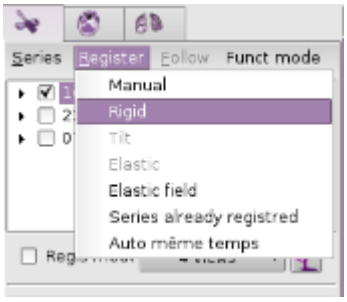

Figure H10. Selecting 'Rigid registration'.

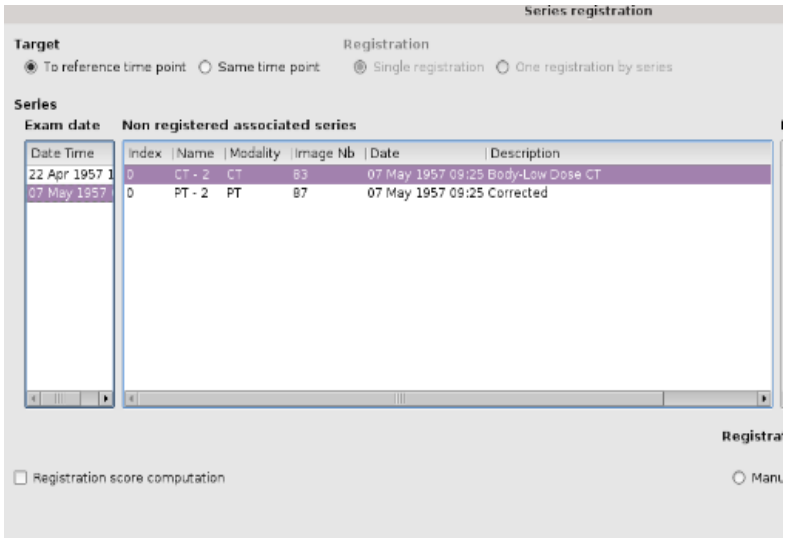

Figure H11. Choosing the CT scans to perform registration on. The process needs to be repeated to perform in on both CT scans (MAA and PET)

3. The semi-manual registration is performed by locating the 'bounding box' around the liver in each view and then clicking on 'Registration' on the left side of the screen, blue box.

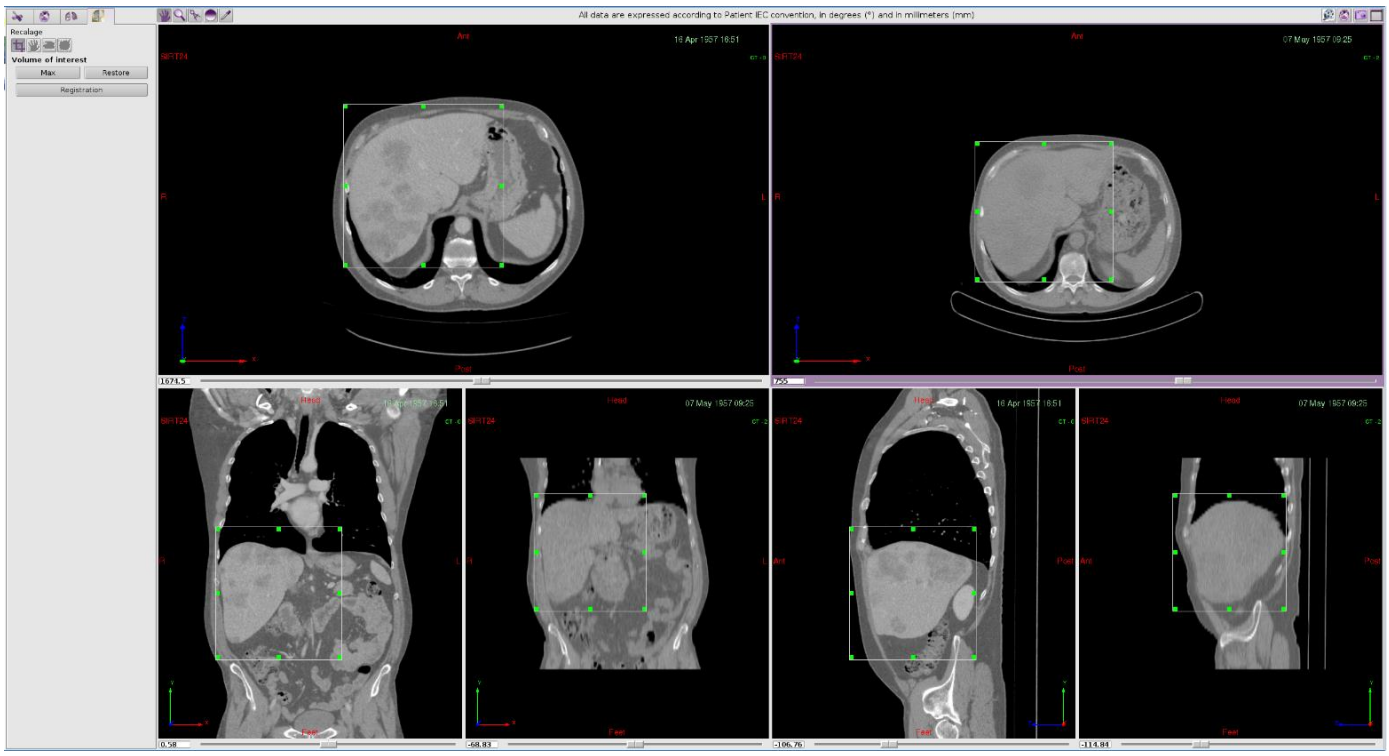

Figure H12. Performing the semi-manual registration by locating the ‘bounding box’ around the liver in each view.

4. In the next screen, the registration can be checked before saving the registration. The registration can be checked visually by clicking on the ‘eye’ icon on the left side of the screen.

Figure H13. Eye icon, which shows the registration visually.

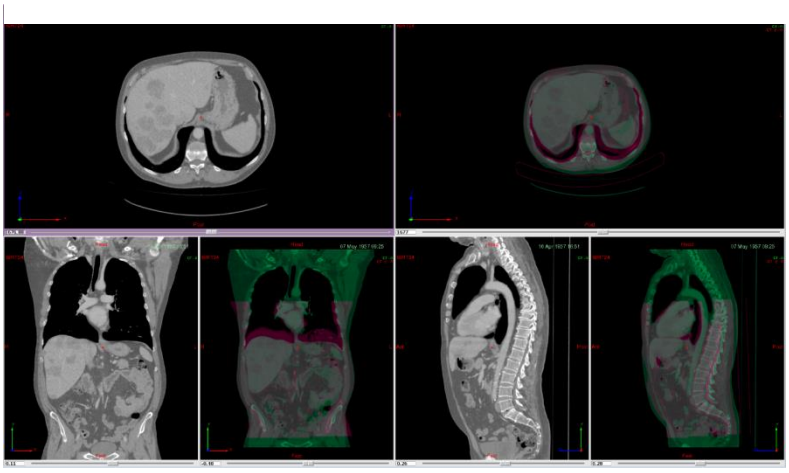

Figure H14. Assessing the registration visually

Warning: After saving a registration, the information about the registration (numbers and visual assessment) cannot be viewed again. Ideally, the information about the registration can be viewed after saving the registration. When dosimetry results are not ideal, one would like to take the accuracy of the registration into account.

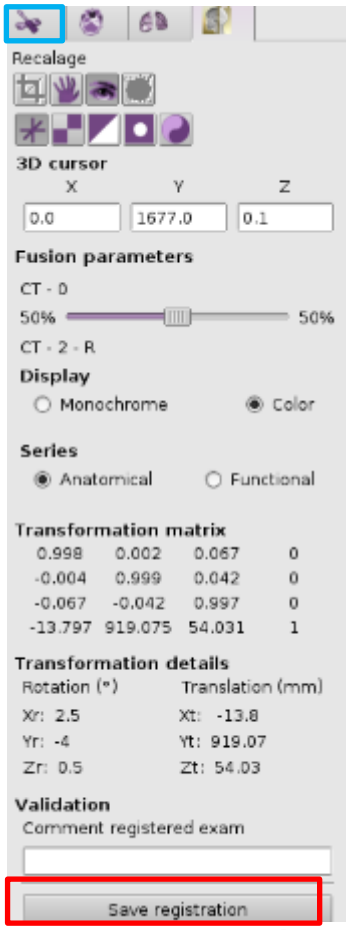

Figure H16. Saving the registration, red box, or returning to the home page, blue box.

5. Save the registration after reviewing the registration, red box. When you are not content with the results of the registration, click on the blue box to return to the starting screen. You can then start the registration process again.

Note: It is not possible to see the results of the registration process after saving the registration.

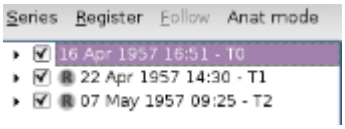

Figure H15. After registration, the registered scans will show a 'R' in front of them at the home page screen

Segmentation

The segmentation process can start when the three CT scans are registered onto each other. Segmenting will be performed on the diagnostic CT, due to the registration, these segmented structures can then be easily propagated to the other two scans. It is needed to segment the liver and all liver lesions separately, this is needed to perform dosimetry on each of these lesions separately.

1. First, a structure needs to be created. This is done by clicking on the heart shaped pictogram button, red box. A structure is created and becomes visible in the 'structures overview' screen, blue box. Names of structures can be changed later in the

segmentation process.

2. Segmentation can be done with several tools, green box. The segmentation process designed for the liver will be described, but look into the other segmentation options for the ideal segmentation tool for your purpose. Select the ‘Shape’ button (purple box), then select the ‘brush’ tool, yellow box. The brush tool has some segmenting presets, ‘liver’ and ‘liver tumor’ (orange box), in which automatically grey value thresholding is applied to regular values for the two tissues. These thresholding values can be manually changed when needed for correct segmentation, pink box.

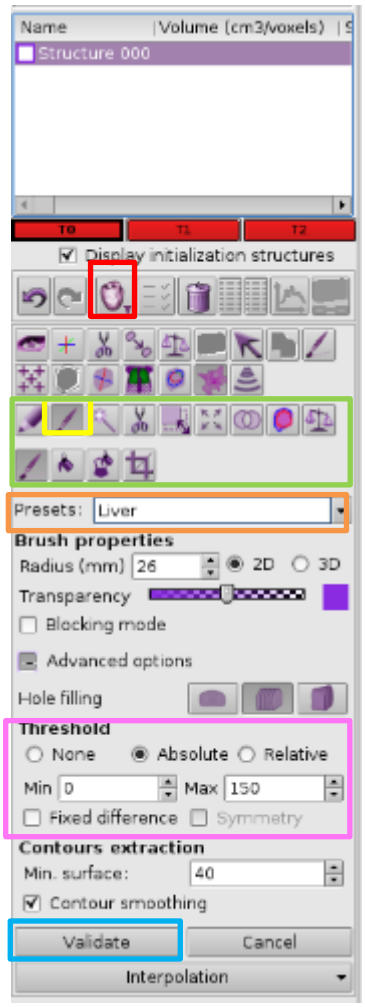

Figure H17. The segmenting toolbox

With the brush tool you can segment a structure, for example the liver on the transversal CT slices. An example is seen in figure H18. It is needed to segment a structure in every two/three slices, containing at least the first and last slide. In this way it is not needed to segment every slide separately. The last slices at both sides, or slices in which the structure changes a lot should be segmented on more slices, to make sure that the segmentation is accurate enough. The sagittal and frontal views can be used to check the correctness of your segmentation.

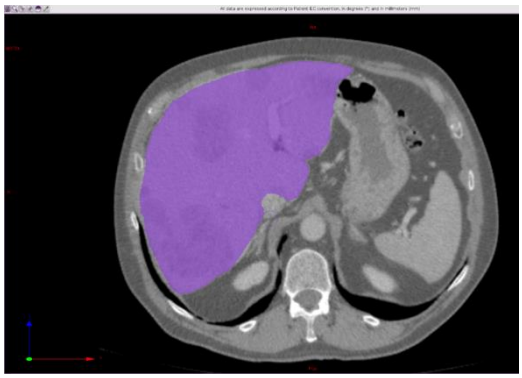

Figure H18. Example of segmenting the liver in one transversal slice.

When you have segmented the complete structure (liver, lesion), click on ‘Validate’, this will save your structure. After this, you should also perform ‘Interpolation’, dark green box. Select the ‘axial transverse’ option. Interpolation is needed, because not all the slices are segmented separately. You can change the name of your structure after you have validated it.

Figure H19. Interpolation options.

3. A structure can have two states: ‘initialization’ or ‘standard’, you have to make a structure ‘standard’ in order to analyze the data from a structure. Select the ‘pointer’ icon to change the status of your structure.

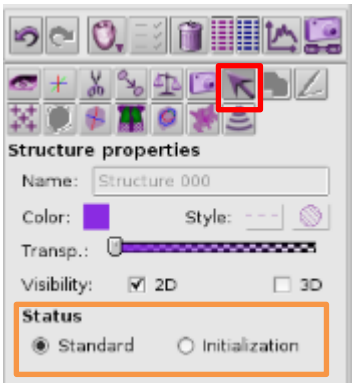

Figure H20. Changing the status of your structure

4. Create in the above described way structures for the liver and all liver lesions separately.

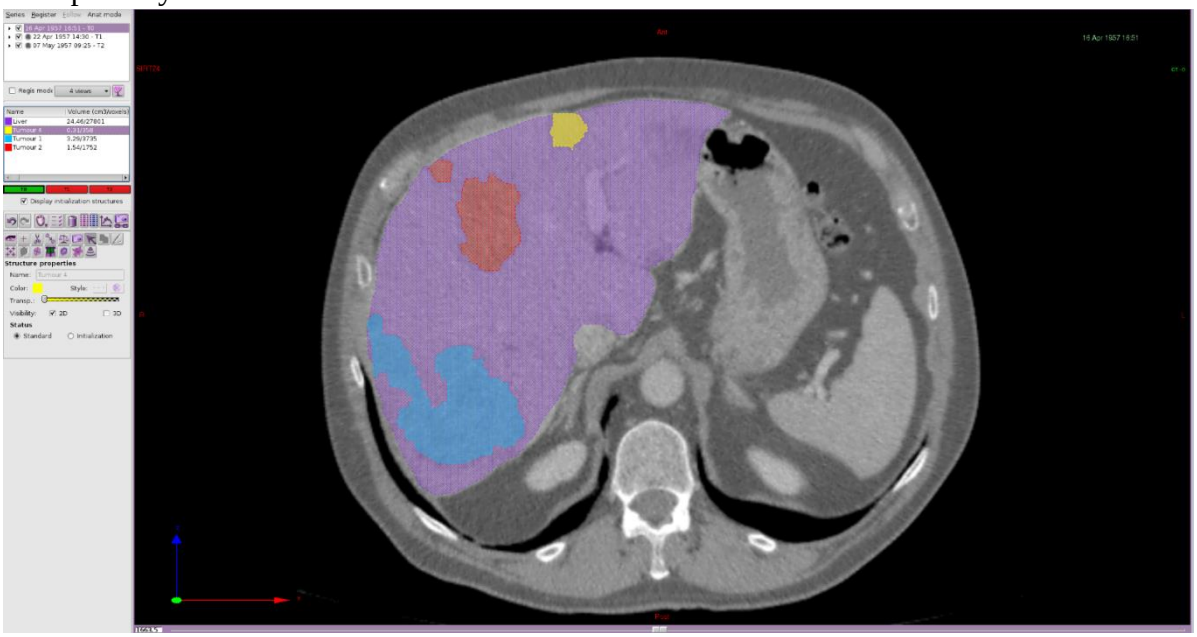

Figure H21. Segmented liver and liver lesions.

5. For dosimetry purposes, it is needed to create a structure for the healthy liver. It is not needed to segment this structure, it can be created from the already existing structures. In the toolbox menu after selecting the ‘shape’ button, select the button of the ‘two circles’, orange and red box. Add the structures already made into the Boolean operations menu. First, add the liver and afterwards the segmented liver lesions, blue box. Select the correct Boolean operation, yellow box, to subtract the volume of the lesions from the whole liver volume. Select ‘Apply’, green box, to create a new structure; ‘Healthy liver tissue’. Perform interpolation, dark blue box, also for this structure.

   Remark: if a liver contains necrotic ablation zones or other zones that are not perfused, like cysts, segment these structures too. It is desired to calculate the doses received by liver tissue. Tissue that is not perfused, will not receive any treatment and therefore should be not considered as healthy liver tissue or Tumor tissue.

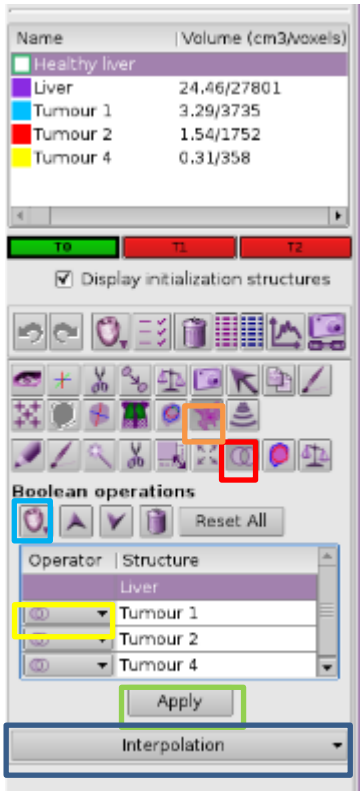

Figure H22. Creating a structure with use of a Boolean operation.

Dosimetry

Now that all structures on which dosimetry should be performed are segmented, dosimetry can be performed. For the dosimetry functionality of the DOSIsoft system, it is needed to transfer to another tab in the system, red box.

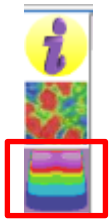

Figure H23. The system contains three tabs, the third one (red box) is the dosimetry tab.

Performing dosimetry

1. To perform dosimetry, a new treatment needs to be created (red box). In this treatment, a treatment step needs to be created (blue box).

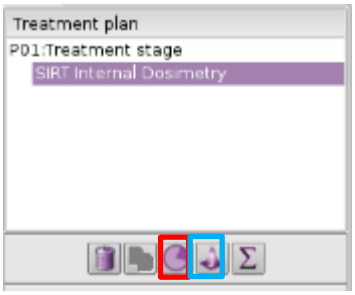

Figure H24. Creating a new treatment (red box) and a treatment step (blue box).

2. Select the scan on which you want to perform dosimetry, in this case PT-2, which is the ^{90}Y-PET/CT scan. The system automatically fills in the scan details, check if these details are correct (red box). A calibration factor is needed, due to the fact that our PET/CT scanners do not have an Yttrium isotope preset (blue box). This correction factor (27966.1) needs to be filled in manually in the blue box. The system then automatically calculates the injected activity, yellow box. This is the total amount of activity that the program can recover in the PET scan. This total activity can be compared to the total amount of activity truly administered. When agreeing on all the data provided, you can start the dosimetry calculations by pressing 'Compute' (green box).

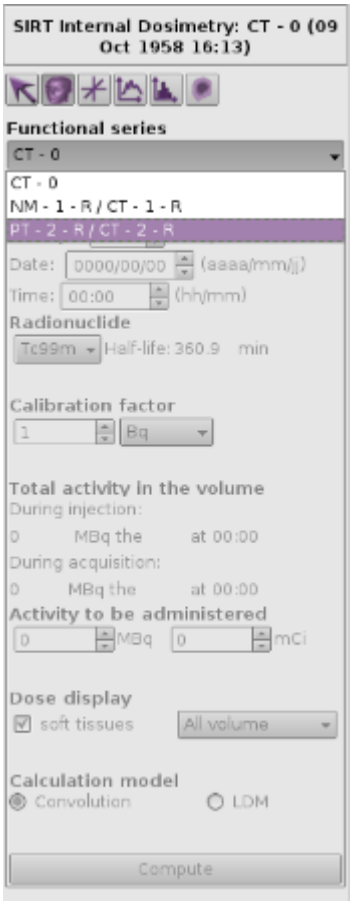

Figure H25. Selecting a scan to perform dosimetry on.

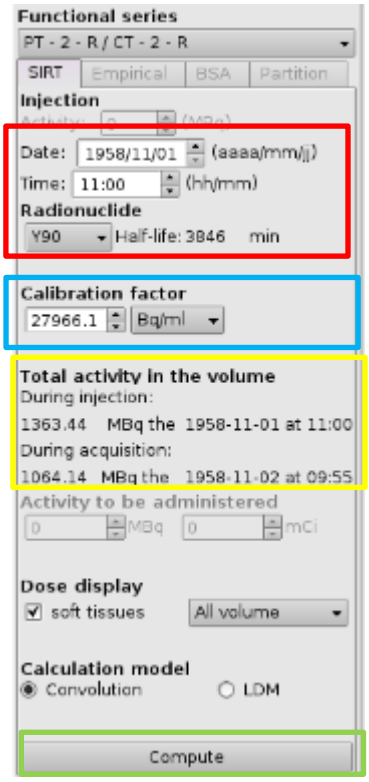

Figure H26. Checking the settings of the system and filling in the calibration factor before performing dosimetry.

Reading the results

The results of the dosimetry calculations are shown. First, the results are shown visually in the three known views.

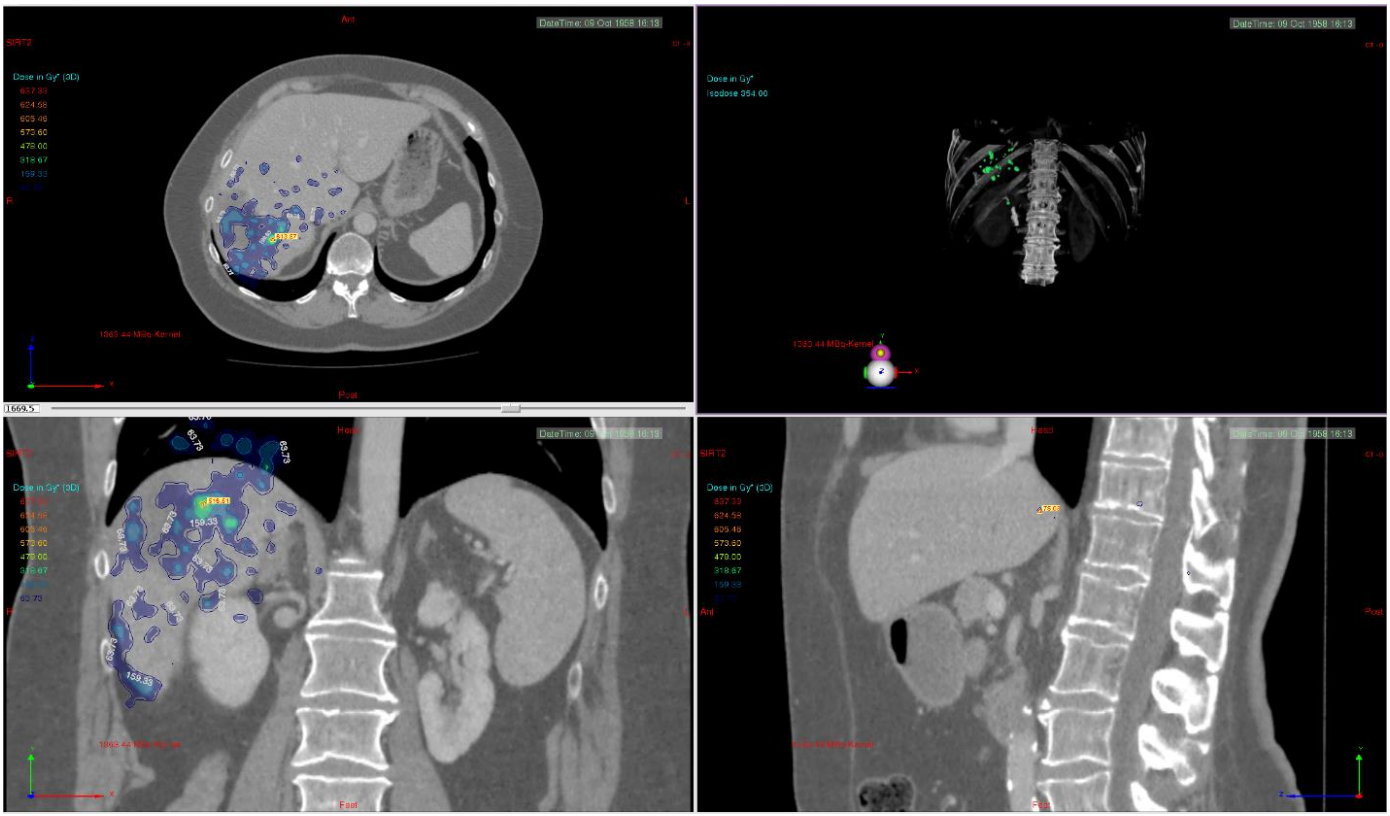

Figure H27. Visual results of the dosimetry.

The results can also be used to calculate several parameters and to obtain dose-volume-histograms (DVH).

1. Click on the ‘graphics’ sign in the toolbar (red box). Add the structures of which you want to calculate the parameters (green box) and then calculate them (yellow box). Results can be exported to excel (figure H29, red box).

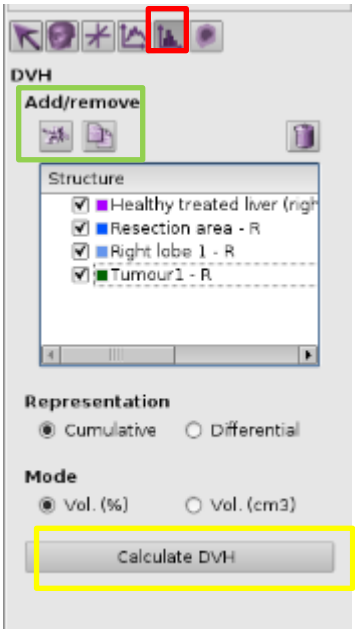

Figure H28. Calculating the data analysis parameters and DVH.

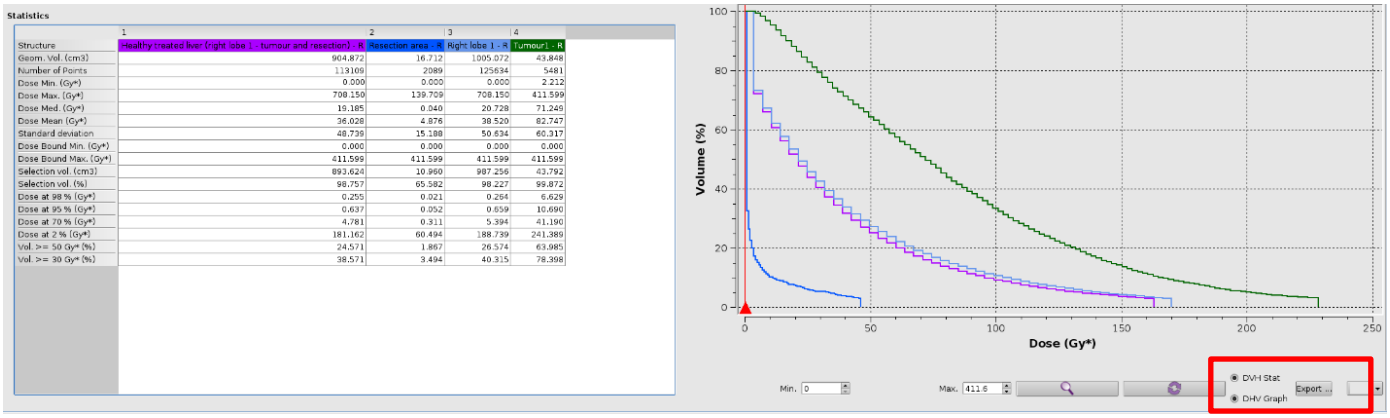

Figure H29. Results of the parameter and DVH calculation and export option (red box).